2004

Modeling the hydrogeochemistry of denitrification in the Elk Valley Aquifer

Paul A. Skubinna
University of North Dakota

MODELING THE HYDROGEOCHEMISTRY OF DENITRIFICATION IN THE ELK VALLEY AQUIFER

by

Paul A. Skubinna
Bachelor of Science, University of North Dakota, 1998

A Thesis
Submitted to the Graduate Faculty

of the

University of North Dakota

in partial fulfillment of the requirements

for the degree of

Master of Science

Grand Forks, North Dakota
December
2004

This thesis, submitted by Paul A. Skubinna in partial fulfillment of the requirements for the Degree of Master of Science from the University of North Dakota, has been read by the Faculty Advisory Committee under whom the work has been done and is hereby approved.

_____
Chairperson

_____

_____

This thesis meets the standards for appearance, conforms to the style and format requirements of the Graduate School of the University of North Dakota, and is hereby approved.

_____
Dean of the Graduate School

_____
Date

PERMISISION

Title Modeling the Hydrogeochemistry of Denitrification in the Elk Valley Aquifer

Department Geology and Geological Engineering

Degree Master of Science

In presenting this thesis in partial fulfillment of the requirements for a graduate degree from the University of North Dakota, I agree that the library of this University shall make it freely available for inspection. I further agree that permission for extensive copying for scholarly purposes may be granted by the professor who supervised my thesis work or, in his absence, by the chairperson of the department or the dean of the Graduate School. It is understood that any copying or publication or other use for financial gain shall not be allowed without my written permission. It is also understood that due recognition shall be given to me and to the University of North Dakota in any scholarly use which may be made of any material in my thesis.

Signature _____

Date _____

TABLE OF CONTENTS

LIST OF FIGURES

LIST OF TABLES

ACKNOWLEDGMENTS

Thanks to the North Dakota State Water Commission for financial assistance, and specifically to William Schuh, Senior Hydrologist, for his technical assistance and wisdom. Thanks to the North Dakota Department of Health for their analytical services and assistance. Thanks to the Water Resources Research Institute and United States Geologic Survey for financial assistance.

Special thanks to Phil Gerla, Ph.D. and Harvey Gullicks, Ph.D., P.E., for their endurance during this process and for their input to this thesis. Special thanks to Scott Korom, Ph.D., PE, for his endurance, patience and commitment to participating in the higher education of willing students.

Very special thanks to my Father, Ray Skubinna, for his continued and unyielding support. Very special thanks to my fiancé, Sarah Dunbar, for her support and unyielding confidence.

To all the “neh-sayers” and skeptics

ABSTRACT

Nitrate (NO_3^-) in groundwater has become an important issue in the last few decades. It is known to cause methemoglobinemia, commonly known as "blue baby syndrome," and is suspected of being a carcinogen. The most common sources for dissolved NO_3^- in shallow groundwater include excessive application of nitrogenous fertilizers, misuse of septic systems, improper disposal of domestic wastewater or sludge, and livestock waste.

Denitrification is the most effective sink for NO_3^-. The Elk Valley aquifer (EVA) of eastern North Dakota is known to support denitrification. The objective of this study was to gain a better understanding of the geochemical processes associated with the denitrification observed in the EVA. The hypothesis tested was that geochemical conditions are proper for organic carbon to be a primary electron donor responsible for denitrification in the Elk Valley Aquifer at the Larimore Field Site (LFS).

This thesis presents data from a second tracer test performed at the LFS. The methodology of this study was to replicate the first tracer test using the same in-situ mesocosms (ISMs) located near Larimore, ND. The approach incorporated fieldwork, analytical lab work and geochemical computer modeling.

The fieldwork consisted of amending groundwater contained within the ISMs with potassium nitrate and potassium bromide on October 8, 1998, followed by monthly sampling and analysis of the amended water. Sample analyses for general anions, cations

and other basic water parameters were performed by North Dakota Department of Health. Bromide analysis, along with duplicate analysis of dissolved carbon, nitrate-nitrogen, and sulfate, were performed at the University of North Dakota, Department Geology and Geological Engineering, Water Quality Lab.

The geochemical modeling code PHREEQC-2 was used to simulate the observed groundwater quality to gain insights regarding a possible a second primary electron donor in addition to pyrite documented during the first tracer test. Additionally, the modeling work was completed in to gain insights into the secondary geochemical reactions resulting from denitrification and reactions caused by the study methodology. The model simulations employ mineral equilibria, cation exchange, dilution and oxidation-reduction calculations to describe the major water quality parameters observed during the study. Ultimately, the model output supports my hypothesis that geochemical conditions are proper for organic carbon to be participating as a primary electron donor to the observed denitrification.

CHAPTER I

INTRODUCTION

In the United States groundwater is a major source for potable water. It is estimated that 41% of the population's fresh water is acquired from the ground (World Wide Web URL http://water.usgs.gov/watuse/spread95.html). Similarly, 44% of North Dakota's population relies on aquifers for its source of fresh water (http://water.usgs.gov/watuse/spread95.html). Many of these freshwater aquifers are shallow; therefore, human practices and natural processes that occur on the land surface can readily affect groundwater quality.

Nitrate (NO_3^-) in groundwater has become an important issue in the last few decades. It is known to cause methemoglobinemia, commonly known as "blue baby syndrome," and is suspected of being a carcinogen (Canter, 1997). Nitrate compounds are highly soluble (Faure, 1998) and are often observed in shallow groundwater systems (Trudell et al., 1986). The United States Environmental Protection Agency (USEPA) Office of Water lists nitrate as the second most common groundwater contaminant observed exceeding its Maximum Concentration Level (MCL) of 10 mg/L nitrate as nitrogen (NO_3^--N) (http://www.epa.gov/ow/resources/9698/chap6c.html).

The proliferation of nitrate (NO_3^-) contamination in many fresh water sources has led to a concerted effort within the research community to characterize the sources and

sinks for the dissolved species of nitrogen. The most common sources for dissolved NO_3^- in shallow groundwater include excessive application of nitrogenous fertilizers, misuse of septic systems, improper disposal of domestic wastewater or sludge, and livestock waste (Canter, 1997). Denitrification is the most effective sink for NO_3^- (e.g., Pauwels et al., 1998; Postma, 1990; Postma et al., 1991; Trudell et al., 1986).

Denitrification, as herein referred to, is the biologically mediated oxidation-reduction (redox) process whereby NO_3^- is irreversibly converted to nitrogen gas ($N_{2(g)}$). The $N_{2(g)}$ end member is not a contaminant and resists conversion back to oxygenated species in most naturally occurring aquifer environments because of its triple bond. In general, there are four requirements for denitrification to occur. These requirements are (Firestone, 1982): (1) the presence of oxygenated species of dissolved nitrogen, (2) available supply of electron donors i.e. sulfide, organic carbon, and reduced iron or manganese (Korom, 1992), (3) anaerobic conditions, and (4) a population of bacteria capable of using nitrogen oxides as electron acceptors during respiration.

Many studies of aquifers that naturally denitrify have revealed important process characteristics such as rates, evidence of the common electron donors and availability, general hydrogeochemistry of the process, the type of bacteria involved, and other useful information that is often site specific. One such aquifer is the Elk Valley aquifer (EVA) of eastern North Dakota. Previous research has concluded that denitrification occurs naturally in the EVA (Mayer, 1992; Patch and Padmanabhan, 1996) and that sulfides are responsible for most of the denitrification observed at the Larimore field site (LFS) (Schlag, 1999).

This thesis presents data from a second tracer test performed at the LFS. The hypothesis tested is that geochemical conditions are proper for organic carbon to be the second major electron donor responsible for denitrification in the Elk Valley Aquifer at the Larimore Field Site. In addition to testing the hypothesis of this research the second tracer test was also designed to confirm the denitrification by pyrite observed by Schlag (1999), monitor denitrification rates under continued loading, gather indicators of the EVA's total denitrification capacity, and gain insights regarding secondary reactions that may be induced by the redox processes and/or the research methodology.

The evidence used to test the hypothesis included replicating the tracer test done by Schlag (1999) using the in-situ mesocosms (ISM) designed and installed for that study. The second tracer test lasted 608 days. The large size of the ISMs affords sampling on an approximate monthly schedule in volumes allowing for analysis of overall water chemistry, with duplicate analysis of ions deemed particularly important to this study. Four nitrogen isotope samples and two sulfur isotope samples were also collected throughout the course of the study and are reported. Bromide (Br^-) was used as the dilution tracer. Changes in the Br^- - NO_3^- ratio and the isotopic enrichment of NO_3^- remaining in solution were used to confirm denitrification. Increases in sulfate (SO_4^{2-}) concentrations were used to estimate the contribution of sulfide minerals to denitrification.

In addition to replicating the first tracer test and comparing data results, PHREEQC-2 (Parkhurst & Appelo, 1999) was used as a tool to further test the hypothesis of this thesis. The capabilities of PHREEQC-2 used for this research include thermodynamically based equations, computation algorithms and a thermodynamic

database (WATEQ4F, Plummer et al. 1976). Most groundwater observed in shallow aquifers is not in thermodynamic equilibrium. Therefore, the boundary conditions input into PHREEQC-2 were specifically chosen based on dissolved ion concentrations, water temperature and pH observed during the study, in an effort to replicate the thermodynamic state of the system. Ultimately, the results of the computer modeling provide evidence that organic carbon is a likely primary electron donor to the observed denitrification. Supplemental to these findings, the model was used to predict a series of potential thermodynamic-based secondary geochemical reactions that resulted in the observed changes in groundwater quality parameter concentrations during the study.

CHAPTER II

REVIEW OF PREVIOUS WORK

This review of denitrification begins with a definition of two types of denitrification reactions and their stoichiometric equations. The stoichiometry discussion is followed by a discussion outlining observed effects of denitrification on the $^{15}N/^{14}N$ stable isotope ratio of NO_3^- remaining in solution. Next, a review of hydrogeochemical modeling work relative to this thesis is presented. Finally, an introduction to the EVA and a brief review of the results of the first tracer test are presented along with an electron donor survey performed at the LFS.

Denitrification Stoichiometry

As defined in the introduction, denitrification is a redox process involving bacteria. It is often qualified as autotrophic or heterotrophic depending on the source of carbon fixed by the bacteria participating in the process (Korom, 1992). Typically, autotrophic bacteria fix carbon from inorganic sources while utilizing inorganic electron donors; heterotrophic bacteria fix carbon from organic sources while utilizing organic electron donors. The most commonly studied electron donor known to participate in denitrification is organic carbon (OC) (e.g. Trudell et al., 1986; van Beek et al., 1989; Korom, 1991; Smith et al., 1991). Therefore, heterotrophic denitrification is commonly defined as the process whereby OC is directly consumed, as represented by the following

oxidation/reduction reaction modified from Trudell et al. (1986):

$$5CH_2O + 4NO_3^- + 4H^+ \rightarrow 2N_2 + 5CO_2 + 7H_2O \quad (1)$$

Reaction (1) involves a labile form of OC (zero valence carbon shown as CH_2O) being oxidized via bacteria using NO_3^- as the terminal electron acceptor during respiration (Trudell et al., 1986). The products of Reaction (1) are nitrogen gas, inorganic carbon as carbon dioxide (+4 valence) and water. Stoichiometrically, each OC atom donates 4 electrons to NO_3^-.

Bacteria that satisfy their need for carbon and other nutrients by fixing them from inorganic sources [e.g., *Thiobacillus denitrificans* (Kolle et al., 1985)] are categorized as autotrophs. Hence, autotrophic denitrification is the process where inorganic carbon and inorganic electron donors are used by bacteria as substrates.

There are many inorganic electron donors available in natural environments. Some common inorganic electron donors in aquifers (in order of most to least available electrons) are, reduced species of sulfur (S^-), manganese (Mn^{2+}) and iron (Fe^{2+}); however Mn^{2+} has not been identified as a significant primary electron donor in natural systems (Korom, 1992) and is therefore often omitted from consideration. It has been suggested that iron sulfide minerals (e.g., pyrite) are the most common inorganic electron donors participating in aquifer denitrification reactions (Kolle et al., 1985; Postma et al., 1991; Tesoriero et al., 2000). Kolle et al. (1985) presented an oxidation/reduction reaction, which provides the stoichiometry for autotrophic denitrification by pyrite

$$5FeS_2 + 14NO_3^- + 4H^+ \rightarrow 7N_2 + 10SO_4^{2-} + 5\ Fe^{2+} + 2H_2O \quad (2)$$

As indicated by Reaction (2), bacteria use reduced sulfur with a negative 1 valence as the electron donor and NO_3^- as the terminal electron acceptor during respiration (Kolle et al., 1985). The stoichiometry indicates that each sulfur atom loses seven electrons to NO_3^--N, assuming complete conversion to $N_{2(g)}$ is achieved. The reaction results in production of SO_4^{2-}, ferrous iron (Fe^{2+}) and water (Kolle et al., 1985).

Kolle et al. (1985) also gave the stoichiometry of an associated secondary oxidation/reduction reaction responsible for denitrification

$$5Fe^{2+} + NO_3^- + 7H_2O \rightarrow 5\ FeOOH + 0.5N_2 + 9H^+ \quad (3)$$

Reaction (3) describes the oxidation of ferrous iron produced in Reaction (2) to ferric iron (Fe^{3+}) by nitrate, and precipitated as the mineral goethite (FeOOH). Each ferrous iron atom is capable of contributing one electron to the overall denitrification process. Nitrogen gas and hydrogen ions are produced. *Gallionella ferruginea* are believed to mediate this process (Postma, 1990).

Buresh and Moraghan (1976) and Postma (1990) suggest that freshly precipitated iron oxyhydroxides, such as the goethite formed in Reaction (3), may act as a catalyst for reduction of dissolved oxygenated nitrogen ions. However, these interactions are not fully understood. Therefore, stoichiometric representation of autotrophic denitrification by pyrite is often summarized through the addition of (2) and (3) to form a combined oxidation/reduction denitrification reaction, (Appelo and Postma 1996)

$$2FeS_2 + 6NO_3^- + 2H_2O \rightarrow 3N_2 + 2FeOOH + 4SO_4^{2-} + 2H^+ \quad (4)$$

Overall, there are two important concepts to consider when regarding the stoichiometry of denitrification as presented by Reactions (1 – 4). The first involves the aqueous products of the described reactions. According to Reaction (1) inorganic carbon is the dominant product of heterotrophic denitrification, observed as HCO_3^- at most commonly observed aquifer pH ranges of 6-8 (Appelo and Postma, 1996). Similarly, (4) indicates SO_4^{2-} and Fe^{3+} (aqueous, sorbed or in an organized mineral structure) are the commonly observed products of autotrophic denitrification, when iron sulfide is the electron donor.

It should be noted that Reaction (1) is strictly a theoretical stoichiometric relationship that does not account for carbon uptake by biomass or the production of organic acids. These aspects of the biogeochemistry were not strictly addressed during this research.

The second concept to note is the origin and relative stoichiometry of the electrons transfers represented by Reactions (1 – 4). An accounting of Reaction (4) reveals that 28 of 30 electrons transferred during denitrification originate from the sulfide, with the remaining 2 originating from Fe^{2+}. Furthermore, it can deducted from (4) that 1 mole of FeS_2 is capable of denitrifying 3 moles of NO_3^--N. Using this approach and normalizing Reaction (1) to the electron donor, it is evident that 1 mole of zero valence OC is theoretically capable of denitrifying 0.8 moles of NO_3^-.

Denitrification Isotopic Signature

The two most common stable isotopes of nitrogen are ^{14}N and the heavier ^{15}N, having one more neutron as indicated by the 15 superscript. The relative enrichment of one isotope over another of the same atom is termed fractionation (Faure, 1998). During denitrification, enrichment of ^{15}N in the remaining NO_3^- occurs during the rate-limiting step (NO_3^- to NO_2^- for most natural aquifer environments) of the unidirectional redox process (Mariotti et al., 1981). Fractionation occurs because bacteria preferentially select the lighter isotope when the N–O bond is broken (Mariotti et al., 1981, 1988). This relative enrichment of ^{15}N in the fraction of nitrogen yet to be denitrified is used to confirm bacterially catalyzed denitrification (e.g. Vogel et al., 1981; Böttcher et al., 1990; Bates and Spalding, 1998).

The magnitude of fractionation is determined by comparing the stable isotope ratio $^{15}N/^{14}N$ of a sample to the $^{15}N/^{14}N$ of atmospheric $N_{2(g)}$. Fractionation is reported as a delta (δ), or change, of the sample from the relatively constant naturally occurring atmospheric isotope distribution. Delta notation is most often given in parts per thousand or permil (‰) due to the small ratios involved in the calculation. Mariotti et al. (1981) presented the following equation for calculating the extent of nitrogen isotope fractionation, or $\delta^{15}N$.

$$\delta^{15}N \text{ ‰} = \{[(^{15}N/^{14}N)_{sample}/(^{15}N/^{14}N)_{atmospheric}] - 1\} \times 10^3 \quad (5)$$

A modification of the Rayleigh equation is applied to quantitatively relate the $\delta^{15}N$ of the portion of NO_3^--N remaining in solution to the $\delta^{15}N$ of the initial NO_3^--N in solution, as calculated using Equation (5) (Vogel et al., 1981; Mariotti et al., 1981).

Rearranging the Rayleigh modification, to solve for an enrichment factor, ε, results in (Mariotti et al. 1981 and 1982):

$$\varepsilon = \{10^3 \times \ln[(10^{-3}\ \delta^{15}N_t + 1)/(10^{-3}\ \delta^{15}N_{t=0} + 1)]\}/\ln(N_t / N_{t=0}) \qquad (6)$$

In Equation (6) N is the concentration of NO_3^--N remaining in solution, $\delta^{15}N$ is the fractionation of the NO_3^--N remaining in solution and t is time.

Mariotti et al. (1988) observed a correlation between denitrification rates and the magnitude of fractionation. They noted that higher rates of denitrification occur at warmer reaction temperatures and/or greater electron donor availability, when all other variable conditions are held constant (Mariotti et al., 1988). Furthermore, elevation of either of these conditions also resulted in lower fractionation of the remaining NO_3^- and computationally a less negative ε (Vogel et al., 1981; Mariotti et al., 1982). Thus, apparently the enrichment factor can be used as a tool for relative comparison of electron donor availability to denitrification occurring at similar reaction temperature.

In summary, years of research have begun to define some of the characteristics of denitrification. In more recent years, studies have involved application of in-situ microcosms, tracer tests and geochemical computer models to gain further insights into denitrification processes. For completeness, a brief review of a selected group of studies regarding the application of in-situ microcosms and tracer test methodologies, similar to those used for this study, is presented in Appendix A. The focus of the literature review below is on studies that directly pertain to the methods utilized during the computer modeling portion of this research.

Geochemical Computer Modeling of Denitrification

Trudell et al. (1986)

Trudell et al. (1986) performed a tracer test whereby an equilibrium mole balance model was executed and discussed to help substantiate their conclusions of heterotrophic denitrification. The geologic setting for the tracer test consisted of an unconfined sand aquifer less than 4 m thick located near Rodney, Ontario, near the north shore of Lake Erie. The site was selected in part because of a small hydraulic gradient, thus minimizing advective dispersion of the chemically-amended tracer test water. Aquifer characteristics at the research site included 2 m of fine-grained brown calcareous glacial-deltaic sand underlain by 1.6 m of gray fine-grained calcareous glacial-deltaic sand. The bottom of the fine-grained calcareous sand was sealed by gray lacustrian clay. The water table varied from 0.93 to 1.89 m below ground surface.

The tracer test employed the single well extraction, amendment, injection and monitor methodology. Hence, 200 L of water was extracted from the aquifer and mixed with 17.0 mg NO_3^--N $\cdot$ L^{-3} as KNO_3, 5.06 mg Br^- $\cdot$ L^{-1} as NaBr and 5.52 mg dissolved oxygen (DO) $\cdot$ L^{-1}. DO concentrations were due to partial equilibration of the extracted fluid with the atmosphere during field operations. The chemically amended water was re-injected back into the aquifer and monitored.

The DO introduced during chemical amendment was reduced within a few hours to less than 2 mg $\cdot$ L^{-1}. After 312 hr of observation, NO_3^- was reduced to 3.6 % (0.47 mg NO_3^--N $\cdot$ L^{-1}) its injected concentration while Br^- remained 40 % (2.00 mg Br^- $\cdot$ L^{-1}) its injected concentration. The pH fluctuated during chemical amendment activities from ~7.2 up to ~7.9 due to CO_2 off-gassing to the atmosphere, finally decreasing back to ~7.6

during post injection monitoring. Dissolved inorganic carbon (DIC) increased as 142 mg $HCO_3^- \cdot L^{-1}$during post re-injection monitoring. Denitrification rates were determined by fitting a curve to the dilution corrected NO_3^- concentrations and finding the slope of the tangent line. Rates ranging from 0.0078 to 0.13 mg NO_3^--N $\cdot L^{-3} \cdot hr^{-1}$are reported. No isotope or SO_4^{2-} data are reported.

A method of mole balance equilibrium modeling was applied to the data. The model employed the Newton-Raphson method for solving a system of equations involving interactions between the carbonate system, NO_3^-, Br^- and a labile form of solid OC, represented by CH_2O. It was assumed that the free energy derived from denitrification by solid OC is equal to that derived from dissolved organic carbon (DOC). This eliminated one unknown and enabled solution of the system of equations. The model boundary conditions were set such that equilibrium distribution of dissolved species was achieved and all activity coefficients were one. Dilution was simulated according to the Br^- concentration profile. Heterotrophic denitrification was allowed to occur freely within the model, simulated by consumption of available OC. Upon execution, the model was allowed to proceed until a predetermined dilution-corrected amount of NO_3^- was completely reduced. The model output depicted heterotrophic denitrification resulting in CO_2 and H^+ production according to Reaction (1). CO_2 produced was observed as HCO_3^- due to ambient pH conditions. Additional secondary HCO_3^- evolution was observed due to the calcareous nature of the aquifer, as indigenous calcite buffered the excess H^+ that resulted from the denitrification. Ultimately, the total HCO_3^- production calculated by the model corresponded well with that observed during the tracer test; furthermore, the pH concluded by the model simulation was 7.98

indicating only a minor deviation from the values observed in the field at the end of the tracer test.

The methodology used to simulate dilution in the model is not clear. It is not clear if the NO_3^- or HCO_3^- concentrations of the dilution water were considered in the total mass balance. It is not clear whether dilution of the HCO_3^- produced during simulated denitrification was accounted for within the model. If not, the concentration of HCO_3^- output by the model should be higher than the diluted concentrations of HCO_3^- recorded in the tracer test. The HCO_3^- produced, as calculated by the model, was slightly less than the observed value.

To further complicate the issue, the state of saturation for calcite or the exchange capacity of the aquifer was not reported. Because the aquifer is calcareous, it could be assumed that background conditions existed such that the water was nearly saturated with respect to calcite. When the groundwater was amended Na^+ and K^+ were also dissolved in the water, potentially inducing exchange for Ca^{2+} and increasing its concentration. Meanwhile, heterotrophic denitrification was occurring, thereby increasing DIC. The combination of an increase in Ca^{2+} and DIC heightens the state of saturation of the water with respect to calcite. Thus, it is more likely to induce calcite precipitation instead of dissolution if the water was near saturation already. This raises issues as to the origin of the observed buffering mechanisms of the aquifer.

The discussion presented by Trudell et al. (1986) does not consider the role, if any, of sulfides and SO_4^{2-}. However, the data reported are compelling evidence outlining some of the fundamentals of natural heterotrophic denitrification. Ultimately, the study

introduces a potentially meaningful methodology to build on for computer modeling of the process.

McMahon et al. (1999)

McMahon et al. (1999) modeled a tracer test they performed in the Pierre Shale below the South Platte River alluvial aquifer. The Pierre Shale underlies 30 % of the alluvial aquifer in northeastern Colorado. One of the purposes of the study was to determine the importance and potential rate of denitrification in the Pierre Shale as a sink for NO_3^- in the overlying South Platte aquifer. Modeling consisted of two phases. First, they determined and modeled the mechanism and rate of NO_3^- transport to the shale. Second, they used NETPATH (Plummer et al., 1991) to model the geochemistry of denitrification in the shale on a mass balance basis.

At the study area the water table was ~3.5 m below land surface in the alluvial aquifer having a saturated thickness of ~6.1 m. The depth to the alluvium/shale contact was 9.6 m. The alluvial aquifer consists mainly of fine to coarse-grained sand composed of quartz and feldspar, with intermittent clay and gravel lenses. The aquifer contained <0.01 % sulfide and 0.06 % OC by weight at the study site. The top 2 cm of the shale at the study site was yellowish-brown, weathered clayey silt. This weathered zone was underlain by dark gray to black clayey silt. The shale samples contained 0.39 % sulfide, and 0.40 % OC by weight. Analysis of the samples indicated 90 % of sulfide was in the form of iron sulfide. Pyrite was the only sulfide mineral identified.

Analysis of the background geochemistry indicated a sharp redoxcline just below the shale alluvium contact. Ambient conditions became reducing in a vertical distance less than a few meters, as indicated by a dramatic decrease in NO_3^- concentrations and a

sharp increase in methane, hydrogen sulfide and ammonia concentrations with depth. There is some isotope evidence presented that seems to indicate a small amount of denitrification in the alluvium. Concentrations and values of $\delta^{15}N$ for $N_{2(g)}$ in the shale indicated alluvial NO_3^- may have been transported into the shale and completely denitrified therein. However, tritium analysis of water collected from three wells screened in the shale and one screened at the base of the alluvial aquifer showed no evidence of post 1950 infiltration of alluvial water into the shale.

A one-dimensional finite difference model was applied to help quantify and qualify transport of NO_3^- to the shale. It was concluded that the primary mechanism was diffusion, because of the hydraulic gradient and low permeability of the shale. Due to the relatively slow nature of this transport mechanism, the supply of alluvial NO_3^- to the shale was determined to be the rate-limiting factor for denitrification in the shale.

The purpose of the tracer test was to evaluate the potential denitrification rate of the shale. They used a single well inject-and-monitor methodology. Approximately 245 L of alluvial water were injected into the shale over a 3-hr period. Following injection the slug was monitored periodically for 233 hrs. Concentrations of Cl^- in the injection water was ~2.5 times that of background concentrations in the shale (1.956 mM and 0.803 mM, respectively). Therefore, due to the conservative nature of Cl^- in redox environments relative to NO_3^-, it was used as the tracer. NO_3^- concentration in the injection water was 0.688 mM having background concentrations of <0.001 mM in the shale well. Redox sensitive analytes were monitored and corrected for dilution according to Cl^- concentrations.

Evidence for denitrification included an increase of $\delta^{15}N$ from +15.3 to +23.6 ‰ in the NO_3^- remaining in solution. The corresponding Rayleigh ε was calculated to be approximately –6 ‰, perhaps indicating an environment with a relatively abundant supply of electron donors. Increases in DIC concentration, having a maximum coincident with the timing of maximum NO_3^- decreases and maximum N_2O increases, indicated heterotrophic denitrification. Calculations indicated a potential first-order rate constant of ~60 yr^{-1} for the observed heterotrophic denitrification.

No detectable SO_4^{2-} evolution was observed, further enforcing an assessment of heterotrophic denitrification. During the tracer test no increases in NH_4^+ concentrations were observed relative to those expected due to dilution with background shale pore water. This indicates that dissimilatory reduction of NO_3^- to NH_4^+ was not a significant NO_3^- sink. Dissolved iron concentrations seemed to indicate that ferrous iron participated as an electron donor during the denitrification; however, it was not considered a significant electron donor.

The computer code NETPATH (Plummer, et al., 1991) was used to construct a mass balance model that included mixing and equilibrium phase interaction. Fractional mixing of background water and injection water was used to simulate dilution of the tracer slug according to Cl^- concentration. Cation exchange along with precipitation and dissolution of compositional phases were allowed to occur within the model simulation to test a possible reaction scenario explaining the observed changes in water quality. The model output presented a series of geochemical interactions to achieve mass balance and the observed concentration profile at 137 hr including: (1) exchange of Ca^{2+} for Na^+, (2) FeOOH precipitation, (3) $N_{2(g)}$ de-gassing, and (4) CH_2O, FeS_2, $CaCO_3$ dissolution.

Model output accuracy for pH was not indicated, Ca^{2+} for K^{+} exchange was not considered, and the potential for losses of $CO_{2(g)}$ was not addressed. However, the study reinforces the applicability of the mass balance model as a sound methodology for analysis and discussion of the fundamental characteristics and reactions associated with redox systems, regardless of the model complexity level.

Postma et al. (1991)

The final journal article reviewed for this thesis is Postma et al. (1991). Postma et al. (1991) worked near Jutland in western Denmark. The methodology included sampling wells (using multilevel samplers) along a transect of a flow path under a portion of arable land known to leach NO_3^- contamination to the groundwater table. This method allowed for the establishment of a vertical profile of groundwater quality and redox conditions. Although no tracer test was performed, the relevance of the study lies in the geochemical modeling efforts.

The purpose was to simulate the general geochemical environment across the redoxcline in an effort to predict its evolution with time. The geochemical data were modeled with the PHREEQM code (Appelo and Willemsen, 1987; Appelo et al., 1990) applying a methodology similar to that used for this thesis. The capabilities of PHREEQM allowed for simultaneous simulation of aqueous speciation, multicomponent ion exchange reactions, redox reactions and mineral dissolution/precipitation reactions combined with a one-dimensional mixing cell transport model.

The aquifer was an unconfined glacial deposit consisting of medium- to coarse-grained sand. The solid matrix consisted mostly of quartz sand known to contain fragments of reworked coal from underlying Miocene deposits. The aquifer was noted to

be calcite deficient in most locations; thus, it was likely to offer little buffering capacity for pH changes caused by redox processes.

The primary electron donors detected within the aquifer matrix consisted of iron sulfide and OC, both increasing in concentration with depth. The iron sulfide detected generally lacked amorphous phases; pyrite was the only sulfide mineral identified. Iron sulfide fractions in the aquifer matrix had an overall average concentration of 3.6 mmol · kg^{-1}. The reworked coal fragments were believed to be the primary form of OC in the aquifer matrix; they were considered to be relatively nonreactive. FeOOH was observed throughout the aquifer in variable concentrations. It appears that the highest concentrations were observed in the oxidized zone of the aquifer; however, Postma et al. (1991) defined the distribution as unaffected by the redox conditions.

The groundwater chemistry along the well transect is best characterized as two general zones. An upper oxidized zone, where DO and NO_3^- were comon; and a lower reduced zone, characterized by higher dissolved iron concentrations. These two zones were separated by the redoxcline defined as the short vertical distance that had a sharp increase in SO_4^{2-} concentration, a minor increase in total inorganic carbon (TIC), and a decrease of NO_3^- and DO concentrations. The pH appeared to be stable in general, varying slightly between 5 and 6. There was no definite trend in pH values observed with depth in any of the three primary redox zones (the oxidized zone, reduced zones, or within the redoxcline itself).

"The sharp decline in nitrate concentration at the redoxcline strongly indicates that NO_3^- reduction is taking place (Postma et al., 1991, pp 2030-2031)." Sulfate increases across the redoxcline seemed to indicate autotrophic denitrification dominated.

However, minor increases in TIC seemed to indicate heterotrophic processes had occurred, based on Reaction (1). Appreciable amounts of NH_4^+ were not detected indicating dissimilatory denitrification was not occurring. Similarly no NO_2^- was detected; thus, they assumed that complete reduction of NO_3^- to $N_{2(g)}$ was occurring. Assessment of the groundwater quality data using the WATEQF database (Plummer et al., 1976) indicated that it was very undersaturated with respect to calcite.

Site conditions made it difficult to identify the extent of denitrification vs. horizontal transport. The groundwater vertical flux rate (although relatively constant compared to the horizontal flux rate) was considerably less than the horizontal flux rate. Additionally, it was determined that the spatial variation of NO_3^- concentrations in recharge water was high, ranging from <0.5 mM to >2 mM.

To overcome these difficulties for denitrification quantification, a "sum of the anions" method was invoked to effectively trace denitrified water across the redoxcline. Using this method of tracing, it was determined that the denitrification kinetics were rapid compared to the progression of the redoxcline downward and the groundwater vertical flux rate. Therefore, a redox equilibrium model was justified to quantify denitrification during vertical transport across the redoxcline.

A series of cells, forming a column, were simulated using the model and the age of the water for the corresponding depth in the field. The model was initialized by determining what the vertical concentration of dissolved species were prior to NO_3^- loading by using the model to flush water in equilibrium with atmospheric oxygen through the simulated column. The cells comprising the upper oxidized zone were allowed to be in equilibrium with goethite. The cells representing the lower reduced zone

of the aquifer were allowed to be in equilibrium with goethite and pyrite, since pyrite was believed to be the only electron donor of consequence. This produced a simulated water quality profile similar to that of the aquifer before nitrate loading. This was evidenced by the simulated water's close match to the vertical water quality profile observed in a monitoring well that had not been influenced by the nitrate plume.

Next, NO_3^- was added to the modeled column influx water at concentrations determined by the age/vertical location vs. the total sum of the anions. The model simulated the beginning of nitrate influx from 1973 to 1988 so the calibration of the model based on field data collected at that time (1988) could be confirmed. The model concentration profile output for 1988 fit within the rather extensive scatter of the water quality data profile measured in that year. The model was then allowed to continue calculation to 2003 to predict the water quality profile of the future.

The modeling results indicated only minor shortcomings in the methods used. The pH was buffered with FeOOH in the absence of calcite. This resulted in iron concentrations that were in excess of observed values. However, Postma et al. (1991) discussed scaling issues in an effort to provide reasons for slight discrepancies in model output vs. observed data. They manipulated the cell lengths at the redoxcline in an attempt to rectify the problem. Ultimately, the pH discrepancies were left unresolved. Furthermore, the model did not include cation exchange because it was felt it did not directly influence redox species under observation. Water analyses were reported for Ca^{2+} and Mg^{2+} and the modeled data fit these data within the scatter.

In conclusion, the degree of accuracy achieved in this study's results reinforces the applicability of building models to gain further understanding of the

hydrogeochemistry of denitrification. Ultimately, the accuracy and complexity of any model is determined by the input data, the boundary conditions applied to the model and the assumptions invoked. These parameters are usually determined based on field sampling and laboratory analysis. Thus, when research data are to be modeled, the field site needs to be described as accurately as possible through the application of sound laboratory and field methods.

Denitrification and the Elk Valley Aquifer

The remainder of the literature review consists of a brief description of the Elk Valley Aquifer (EVA) and the Larimore Field Site (LFS). This is accomplished via a summary of studies conducted at, or pertaining directly to, the LFS. A description of the general chemical and physical characteristics of the aquifer is provided, including a description of the specific aquifer characteristics believed to be pertinent to the hydrogeochemistry of the denitrification observed during this study.

Geography of the Larimore Field Site

The EVA underlies approximately 725 km^2 of eastern North Dakota ranging in thickness up to 20 m (Mayer, 1992; Kelly and Palson, 1970). The LFS is located approximately 1 km west of Larimore, North Dakota, along county road 4. The ISMs (Schlag,1999) were installed next to an access road on the western edge of SW ¼ SE ¼ Section 11, T. 151 N., R. 55 W. The area surrounding the ISMs is arable land, cropped with beans and small grains during the growing seasons spanned by this study. The half section containing the ISMs has minimal relief, totaling about 60 cm (approximated from water stains resulting from flooding during the summer of 2000). The ISMs are approximately 5 m apart in a north-south orientation. The tops of the chambers are ~4.6

m below land surface within the sediments of the EVA. For a complete description of the ISM design and installation see Schlag (1999).

Regional Deposition Environment for EVA

Glacial activity sculpted many of the landforms observed today in the upper Midwest. The Red River Valley, for example, was not truly formed from erosion by the Red River as its name suggests, rather it is the lake bottom plain of the pro-glacial Lake Agassiz. The name "Lake Agassiz" is assigned to the last two phases of four pro-glacial lakes that covered large portions of the upper Midwest during the Laurentide time. The EVA was deposited along the west shore of the Lake, during one of the last phases of its pro-glacial occurrence, as a glacial outwash lacustrian delta/underflow fan (Harris, 1997).

Source material for the EVA consisted mostly of reworked Cretaceous upland deposits including the Pierre Shale and equivalent rocks. The deposition mechanisms and source material have directly influenced the physical and chemical characteristics of the Elk Valley sediments. For a more complete description of the depositional environment, sequence and source rock for the EVA and sediment physical analyses at the LFS see Schlag (1999).

Hydrogeology and Geochemistry of EVA

In recent decades, research has been conducted to characterize the EVA hydrogeologically and geochemically. The sediments of the EVA are generally graded north to south. Near Northwood (south) the aquifer consists of very fine sand, silt and clay, becoming coarser in the north to sand and gravel near Inkster (Kelly and Paulson, 1970). The LFS is near the middle of the sediment N-S gradation and is mainly fine to medium grained sands, becoming slightly coarser with depth (Schlag, 1999). Sieve

testing of ISM-depth LFS sediment revealed a size distribution of 11.1 % clay, 9.7 % silt, 79.0 % fine sand and 0.2 % coarse sand by weight (Schlag, 1999).

In general, the EVA sediment matrix is porous and has a moderately high hydraulic conductivity. The porosity is estimated to be 35 % and hydraulic conductivities of the aquifer are estimated to be 400 $m \cdot day^{-1}$ and 40 $m \cdot day^{-1}$ in the horizontal and vertical direction, respectively (Schlag, 1999; Gerla, 1992, Table 2 pg 746). The groundwater flow direction is generally west to east (Gerla, 1992). The infiltrative nature of the overlying soils is manifested in the poorly developed surficial drainage system (Kelly and Paulson, 1970). One extreme incident illustrating the low relief was observed during the summer of 2000. An unusually heavy rain caused ponding to depths of 40 cm above land surface at the ISM location. Approximately 90 % of the land area within the half section the ISMs are located was inundated for approximately one week until the surface water evaporated and/or infiltrated. Infiltration events cause fluctuations in the groundwater table; however, it is estimated that total average annual water table fluctuation is less than two meters in magnitude. Depth to the water table at the LFS is rarely >3 m below land surface.

Gerla (1992) described the geochemistry of the EVA as a Ca^{2+} - Mg^{2+} - HCO_3^- type water in the west, evolving along easterly flow paths into a more SO_4^{2-} - Na^+ type water. Gerla (1992) also noted that most water samples from the EVA were undersaturated with respect to gypsum ($CaSO_4 \cdot H_2O$) and near saturation with respect calcite ($CaCO_3$) and dolomite [$CaMg(CO_3)_2$]. The geochemical mechanisms believed controlling these observations are Ca^{2+} and Mg^{2+} exchange for Na^+ within the montmorillonite clays, accompanied by calcite precipitation (Gerla, 1992). Overall the

water quality of the EVA is potable; however, concerns regarding parameters such as nitrate, hardness and the potential for increased metal and metalloid concentrations have been noted (Mayer, 1992; Kelly and Paulson, 1970; Schlag 1999). Ultimately, most of the water quality parameters are directly influenced by the chemical and mineralogical composition of the aquifer matrix.

Kammer (2001) investigated the chemical and mineralogical character of EVA sediments during a laboratory study of electron donors present at the LFS. She reported the mineralogical composition of the bulk matrix via X-ray diffraction (XRD) analysis. One sample taken at the LFS from ISM depth (4.9-5.8 m) was reported to contain mostly silica, in the form of quartz, chalcedony and other amorphous hydrated silica species. Other XRD peaks showing strong intensity were potassium feldspar, plagioclase feldspar (albite → anorthite solid solution series), calcite, dolomite and smectite. Minor peaks identified were amphibole, pyrite, illite/mica, and kaolinite. The fifth tallest peak observed on the XRD scan was not identified. The analysis of this sample is considered to be representative of the general matrix chemistry within the ISM chambers due to the sample collection location (near the ISMs at the LFS) and depth. The presence of feldspars seems to reinforce the notion of a short depositional period with minimal chemical weathering.

The sedimentary nature of the aquifer source material is discernable in hand samples. Fine sand and silt size grains of black shale aggregates within most of the sediment samples from the LFS are readily identifiable by eye. The aquifer electron donors are often associated with this shale fraction.

Kammer (2001) determined the abundance of potential electron donors within the EVA at the LFS. She reported total organic carbon (TOC) and sulfide fractions of 0.43 % and 0.41 % by weight, respectively. Similarly, Schlag (1999) reported values for TOC ranging from 0.195 to 0.304 % at the LFS ISM depth.

Schlag (1999) also reported the metal and metalloid compositions of sediment samples taken from the LFS over the range of ISM depth. Mo, Cu, Pb, Zn, Ag, As, Cd, Sb, Bi, Ti, Hg, Se, Te, Ga and Au were all detected in varying concentrations. Many of the elements detected are known to be associated within the organic fraction of the Pierre Shale (Schultz et al., 1980); others commonly occur as impurities in pyrite by substituting for iron in the crystal lattice (Kölle et al., 1990).

Previous Research on Denitrification in the EVA

In recent years, concerns regarding the effects of increased irrigation and application of nitrogen-based fertilizer have fueled efforts to establish the occurrence and fate of nitrate contamination within the EVA.

Mayer (1992) established the occurrence of nitrate concentrations in the EVA, often in excess of EPA drinking water standards. In general Mayer (1992) observed the greatest NO_3^- concentrations in samples from wells screened at the water table. A vertical nitrate concentration profile exhibited a decrease of NO_3^- concentration to below detection within three meters below the water table. Mayer (1992) also determined that the other major requirements for denitrification were met at his field site. He presented direct evidence of the presence of denitrifying bacteria and electron donors in the form of OC. Mayer concluded that heterotrophic denitrification was occurring within the EVA,

based on the data presented. Mayer (1992) also suggested that autotrophic denitrification may also be an important nitrate sink within the aquifer.

Patch and Padmanabhan (1996) also discussed the occurrence and distribution of NO_3^- concentrations in the EVA. Their study was designed to investigate a method for sampling vertical NO_3^- concentration profiles and discern the cause of concentration gradients. They observed nitrate concentrations that decreased with depth, similar to those presented by Mayer (1992). To determine the cause of the NO_3^- concentration gradient, nitrogen isotope analyses were performed. Generally, they found a relative enrichment of ^{15}N in the NO_3^- remaining in solution with depth. This observation was interpreted as an indication of heterotrophic denitrification; however, no direct evidence is reported identifying the electron donor(s) participating in the denitrification.

In October of 1997, Schlag (1999) started the first in a series of tracer tests at the LFS. This first tracer test was intended to provide evidence supporting sulfide minerals as a major electron donor for denitrification in the EVA. Prior to amending the groundwater Schlag (1999) designed and installed two stainless-steel chambers called in-situ mesocosms (ISM) below the redoxcline of the aquifer. The ISMs are cylindrical, having an open bottom, effectively isolated approximately 185.5 L of the aquifer from lateral transport and advective effects. Assuming 35 % porosity for the aquifer the pore volume of the ISMs is estimated to be 64.9 L.

Schlag (1999) observed dissolved nitrogen attenuation of 4.18 mmol $\cdot$ L^{-1} NO_3^--N within the R-ISM that could not be attributed to dilution, as measured by the Br^- tracer. Simultaneously a 1.70 mmol $\cdot$ L^{-1} SO_4^{2-} increase was observed during the study, identifying pyrite as the electron donor accountable for 61 % of the observed

denitrification. $\delta^{15}N$ of the NO_3^- remaining in the R-ISM progressively increased during the study from 2.4 to 43.5 ‰ further indicating denitrification and suggesting an electron donor deficient environment (relative to electron acceptor abundance). Schlag (1999) reported an average denitrification rate of 15 μmol NO_3^--N · L^{-1} · day^{-1} (0.21 mg · L^{-1} · day^{-1}).

No direct aqueous phase evidence supporting heterotrophic denitrification within the R-ISM was reported; however, Schlag (1999) described the potential for carbonate phase precipitation as a DIC sink. He substantiated his hypothesis with mass balance calculations and XRD data of sample bottle precipitate observed during TT1.

The phenomenon proposed by Schlag (1999) explained why the expected increases in DIC concentration, as a result of heterotrophic denitrification in the R-ISM, were not observed. Ultimately, he inferred from the overall aqueous geochemistry and other observations made during the study that the remaining 39 % of the denitrification could have been due to heterotrophic processes.

CHAPTER III

FIELD AND LABORATORY METHODS AND RESULTS

The effectiveness of the ISMs and protocols applied during the first tracer test (TT1) warranted a second tracer test (TT2) to observe the effects of continued NO_3^- loading on the portion of the aquifer isolated within the ISMs.

Prior to commencement of TT2 some minor maintenance was performed on the ISMs to mitigate suspected leaks detected during TT1. Subsequently, the ISMs were purged and sampled for Br^- to ensure that geochemical remnants of TT1 had been effectively removed. After ISM maintenance and purging the target concentrations and duration of TT2 were determined based on the observation made during TT1. TT2 was designed to last approximately 10 to 14 months. TT2 target groundwater amendment concentrations for the research ISM (R-ISM) were 7.8 mmol $\cdot L^{-1}$ NO_3^--N and 1.4 mmol $\cdot L^{-1}$ Br^- (110 mg $\cdot L^{-1}$for both parameters), delivered as KNO_3 and KBr. The control ISM (C-ISM) was to receive an equivalent amendment of only KBr, such that the ionic strength of the amendment to both ISMs was equal or approximately 9.2 mmol $\cdot L^{-1}$ (737 mg $\cdot L^{-1}$) Br^-. Thus each ISMs would theoretically receive an increase of 9.2 mmol $\cdot L^{-1}$ of both negatively and positively charged ions per liter.

On October 8, 1998, 83 L of water were pumped out of each ISM into precalibrated plastic containers, amended and gravity-fed back into the ISMs. The R-ISM received 65.90 g KNO_3 and 13.60 g KBr. The C-ISM received an ionic equivalent

91.16 g KBr. Dissolved oxygen and pH were monitored during field operations. Samples BC-10-08-98 and BR-10-08-98 (B signifying before amendment) were collected from both ISMs before amendment water withdrawal. After addition of the premeasured allotment of lab grade reagents the bulk solution was mixed and samples AC-10-08-98 and AR-10-08-98 (A signifying after amendment) were collected from the plastic reservoirs. The laboratory analytical results indicated resultant concentrations of NO_3^--N and Br^- were similar to the design concentrations desired for both ISMs.

Sampling Protocol and Analytical Methods

The sampling protocol and field methods used for TT2 were identical to those used in TT1 (see Schlag, 1999 pp. 20-22) except for the three minor changes. The total initial purge volume (500mL) was taken in two installments during TT2. The first 250 mL of purge were discarded; the following 250 mL of purge water were used for pH and DO measurements. This protocol change was adopted in an attempt to stop suspicious DO readings observed in TT1. No significant differences were observed between the TT1 and TT2 DO observations.

Two other sampling protocol changes involved decontamination procedures for the peristaltic pump tubing and ion chromatograph (IC) anion sample volume for the University of North Dakota, Department of Geology and Geological Engineering Water Quality Laboratory (WQL). Pump tubing was still rinsed after sampling; however, new tubing was purchased for TT2 and each ISM had its own sampling tubing. This was done to eliminate the possibility of sample cross contamination. In May 1999 sample volumes for WQL IC anion samples were reduced (from 250 mL) to 60 mL.

Laboratory analytical methods used during TT2 were the same as those used during TT1 (see Schlag, 1999, pp 22-24) except that the mobile phase eluent used in the WQL IC. Starting March 13, 1999, the IC mobile phase anion eluent was switched to a 4.0 mM P-Hydroxybenzoac acid solution adjusted to pH 8.5 with NaOH. The new eluent significantly reduced machine run time while maintaining analytical accuracy. During TT2 cation exchange capacities (CEC) were measured for sediments taken near the ISMs. Laboratories, methodologies and detection limits for all parameters reported in this study are summarized in Table 5 of Appendix B. The use of similar methods during TT1 and TT2 facilitated comparison of the two data sets.

Analytical Results

TT2 lasted 608 days, starting 10-08-98 and ending 06-07-00. During this time the products and reactants presented in Reactions (1-4), as well as the general aqueous chemistry species, were monitored to evaluate denitrification. These denitrification-sensitive reactants and products, and other ions that are considered to be closely associated with denitrification processes, are presented in Tables 1 and 2.

Major Anions

The denitrification reactions presented as (1-4) relate the stoichiometric importance of three major anions NO_3^-, SO_4^{2-} and DIC as potential indicators of denitrification. Equally important to this study is the relative change of the dilution-tracing Br^- compared to these three anions. To show concentration trends and relative changes compared to dilution, these major anions are displayed in Figure 1 and 2 as normalized concentrations of the C and R-ISM, respectively.

Table 1. Important analytes of the Research ISM.

		Important cations, reported by NDDH.									
Sample #		K^+	Na^+	Ca^{2+}	Mg^{2+}	Mn^{2+}*	Fe^{2+}*	NH_3-N	total As	Field	IB
ISM-mm-dd-yy	Time	mmol/L	mmol/L	mmol/L	mmol/L	mmol/L	mmol/L	mmol/L	mmol/L	pH	% Error
BR-10-08-98	0	0.25	0.16	2.06	1.23	0.010	<1.2e-04	<0.0007	1.9E-05	7.6	4.90
AR-10-08-99	0	9.44	0.19	1.99	1.17	0.010	<1.2e-04	0.0037	1.1E-04	7.7	2.37
R-10-27-98	19	8.39	0.29	2.28	1.33	0.011	<1.2e-04	<0.0007	1.7E-04	7.6	-0.53
R-12-01-98	54	7.42	0.39	2.21	1.29	0.011	<1.2e-04	<0.0007	1.5E-04	7.1	-0.16
R-01-16-99	100	9.11	0.37	2.26	1.32	0.011	<1.2e-04	0.004	1.1E-04	7.1	3.28
R-02-15-99	130	7.72	0.39	2.11	1.21	0.010	<1.2e-04	0.002	3.5E-04	7.4	-1.04
R-03-12-99	156	6.75	0.33	2.07	1.19	0.010	<1.2e-04	<0.0007	9.0E-05	7.8	-4.12
R-04-17-99	192	6.85	0.40	2.01	1.16	0.009	<1.2e-04	0.046	1.9E-04	7.5	1.20
R-05-25-99	229	5.91	0.40	1.95	1.11	0.009	<1.2e-04	0.100	4.2E-04	7.7	-1.42
R-06-22-99	257	5.78	0.41	1.95	1.11	0.009	<1.2e-04	0.009	1.8E-04	7.6	1.71
R-07-20-99	285	5.01	0.40	1.68	0.98	0.008	<1.2e-04	<0.0007	2.2E-04	7.7	-2.62
R-08-17-99	314	4.89	0.42	1.63	0.95	0.008	<1.2e-04	0.002	8.7E-04	7.6	0.03
R-10-26-99	383	4.53	0.43	1.43	0.84	0.005	<1.2e-04	<0.0007	2.7E-04	7.6	1.27
R-11-30-99	418	4.55	0.42	1.39	0.81	0.005	<1.2e-04	0.001	5.4E-04	7.4	3.05
R-02-19-00	499	3.94	0.41	1.49	0.86	0.007	<1.2e-04	<0.0007	7.5E-04	7.5	1.79
R-06-07-00	608	3.35	0.35	1.43	0.82	0.007	<1.2e-04	<0.0007	1.8E-04	7.5	-0.86

		Important anions and dissolved carbon, reported by WQL.									
Sample #		NO_3^--N**	Br^-	HCO_3^-***	SO_4^{2-}	CO_3^{2-}***	CO_2***	TDC	DIC	DOC	DO
ISM-mm-dd-yy	Time	mmol/L	mmol/L	mmol/L	mmol/L	mmol/L	mmol/L	mmol/L	mmol/L	mmol/L	mmol/L
BR-10-08-98	0	0.001	nd	5.54	0.26	0.02	0.38	6.95	5.95	1.00	0.25
AR-10-08-99	0	7.52	1.33	nr	0.23	nr	nr	nr	nr	nr	0.28
R-10-27-98	19	7.55	1.38	5.66	0.62	0.03	0.32	6.06	6.01	0.05	0.31
R-12-01-98	54	7.18	1.40	4.74	0.68	0.01	1.06	5.79	5.80	-0.01	0.23
R-01-16-99	100	6.90	1.39	5.43	0.85	0.01	0.72	6.83	6.15	0.68	nr
R-02-15-99	130	6.38	1.41	5.14	0.96	0.01	0.52	6.02	5.68	0.35	nr
R-03-12-99	156	5.59	1.36	5.69	0.92	0.04	0.26	6.50	5.98	0.52	0.24
R-04-17-99	192	5.03	1.22	4.97	0.93	0.01	0.48	6.22	5.46	0.76	0.16
R-05-25-99	229	4.45	1.18	5.12	0.93	0.03	0.28	5.47	5.43	0.05	0.13
R-06-22-99	257	3.57	1.04	4.88	1.12	0.02	0.32	5.38	5.22	0.16	0.11
R-07-20-99	285	2.41	0.92	5.05	1.33	0.03	0.23	5.45	5.30	0.15	0.14
R-08-17-99	314	1.66	0.80	4.97	1.40	0.02	0.33	5.47	5.32	0.15	0.13
R-10-26-99	383	0.55	0.63	4.80	1.52	0.02	0.30	5.71	5.11	0.60	0.11
R-11-30-99	418	0.13	0.60	4.64	1.63	0.01	0.51	5.87	5.16	0.70	0.11
R-02-19-00	499	0.001	0.49	4.74	1.65	0.01	0.40	5.19	5.15	0.04	nr
R-06-07-00	608	0.001	0.41	4.88	1.39	0.02	0.31	5.39	5.21	0.18	0.08

* Dissolved Fe and Mn are assumed to be in more soluble 2+ valence.

** NDDH value for nitrate is reported when concentration was below WQL detection limit of 0.07mmol/L and above NDDH detection limit.

*** Dissolved inorganic carbon species concentrations were calculated by PHREEQC-2 using DIC, pH and water temperature. Aqueous complexes of inorganic carbon species are included in reported value.

DIC = Dissolved inorganic carbon.

DOC = Dissolved organic carbon.

TDC = Total dissolved carbon.

nd = Indicates non-detect.

nr = Not reported.

IB = Ion Balance.

Table 2. Important analytes of the Control ISM.

		Important cations, reported by NDDH.									
Sample #		K^+	Na^+	Ca^{2+}	Mg^{2+}	Mn^{2+}*	Fe^{2+}*	NH_3-N	total As	Field	IB
ISM-mm-dd-yy	Time	mmol/L	mmol/L	mmol/L	mmol/L	mmol/L	mmol/L	mmol/L	mmol/L	pH	% Error
BC-10-08-98	0	0.38	0.20	2.10	1.05	0.011	<1.2e-04	<0.0007	nd	7.7	2.53
AC-10-08-98	0	10.13	0.23	2.20	1.10	0.012	<1.2e-04	<0.0007	2.1E-04	7.6	2.96
C-10-27-98	19	5.17	0.35	3.62	1.78	0.011	<1.2e-04	0.0024	2.9E-04	7.3	3.34
C-12-01-98	54	5.12	0.56	2.99	1.50	0.015	<1.2e-04	0.0034	2.8E-04	7.1	-0.13
C-01-16-99	100	5.40	0.48	3.07	1.51	0.017	<1.2e-04	0.0049	1.9E-04	7.3	0.92
C-02-15-99	130	4.73	0.47	3.09	1.52	0.017	0.001	0.0027	8.0E-04	7.5	1.85
C-03-12-99	156	4.09	0.39	3.07	1.49	0.017	<1.2e-04	0.0028	1.1E-04	7.6	-0.97
C-04-17-99	192	4.60	0.46	3.29	1.63	0.019	<1.2e-04	0.0033	1.9E-04	7.6	-0.32
C-05-25-99	229	3.89	0.47	3.37	1.64	0.020	<1.2e-04	<0.0007	6.0E-04	7.4	-2.23
C-06-22-99	257	4.45	0.47	3.17	1.66	0.021	<1.2e-04	0.0095	3.1E-04	7.3	0.09
C-07-20-99	285	3.84	0.48	3.59	1.80	0.021	<1.2e-04	<0.0007	3.2E-04	7.5	3.09
C-08-17-99	314	3.79	0.48	3.39	1.70	0.022	<1.2e-04	0.0015	2.9E-03	7.4	1.87
C-10-26-99	383	3.53	0.47	3.14	1.57	0.021	<1.2e-04	<0.0007	1.6E-03	7.4	0.27
C-11-30-99	418	4.02	0.57	3.62	1.80	0.022	<1.2e-04	0.0047	3.7E-03	7.3	1.15
C-02-19-00	499	3.32	0.47	3.24	1.60	0.024	0.001	<0.0007	2.4E-03	7.7	0.46
C-06-07-00	608	2.97	0.43	3.04	1.53	0.024	<1.2e-04	0.0016	8.7E-04	7.7	-0.41

		Important anions and dissolved carbon, reported by WQL.									
Sample #		NO_3^--N**	Br^-	HCO_3^-***	SO_4^{2-}	CO_3^{2-}***	CO_2***	TDC	DIC	DOC	DO
ISM-mm-dd-yy	Time	mmol/L	mmol/L	mmol/L	mmol/L	mmol/L	mmol/L	mmol/L	mmol/L	mmol/L	mmol/L
BC-10-08-98	0	0.001	nd	5.01	0.67	0.02	0.37	5.80	5.40	0.39	0.23
AC-10-08-98	0	0.001	9.31	nr	0.67	nr	nr	nr	nr	nr	0.28
C-10-27-98	19	0.003	9.35	4.50	0.62	0.02	0.48	5.22	5.00	0.22	0.39
C-12-01-98	54	0.002	9.11	4.12	0.65	0.01	0.85	7.01	4.98	2.04	0.37
C-01-16-99	100	<0.001	8.56	4.79	0.62	0.01	0.63	5.89	5.43	0.47	nr
C-02-15-99	130	<0.001	8.16	4.52	0.53	0.02	0.42	5.77	4.96	0.82	nr
C-03-12-99	156	<0.001	8.70	5.00	0.57	0.02	0.33	6.12	5.34	0.78	0.24
C-04-17-99	192	0.001	9.07	4.66	0.53	0.02	0.31	5.57	4.99	0.58	0.23
C-05-25-99	229	0.003	9.17	4.45	0.60	0.02	0.42	5.29	4.88	0.40	0.13
C-06-22-99	257	0.001	8.82	4.51	0.53	0.02	0.49	5.25	5.01	0.24	0.23
C-07-20-99	285	0.001	8.23	4.70	0.55	0.03	0.36	5.21	5.08	0.13	0.18
C-08-17-99	314	0.001	8.13	4.63	0.49	0.02	0.44	5.22	5.09	0.13	0.15
C-10-26-99	383	<0.001	7.53	4.53	0.56	0.02	0.50	5.60	5.04	0.56	0.15
C-11-30-99	418	<0.001	7.35	4.52	0.56	0.01	0.63	5.64	5.17	0.48	0.15
C-02-19-00	499	<0.001	7.13	4.88	0.56	0.03	0.29	5.86	5.21	0.66	nr
C-06-07-00	608	0.001	6.71	4.59	0.57	0.01	0.56	5.40	5.16	0.24	0.09

* Dissolved Fe and Mn are assumed to be in more soluble 2+ valence.

** NDDH value for nitrate is reported when concentration was below WQL detection limit of 0.07mmol/L and above NDDH detection limit.

*** Dissolved inorganic carbon species concentrations were calculated with PHREEQC-2 using DIC, pH and water temperature. Aqueous complexes of inorganic carbon species are included in reported value.

DIC = Dissolved inorganic carbon.

DOC = Dissolved organic carbon.

TDC = Total dissolved carbon.

nr = Not reported.

IB = Ion Balance.

The NO_3^--N concentration in the R-ISM (Figure 1) began at 7.52 mmol · L^{-1} and established a downward trend until falling below detection (0.02 mg · L^{-1}) at 418 days. The NO_3^--N concentration for the C-ISM is not displayed on the normalized graph due to

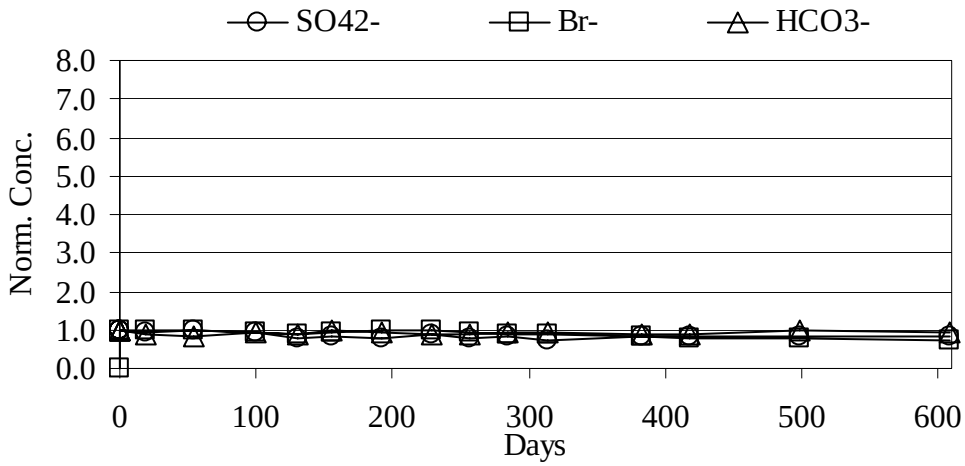

Figure 1. Control ISM major anions normalized to AC-10-08-98.

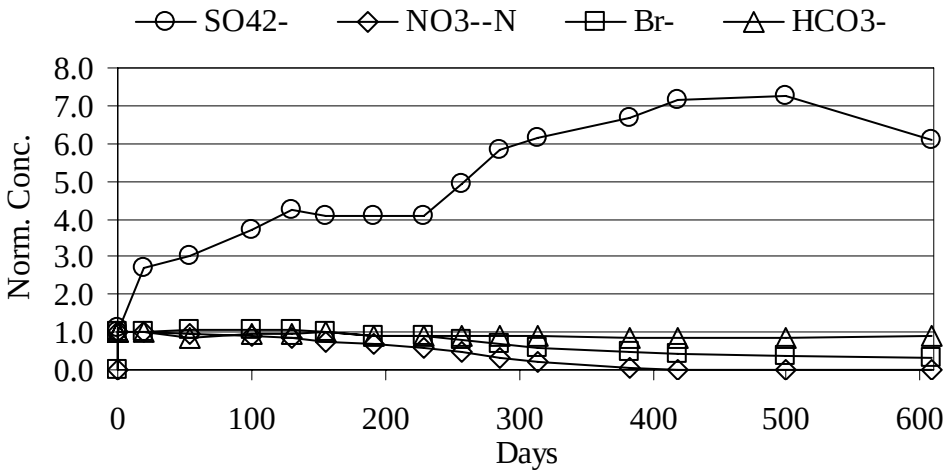

Figure 2. Research ISM major anions normalized to AR-10-08-98.

its lack of detection or low concentration throughout the tracer test.

The Br^- concentration in the R-ISM (Figure 1) started at 1.33 mmol $\cdot L^{-1}$ and remained within a few percent of the desired amendment concentration (1.38 mmol $\cdot L^{-1}$) for 156 days. Then, the concentration profile establishing a downward trend due to dilution to a final concentration of 0.60 mmol $\cdot L^{-1}$ (45 % of initial concentration) to 418 days, at which time, the NO_3^- concentration had been effectively zeroed. After that time the Br^- concentration continued in a downward trend ending the tracer test at 31 % (0.41 mmol $\cdot L^{-1}$) of its initial concentration. Br^- concentrations in the C-ISM (Figure 2) began at 9.31 mmol $\cdot L^{-1}$, decreased to 88 % (8.16 mmol $\cdot L^{-1}$) at 130 days and returned to 98 % its initial concentration at 229 days. After this point it established a downward trend ending at 6.71 mmol $\cdot L^{-1}$, 72 % its initial concentration, at 608 days.

The SO_4^{2-} concentration in the R-ISM (Figure 1) began the tracer test at 0.23 mmol $\cdot L^{-1}$ and immediately established an upward trend. Its concentration rose to 1.62 mmol $\cdot L^{-1}$ (714% its initial concentration) when NO_3^- was effectively zeroed after 418 days and continued to rise to its maximum value of 1.65 mmol $\cdot L^{-1}$ at 499 days. After 499 days its concentration decreased to a concentration of 1.39 mmol $\cdot L^{-1}$ by the end of the study. Sulfate concentration in the C-ISM (Figure 2) started the tracer test at its maximum value of 0.67 mmol $\cdot L^{-1}$ and fluctuated throughout the rest of the experiment from 0.65 to 0.53 mmol $\cdot L^{-1}$, failing to establish a discernable trend.

The DIC concentrations are represented by HCO_3^-, the dominant species at the observed pH and temperature. DIC analysis was not included for the AR/AC-10-08-98 sample. It was expected that little change would occur to the DIC concentration during water amendment. In retrospect, the potential for CO_2 degassing during atmospheric exposure while the amendment took place, decreasing DIC, should have been considered.

Regardless, HCO_3^- values are normalized to the AC and AR values, which are assumed to have equal DIC as the BC and BR samples; however, HCO_3^- concentration values are reported as speciated according to temperature and pH measurements taken after the amendment directly prior to injection.

The HCO_3^- concentration in the R-ISM (Figure 1) began the study at 5.54 mmol $\cdot$ L^{-1} and fluctuated between 4.64 mmol $\cdot$ L^{-1} and its maximum 5.69 mmol $\cdot$ L^{-1} the entire study. The R-ISM HCO_3^- failed to establish a discernable trend, having a concentration of 4.88 mmol $\cdot$ L^{-1} upon termination of the tracer test. HCO_3^- concentration in the C-ISM (Figure 2) also failed to establish a discernable trend. It began the tracer test at its maximum value of 5.01 mmol $\cdot$ L^{-1}. After 54 days it reached its minimum value of 4.12 mmol $\cdot$ L^{-1}, 82 % of its initial value. After 54 days the C-ISM HCO_3^- concentration continued to fluctuate ranging from 5.00 to 4.45 mmol $\cdot$ L^{-1} ultimately ending at 91 % (4.59 mmol $\cdot$ L^{-1}) its initial concentration.

Major Cations

The cations contributing the majority of positive charge to ion balances include Na^+, Ca^{2+}, Mg^{2+} and K^+. Ca^{2+} and Mg^{2+} concentrations have a significant importance in the carbonate system equilibrium, which ultimately can control pH and other parameters. K^+ is the cation of the Br^- and NO_3^- amendments, and Na^+ can be an important indicator of cation exchange. Therefore, monitoring of cation trends is important to the overall understanding of the geochemical system. Comparison of the R-ISM data to C-ISM data is fundamental to discerning methodology versus redox-induced reactions. Methodology reactions are not believed to be directly or secondarily associated with the redox processes and are referred to as amendment-induced reactions or amendment-

methodology-induced reactions. Concentrations of these major cations are presented in Figures 3 and 4, normalized to AR and AC-10-08-98, respectively.

The K^+ concentration in the R-ISM (Figure 3) started the tracer test by making an abrupt jump upward on day zero due to the amendment. After the amendment the K^+ concentration was 9.44 mmol $\cdot L^{-1}$. It made another abrupt jump to 79 % the amended concentration (7.42 mmol $\cdot L^{-1}$) after only 54 days during a period when Br^- concentrations remained constant. The concentration then rebounded to 9.11 mmol $\cdot L^{-1}$ (96.5 % its amended concentration) at 100 days, finally establishing a downward trend ending with a post amendment minimum of 0.36 mmol $\cdot L^{-1}$ (3.8 % of amended

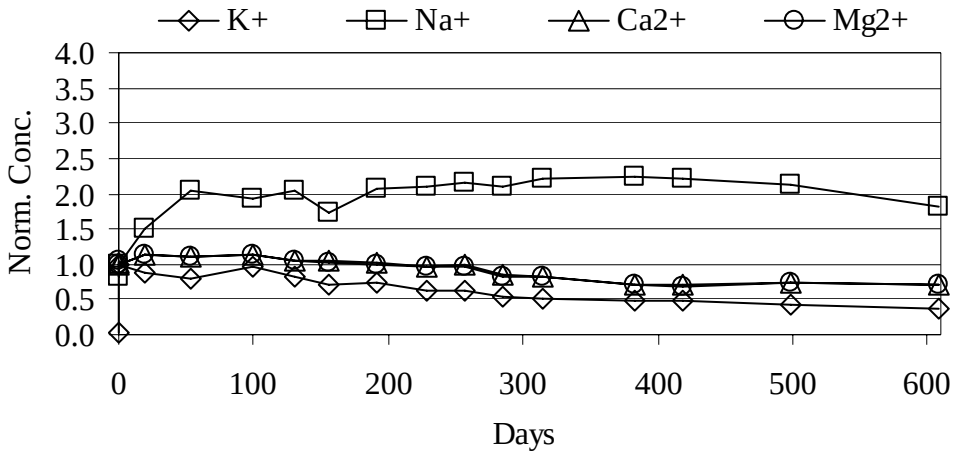

Figure 3. Research ISM major cations normalized to AR-10-08-98.

concentration) at 608 days. The K^+ concentration in the C-ISM (Figure 4) also made a positive day-zero jump from 0.38 mmol $\cdot L^{-1}$ to a post amendment concentration of 10.13 mmol $\cdot L^{-1}$. Within 19 days its concentration had decreased to 51 % (5.17 mmol $\cdot L^{-1}$) the AC-10-08-98 concentration. After the initial drastic drop the K^+ concentration

established a much more gradual downward trend throughout the rest of the tracer test. At 608 days a concentration of 2.97 mmol $\cdot L^{-1}$ was observed, being 29 % of the post amendment concentration.

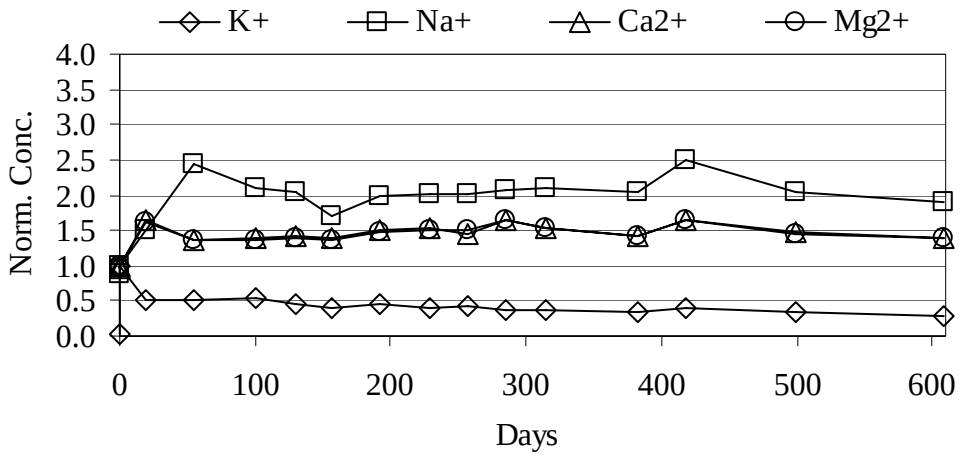

Figure 4. Control ISM major cations normalized to AC-10-08-98.

The other major monovalent cation is Na^+. In the R-ISM (Figure 3) Na^+ started the tracer test at a concentration of 0.16 mmol $\cdot L^{-1}$ and increased sharply to 205 % (0.39 mmol $\cdot L^{-1}$) in 54 days. After this time Na^+ failed to establish a clear trend varying from a minimum of 0.33 mmol $\cdot L^{-1}$ (173 % the post amendment concentration) at 156 days, to the maximum of 0.43 mmol $\cdot L^{-1}$ (225 % post amendment concentration) at 383 days. Na^+ ended the tracer test at 182 % the initial post-amendment concentration with a value of 0.35 mmol $\cdot L^{-1}$ at 608 days. In the C-ISM (Figure 4) the Na^+ concentration profile was similar to that observed in the R-ISM. Na^+ increased rapidly for 54 days from its post amendment concentration of 0.20 mmol $\cdot L^{-1}$ to 243 % (0.56 mmol $\cdot L^{-1}$) that value. After the first 54 days the Na^+ concentration in the C-ISM failed to establish a clear trend

having a minimum concentration of 0.39 mmol $\cdot L^{-1}$ at 156 days and a maximum concentration of 0.57 mmol $\cdot L^{-1}$ at 418 days, both coincident with the time of the R-ISM minimum and maximum. Na^{+} ended the tracer test with a concentration 189 % of the post amendment concentration with a value of 0.43 mmol $\cdot L^{-1}$ at 608 days.

The major divalent cations were Ca^{2+} and Mg^{2+}. The percent concentration changes of Ca^{2+} and Mg^{2+} in both ISMs during TT2 match each other closely. In the R-ISM Ca^{2+} and Mg^{2+} (Figure 3) started the tracer test with concentrations of 2.06 mmol $\cdot L^{-1}$ and 1.23 mmol $\cdot L^{-1}$, respectively. Both cation concentrations immediately increased to the TT2 maximums of 2.28 mmol $Ca^{2+} \cdot L^{-1}$ and 1.33 mmol $Mg^{2+} \cdot L^{-1}$ (both 114 % of the initial concentrations) at 19 days and remained near these concentrations through 100 days. After day 100 both Ca^{2+} and Mg^{2+} established a downward trend that reached a minimum of 70 % and 69 %, respectively, at 418 days. Day 418 is considered to be when NO_3^{-} concentrations were, effectively, zeroed. Neither cation concentration varied more than a normalized 5 % for the next 190 days, ending TT2 at 72 % and 70 % of the initial concentrations.

Percent changes of Ca^{2+} and Mg^{2+} in the C-ISM (Figure 4) also matched each other very closely. Concentrations of these cations started TT2 at minimum values of 2.10 mmol $Ca^{2+} \cdot L^{-1}$ and 1.05 mmol $Mg^{2+} \cdot L^{-1}$ increasing to a maximum of 3.62 mmol $Ca^{2+} \cdot L^{-1}$ and 1.78 mmol $Mg^{2+} \cdot L^{-1}$ (164 % and 162 % of the initial concentrations) after 19 days. By day 54 both Ca^{2+} and Mg^{2+} concentrations had dropped to 136 % (2.99 mmol $\cdot L^{-1}$ and 1.50 mmol $\cdot L^{-1}$, respectively) of the initial concentrations. After 54 days neither Ca^{2+}or Mg^{2+} established an obvious trend, finishing TT2 at 608 days with

concentrations of 3.04 mmol · L^{-1} and 1.53 mmol · L^{-1}. The relative changes for both Ca^{2+} and Mg^{2+} in each ISM are remarkably similar

Isotope Data

Four nitrogen isotope analyses were performed on samples of the nitrate remaining within the R-ISM during TT2. These analyses were acquired for samples R-10-27-98 (19 days), R-02-15-99 (130 days), R-04-17-99 (191 days) and R-06-22-99 (237 days). Results of the N-isotope analyses indicate an enrichment of $\delta^{15}N$ throughout TT2 (Figure 6); values reported for the four samples were 4.5 ‰ at 19 days, 14.9 ‰ at 130 days, 20.25 ‰ at 192 days and 26.95 ‰ at 257 days.

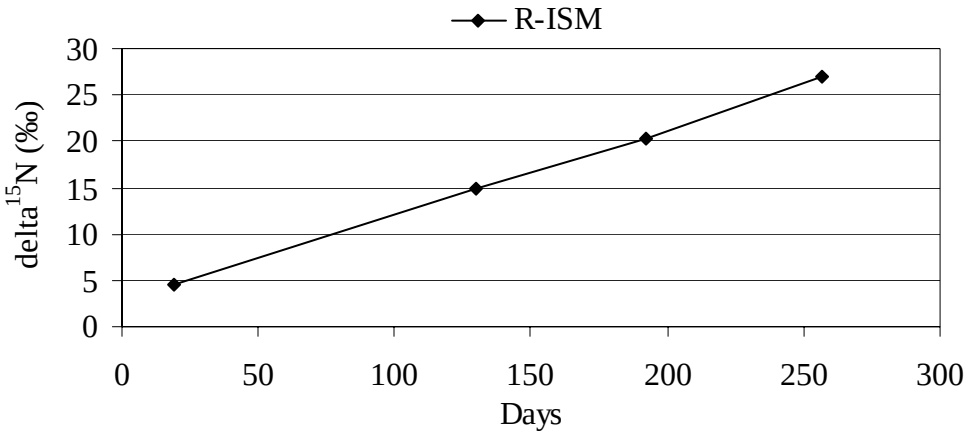

Figure 5. Increase in $\delta^{15}N$ in the R-ISM during TT2 vs. time.

Geochron Laboratories of Cambridge, MA, was contracted to perform two sulfur isotope analyses during TT2. Analyses were performed on samples taken from both ISMs after 19 and 155 days. Within the C-ISM $\delta^{34}S$ values were nearly equal for these first two analyses, values of –18.1 and –18.5 ‰ were reported. The $\delta^{34}S$ of SO_4^{2-} in the

R-ISM was also consistent for the first two isotope samples, –15.9 and -15.5 ‰. Due to the lack of enrichment or depletion of $\delta^{34}S$ within either ISM during TT1 and the first two data points of TT2, sulfur isotope analysis was discontinued.

See Appendix C for a discussion on minor analyte data and trends.

CHAPTER IV

DISCUSSION OF FIELD AND LABORATORY RESULTS

Comparing the evolution of dissolved species and parameters within the C-ISM and R-ISM leads to three lines of evidence supporting the occurrence of denitrification in the R-ISM during TT2. These three lines of evidence, listed in order of discussion, are: (1) NO_3^- attenuation exceeding Br^- attenuation, (2) observed isotopic enrichment of ^{15}N in the NO_3^- remaining in the R-ISM, and (3) production of SO_4^{2-} within the R-ISM corresponding to NO_3^- attenuation.

NO_3^- Attenuation Exceeding Br^- Dilution

Br^- was used in this study to quantify dilution in the ISMs. Tracking dilution via Br^- in the R-ISM results in a direct comparison for NO_3^- attenuation via dilution and NO_3^- attenuation via some other sink. Although TT2 lasted for 608 days, NO_3^- concentrations effectively disappeared after 418 days (Figure 1.). At 418 days Br^- concentrations in the R-ISM were 0.60 mmol $\cdot$ L^{-1} having 42.5 % its total amended concentration remaining. This suggests that 42.5 % or approximately 3.19 mmol $\cdot$ L^{-1} of the missing nitrate was attenuated due to some process other than dilution. This observation forms the first line of evidence for denitrification. Based on this calculation, the average denitrification rate was 7.6 μmol $\cdot L^{-1} \cdot day^{-1}$ (0.11 mg $\cdot$ L^{-1} $\cdot$ day^{-1}) for TT2, which was half the reported 15 μmol $\cdot L^{-1} \cdot day^{-1}$ (0.21 mg $\cdot$ L^{-1} $\cdot$ day^{-1}) reported by Schlag (1999) for TT1.

Observed Isotopic Enrichment of ^{15}N

The isotopic composition of NO_3^- remaining within the R-ISM during TT2 is an important parameter to consider; it may be used as an established indicator of biologically-mediated denitrification (Aravena and Robertson, 1998; Böttcher et al., 1990; Mariotti et al., 1988). As time progressed significant increases the $\delta^{15}N$, from 4.5 ‰ to 26.95 ‰, were observed in the NO_3^- remaining in solution within the R-ISM (Figure 5). The observed enrichment of ^{15}N appears to be nearly linear with respect to time.

Nitrogen isotope data are commonly presented as a graphical representation of the Rayleigh Equation (6), which is used as a tool for describing the environment of the microbial mediated denitrification (Mariotti et al., 1981; Mariotti et al., 1982; Mariotti et al., 1988). This graphical method consists of plotting the numerator of Equation (6) vs.

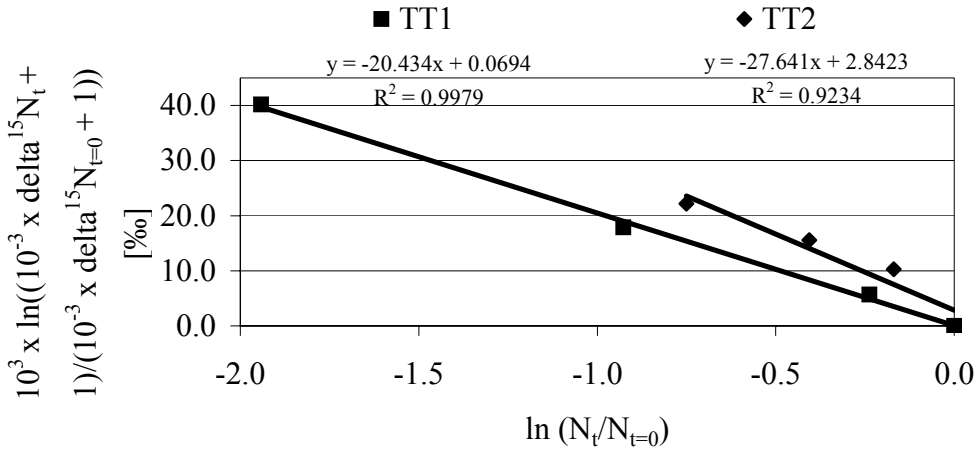

Figure 6. Graphical comparison of $\delta^{15}N$ enrichment in Rayleigh equation format. (Data set for TT1 from Schlag, 1999.) Enrichment, ε, is the slope of the best-fit line.

the denominator and fitting a linear trend line to the data (Figure 6). A strong linear correlation of the data indicates the occurrence of biologically mediated denitrification (Mariotti et al., 1981; Mariotti et al., 1982; Mariotti et al., 1988). As indicated by Figure 6, a strong linear relation exists within the isotope data, as the R^2 value of the linear regression calculation for the best-fit line is 0.92. This forms a second line of evidence that bacterially mediated denitrification did occur during TT2.

As indicated by Figure 6, the enrichment, ε, for TT2 was –27.6 ‰; for TT1 ε was –20.4 ‰. Both values are consistent of a denitrification environment limited by the availability of electron donors, as discussed in a previous chapter of this thesis (REVIEW OF PREVIOUS WORK).

Production of SO_4^{2-} in R-ISM

According to Reaction (4), sulfate production can be an indicator of autotrophic denitrification. The R-ISM sustained a 1.01 mmol · L^{-1} SO_4^{2-} increase, whereas the C-ISM exhibited a slight decreasing trend in SO_4^{2-}. The only significant sulfur-bearing mineral identified by XRD of EVA sediments at the LFS is pyrite (Kammer, 2001), which is known to participate as an electron donor to denitrification. These observations are another line of evidence supporting the occurrence of denitrification and indicate that a portion of the observed denitrification is autotrophic in nature.

Using the method in Schlag (1999), the increase in SO_4^{2-} observed in the R-ISM explains 49 % to 61 % of the attenuated NO_3^- beyond that explained by dilution of the Br^- tracer at 418 days, depending on which data point is used to initialize the mathematical computations (see Appendix D). For TT1, the increase in SO_4^{2-} explained 61 % of the observed denitrification (Schlag 1999).

Based on the observation made during TT1, Schlag's hypothesis (1999), and the hypothesis of this thesis, was that denitrification by organic carbon accounted for the nitrate attenuation not accounted for by dilution or SO_4^{2-} evolution. Assessment of this hypothesis becomes computationally intensive when numerous water quality parameters and potential secondary geochemical reactions are considered. Therefore, to test the hypothesis that geochemical conditions in the EVA at the LFS are proper for organic carbon to act as the second primary electron donor to denitrification, the data from TT2 were analyzed using the modeling code PHREEQC-2 (Parkhurst and Appelo, 1999).

CHAPTER V

MODEL DESCRIPTION

The geochemical modeling software PHREEQC-2 (Parkhurst and Appelo, 1999) was used for this research. The following statement is taken from the PHREEQC-2 Users Guide and serves as a summary description of the code and its capabilities.

> PHREEQC version 2 is a computer program written in the C programming language that is designed to perform a wide variety of low-temperature aqueous geochemical calculations. PHREEQC is based on an ion-association aqueous model and has capabilities for (1) speciation and saturation-index calculations; (2) batch-reaction and one-dimensional (1D) transport calculations involving reversible reactions, which include aqueous, mineral, gas, solid-solution, surface-complexation, and ion-exchange equilibria, and irreversible reactions, which include specified mole transfers of reactants, kinetically controlled reactions, mixing of solutions, and temperature changes; and (3) inverse modeling, which finds sets of mineral and gas mole transfers that account for differences in composition between waters, within specified compositional uncertainty limits.
>
> (Parkhurst and Appelo, 1999, p. 1)

For a more complete description of PHREEQC and the added capabilities of version 2 see Parkhurst and Appelo (1999).

Input files for PHREEQC-2 are built via a window type interface, in which the specific calculations to be executed by the model and the boundary conditions for those calculations are delineated by invoking "keywords." The model acknowledges and performs calculations and gives specific output and output formats as it reads and recognizes these keywords. In the input file the keywords are most often followed by boundary conditions and numeric parameters that help describe and guide the model through a series of complex geochemical calculations. The type of model built, the

modeling methodology applied, the keywords invoked and values for boundary condition parameters designated in the input file are ultimately determined by the goals and objectives of the modeling efforts, and the conceptual model and assumptions for the geochemical system being studied.

Modeling Objectives

There were two major objectives and one minor objective for the modeling portion of this thesis. The first objective was to simulate the observed state of geochemical thermodynamic disequilibrium within the ISM during the tracer test. The second major objective was to gain evidence to substantiate the hypothesis that OC is a primary electron donor to the denitrification observed at the EVA LFS. The third objective was to gain insights and propose a possible scenario of geochemical reactions occurring within the mesocosms that are associated with the study methodology and redox reactions. In addition to denitrification, the amendment of groundwater with a strongly concentrated solution of K^+ is expected to influence the geochemistry of the aquifer. These reactions are not believed to be directly associated with the redox processes and are referred to as amendment-induced reactions or amendment-methodology-induced reactions.

Modeling Conceptual Method, Construction and Assumptions

The overall methodology used to achieve these objectives is best described as a "circular" (Figure 7) approach involving two separate input simulations for each ISM. The conceptual method used to achieve the first objective accounts for the first half of the circular methodology. It consists of inputing the total concentrations for all major and

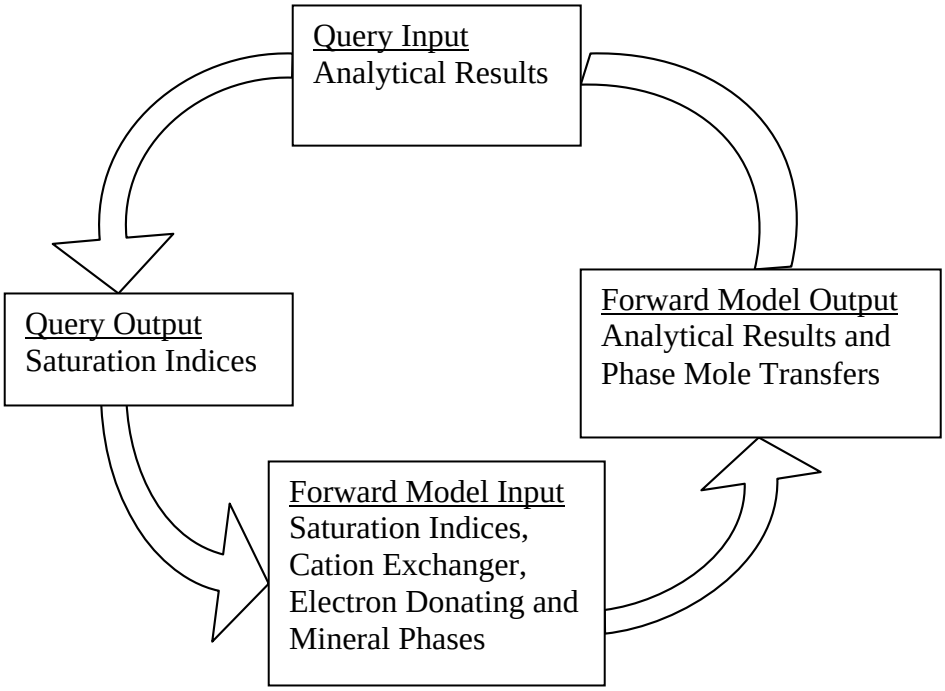

Figure 7. Conceptual representation of modeling methodology.

many minor ions, as well as, the other chemical parameters observed in the water chemistry analytical results for each sampling date (see Appendix E, Tables 6 and 7). The model speciates the dissolved parameters, computes/confirms the charge balance (ion balance) of the water, as well as, calculates the state of redox sensitive analytes based on the groundwater temperature and pH observed in the field. The model also calculates the saturation state of the water with respect to solid/mineral and gaseous phases. The state of saturation is reported in the form of a saturation index (SI).

$$SI = \log[IAP/K] \quad (7)$$

Equation (7) is derived from the second law of thermodynamics and defines the SI as the log of the ion activity product (IAP) divided by the solubility constant (K) of a particular phase and its ions. Hence, the SI is calculated based on the pH, temperature, and the total and/or speciated concentration values input into and/or calculated by the model. As indicated by the second law of thermodynamics, an SI equal to 0 means the water is in equilibrium, or saturated, with respect to the phase in question.

Next, the XRD data presented by Kammer (2001) were inspected to determine which solid and mineral phases are known to exist in the EVA at the LFS in the range of depths spanned by the ISMs (see Kammer, 2001, for summary of mineralogy). In particular the carbonate system was focused on because of the potential effects of denitrification by OC on the carbonate system equilibrium, as indicated by the products of Reaction (1). The model was queried regarding the state of saturation for these phases and the SIs were recorded for all 17 sets of water analyses. In addition to the mineral phases, the model was also queried for the SI of dissolved $CO_{2(g)}$. The state of saturation for dissolved $CO_{2(g)}$ is reported as a SI; however, for this phase, and all gaseous phases, the SI reported by the model is truly the log of the partial pressure of that gas dissolved in solution.

The saturation states of the ISM waters with respect to alumino-silicate minerals were considered initially; however, these phases should not be directly related to denitrification as presented by Reactions (1-4) and were omitted from interaction within the model for simplicity.

Iron was also a target analyte during TT2 due to the implications of Reactions (2-4); however, concentrations were below detection within all data sets except two

recorded for the C-ISM during the study. Therefore an assumption with regard to iron concentrations was made. It is assumed the initial amendment water and the dilution water contained iron just below the detection limit of 0.125 μmol · L^{-1}. The model was queried for the state of saturation with respect to goethite in the R-ISM based on the products of Reaction (4).

At this juncture, the information to build a forward model has been realized and half of the circle represented by Figure 7 is complete. Appendix F, Tables 12 and 13, list the state of saturation for the mineral phases as discussed in the previous paragraph.

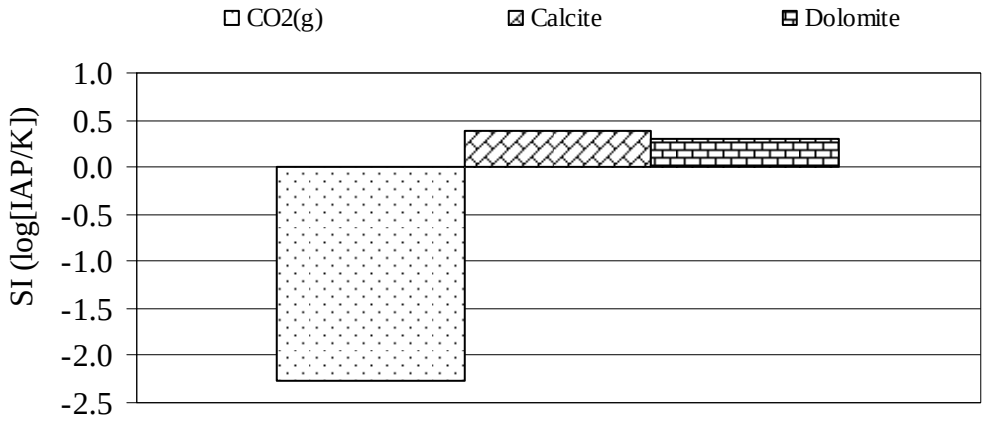

Figure 8. Carbonate system SIs for C-3-12-99.

Figures 8 and 9 present the state of saturation for data points C- and R-3-12-99, which are presented as being representative examples of the state of thermodynamic equilibrium throughout the study for goethite and for the carbonate phases known to exist in the aquifer.

Next, a new input data set was constructed for the forward model, using the information gained from the first half of the circle as the boundary conditions. The forward model simulates each data point as a batch reaction occurring from day zero to the date of the sample (see Table 8 and 9 of Appendix E for input files used for forward models). The two initial solutions, which include the pre-amendment sample BC & BR-10-08-98 (Solution 0) as the dilution water and AC- and AR-10-08-98 (Solution 1) as

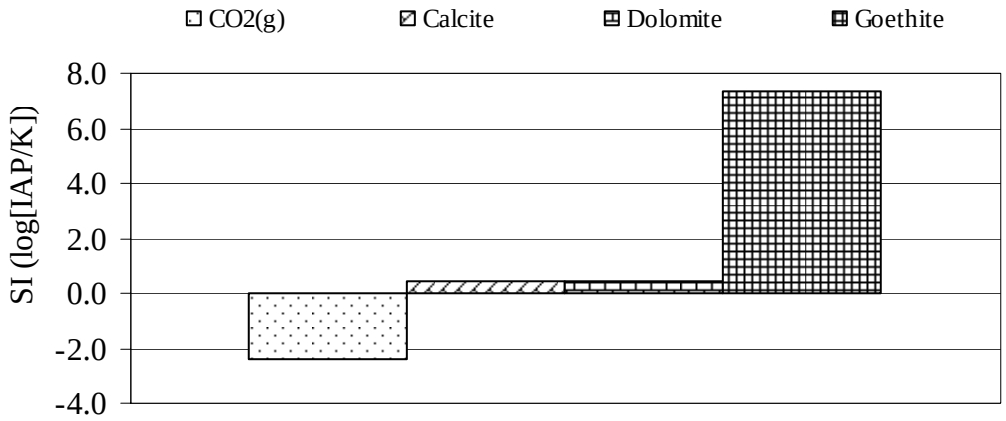

Figure 9. Carbonate system SIs for R-3-12-99.

the amendment water, have been defined in the model. However, some assumptions with regard to the initial concentrations of Br-, NO_3^--N and SO_4^{2-} within these initial chemically amended solutions were made for modeling purposes.

It was assumed that the maximum value reported for Br^- concentration during TT2 was the Br^- concentration of the original amendment water and that initial values of Br^-, which were less than maximum concentrations reported later, are a result of minor analytical and field errors. NO_3^--N concentrations within the R-ISM are dealt with in same manner.

Assumptions regarding SO_4^{2-} of the dilution water (Solution 0) and the amendment water (Solution 1) are also made. The SO_4^{2-} increase observed during the first 19 days in the R-ISM can not be accounted for by reduction of NO_3^--N according to Reaction (4) or DO. Therefore, it is assumed that the concentration of 0.62 mmol $\cdot L^{-1}$ (day 19 concentration) was the initial concentration in the R-ISM for modeling purposes. Solutions 1 and 0 (amendment and dilution, respectively) are defined as having a SO_4^{2-} concentration of 0.62 mmol $\cdot L^{-1}$. Ultimately, this assumption results in a conservative estimate of denitrification accounted for by SO_4^{2-} evolution. The actual SO_4^{2-} concentrations reported at the beginning of TT2 for the BC and AC-10-08-98 analyses are used for initialization of Solutions 0 and 1 during simulation of the C-ISM.

Within the model, dilution is simulated using the MIX keyword. The "mixing fraction" or, dilution factor, of Solutions 0 and 1 are input as a decimal fraction determined from the Br^- concentration with respect to the maximum Br^- concentration observed in that ISM.

Next, the solution resulting from the mixture reacts to a new equilibrium with an exchanger (via the "Use Exchanger 1" command) that has been initialized earlier in the input to be in equilibrium with the native/dilution water (BC and BR samples). Some assumptions have also been made in regard to initializing the exchanger.

The cation exchange capacity (CEC) of aquifer is defined using the EXCHANGE keyword. In this case the composition of the exchanger is initialized to be in equilibrium with the BR- and BC-10-08-98 samples with the "equilibrate 0" command. Purging of the ISMs was completed as of 9-18-98. The water drawn out of the ISMs for amendment on 10-8-98 had resided within the ISMs for 19 days. Due to the nature of cation

exchange reactions, exchanger equilibrium is achieved quickly (Appelo and Postma, 1996); therefore, the exchangers within the ISMs were assumed to be in equilibrium with the amendment water prior to the amendment as recorded by the BR- and BC-10-08-98 analytical results.

The moles of exchange sites available per liter of water are defined within the EXCHANGER keyword input data block. The exchanger is defined as "X" followed by a numerical value for the number of moles of exchange sites. The number input as available exchange sites was fitted according to the analytical results.

A CEC test was performed on EVA sediments from LFS across the depth of the ISMs. The results of the CEC test indicated an average value of 9.9 meq $\cdot$ 100 g^{-1} of sediment. Assuming a porosity of 35 % and a bulk density of 1.63 g $\cdot$ cm^{-3} (Das, 1994) the calculated number of exchange sites is 0.46 eq $\cdot$ L^{-1} of ISM water using the method described by Appelo and Postma (1996, pg 149). When this value is used in the input of the forward model as the number of exchange sites per liter of water the cation concentrations calculated by the model are grossly in error of the observed analytical results.

Personal observation of the EVA sediments from ISM depth at the LFS reveals fine sand size shale aggregates abundant enough that they are readily identifiable with the naked eye. The methodology used for analytical determination of the total CEC involved grinding the samples. Therefore, it is argued that these small shale conglomerates were broken apart. Thus, it is believed that this analytical methodology caused the laboratory results of the CEC test to be a gross over-estimation of the number of sites immediately available for exchange.

These difficulties were overcome by fitting a value by trial and error according to the analytical results from ISM water cation analyses for R- and C-10-27-98. Under the assumption that cation exchange is much more rapid than mineral dissolution or precipitation it was assumed that the only major reaction affecting cation concentrations in the first 19 days of the study would be cation exchange. Cation exchanger equilibrium distribution is determined by relative concentrations of any cation on the exchanger and in solution (Appelo and Postma, 1996). The model, inherently deals with this exchanger equilibrium phenomenon.

To determine a fitted value for the number of moles of exchange sites to be input into the model, the analytical results for cations from R- and C-10-27-98 were directly compared to the model output concentrations. Model simulations where conducted such that the initial solutions were defined, mixed according to dilution, and allowed to react to equilibrium with the exchanger. When too many exchange sites were input into the model, concentrations output by the model for K^+ were lower and concentrations for Ca^{2+}, Mg^{2+}, and Mn^{2+} were higher than the water quality analytical results. Conversely, when too few exchange sites were input into the model, the K^+ concentrations output by the model for R- and C-10-27-98 were too high and the other major cations were too low. Ultimately, the number of exchange sites input into the model were fitted values of 0.0395 eq $\cdot$ L^{-1} and 0.00365 eq $\cdot$ L^{-1} for the C and R-ISM, respectively.

Next the exchanger-equilibrated water was allowed to react with a set of EQUILIBRIUM_PHASES, all of which were positively identified by Kammer (2001) in XRD of the EVA sediments. The first number after the phase name, reading left to right in Tables 8 and 9, is the SI (see Tables 10 and 11 in Appendix F for list of SIs). The SI is

input exactly as recorded in the first half of the circle (Figure 7), when the raw data were input and the model was queried about each phase. The SI tells the model to allow that phase to react until it reaches that particular state of thermodynamic disequilibrium or state of saturation. The second number is the amount in moles of that phase available to react per liter of water. When this number is 0 no moles of that phase were available to react, thus it is allowed to precipitate or exit solution only. The default value of 10 is used for most phases, signifying that the quantity or availability of the phase does not limit its reactive capability.

The phases allowed to react with the ISM waters were calcite ($CaCO_3$), dolomite [$CaMgCO_3)_2$], carbon dioxide gas ($CO_{2(g)}$), pyrite (FeS_2), goethite (FeOOH),and OC (CH_2O). The SI index (Tables 10 and 11) for each of these phases, except FeS_2 and OC was set according to the results of the first half of the model conceptual circle (Figure 7).

The use of dolomite, when it is observed precipitating from solution in the model, is strictly for stoichiometric purposes. Although the phase exists at the LFS, it is not accepted that dolomite could form from solution at the site. The "dolomite problem," as referred to by Boggs (1995, pg 221) has been a topic of extensive study in sedimentology. There are numerous theories and models describing the formational processes of penecontemporaneous dolomites vs. ancient diagenetic dolomites (Boggs, 1995). Penecontemporaneous dolomites are "early-formed" dolomites that form from solution in shallow unconsolidated geochemical environments as opposed to the classic diagenetic dolomitization, which involves replacement processes within consolidated limestones (Boggs, 1995). Ultimately, dolomite synthesis has not been successfully achieved in laboratory experiments at temperatures less than 100 °C (Boggs, 1995). For

this thesis, attempts to solve the “dolomite problem” are not presented, rather the combination of dolomite and calcite precipitating in concert is allowed in the model in an attempt to simulate precipitation of a Ca-Mg carbonate solid solution series member, such as the sample bottle precipitate observed in TT1 (Schlag, 1999).

The electron-donating phases and the quantity of moles of these phases allowed to react were determined and input according to concentrations of indicator parameters in the output, as compared to the actual data.

During simulation of the R-ISM pyrite was used as a primary electron donor. The moles of pyrite allowed to react, for any given time period, were based on the analytical data for sulfate recorded for that particular sampling date. Again, the model was initialized and the dilutive mixing was simulated in the presence of the fitted number of exchange sites. The appropriate amount of pyrite was allowed to react to generate the amount of sulfate observed in the analytical data based on Reaction (4).

Goethite was also allowed to react in the simulations of the R-ISM as an iron-oxide sink. Denitrification by pyrite was expected to yield precipitation of an iron oxy-hydroxide according to Reaction (4). Goethite was allowed to react to its recorded SI. This resulted in dissolved iron concentrations in the model output below the analytical detection range, therefore making observed dissolved iron and model output dissolved iron concentrations congruent. As expected from the calculation discussed previously, the increase in SO_4^{2-} from pyrite denitrification did not explain all of the attenuated NO_3^-. OC was considered as a potential primary electron donor for the remaining NO_3^- lost.

The OC used in the modeling simulations for both the R- and C-ISM is a zero valence labile form CH_2O as described in Reaction (1). This phase did not exist in the

model thermodynamic database, so it was defined at the beginning of the model input under the PHASES keyword. The log_k was input as 0.0, thereby signifying that the phase was extremely soluble. This allowed OC interaction with the solutions within the model to be dictated by the modeler such that only the number of moles available, and not solubility, limited its participation.

After sufficient NO_3^- was reacted with pyrite to generate the SO_4^{2-} measured in the R-ISM, small amounts of OC were allowed to react until the concentrations of NO_3^- output by the model were equal to those observed in the analytical data. This resulted in the simulation of denitrification as described by Reaction (1). The products of these reactions were allowed to react with the aqueous chemistry, as well as participate in dissolution or precipitation along with the other "EQUILIBRIUM_PHASES." Small amounts of OC were also allowed to react during simulation of the C-ISM. DOC was observed in the C-ISM analytical data and thus, was made available to react within the modeling simulation of the C-ISM.

Application of the pN_2 value output in the SI query simulation, within the forward model for both ISMs, as a calibration method was considered and tested. However, it was discovered that neither solution approached saturation with nitrogen gas, therefore, it was not a limiting boundary condition. For simplicity it was eliminated as an active boundary condition and excluded from the input. Ultimately, it was believed that the observed analytical data for SO_4^{2-} were a more representative and accurate method of calibration for nitrate and redox processes.

The partial pressure of $CO_{2(g)}$ in solution was considered and included as a boundary condition in the forward model simulations. This was done due to the

interdependence of carbonate system equilibrium phases and pH on this parameter. This parameter was input into the forward model, as a SI, with the exact value observed in the SI query simulation, as was done for other equilibrium phases.

The temperature of all reactions was input using the keyword REACTION_TEMPERATURE. This reaction parameter was entered into the model input according to the data gathered in the field during sampling. Finally, the end of calculations for each data point was signified by the END keyword.

During and after model construction, all indicator parameters output by the forward model, such as pH, dissolved concentrations and speciated concentrations of major and minor ions and other water quality parameters, were compared to the actual water quality data. Upon arriving at a satisfactory match between model parameter output and analytical data believed to be directly or secondarily influenced by the denitrification, the reactions and interactions within the forward model were considered to be a possible representation of the in-situ geochemical environment. It was found that the model output matched analytical data most accurately under a relatively unique set of boundary conditions and when a specific set of phases, included in the geochemical conceptual model of the aquifer, were used in the model. This created the perception that these phases were controlling of, and integral to, the water quality observed. At this point the modeling efforts have made a full "circle" (Figure 7). That is, the model output concentrations satisfactorily matched the analytical results, and indicated OC as a potential second primary electron donor.

The final step was to query the model as to the composition of the exchanger and the phase mole-transfers that had occurred in the calibrated forward model using the

"SELECTED_OUTPUT" keyword. This keyword was invoked at the beginning of the model input to facilitate reporting of specified queried parameters throughout the model calculations.

The ISMs were modeled to gain insights into denitrification reactions and secondary reactions induced by the denitrification, while assessing amendment-methodology reactions as discovered in the C-ISM model. Amendment-methodology-induced reactions and denitrification-induced reactions could be discerned, tracked, compared and ultimately, assessed for their geologic validity. This final validation of the model was accomplished via analysis of the phase mole transfers that occurred as presented by each model within the "SELECTED_OUTPUT" file.

In summary, the modeling methodology included using the actual water analyses to gain information about the state of thermodynamic disequilibrium during the query simulation. That information was then applied as the boundary conditions for phases in a forward model simulation, along with cation exchange, to gain information pertaining to the tracer test amendment-methodology reactions and denitrification-induced geochemical processes.

CHAPTER VI

MODELING RESULTS AND DISCUSSION

The results of the forward models are presented in two parts. First, the concentrations of dissolved ions and other indicator parameters output by the model are compared to the analytical results of the tracer test. Hence, the first objective of modeling the observed state of disequilibrium and is achieved. This objective also serves to help validate the model. Second, phase mole transfers for the partially validated model are presented. This provides final validation of the model and accomplishment of the second and third objectives, and promotes discussion and comparison of the observed geochemical interactions within each ISM. All concentrations and phase mole transfers are presented in mmol $\cdot$ L^{-1} in this section.

Modeled vs. Measured Concentrations

Forward modeling for the C-ISM was completed first. It was assumed that the geochemistry involved in this ISM would be relatively simple with no significant redox reactions anticipated. All output concentration data can be viewed in Appendix G Tables 12 and 13.

Figure 10 and 11 present the model output concentrations compared to the actual analytical data for pH and ions believed to be most influenced by redox or amendment-methodology reactions. Modeled concentrations for each analyte or ion are plotted using the same symbol, model concentration output are indicated by dashed line and analytical

results are indicated by solid lines. There is a close agreement between modeled output values and the analytical results.

Figure 10 compares important cations modeled vs. measured concentrations for the C-ISM. The concentration of the cations were calculated by the model according to the boundary conditions delineated in the previous section. Model output concentrations deviate slightly for certain data points. However, considering the ion balances of the analytical data compared to the ion balances for the solutions output by the model, the modeled vs. measured differences can be accounted for by the accuracy of analytical methods and the convergence limits of the model.

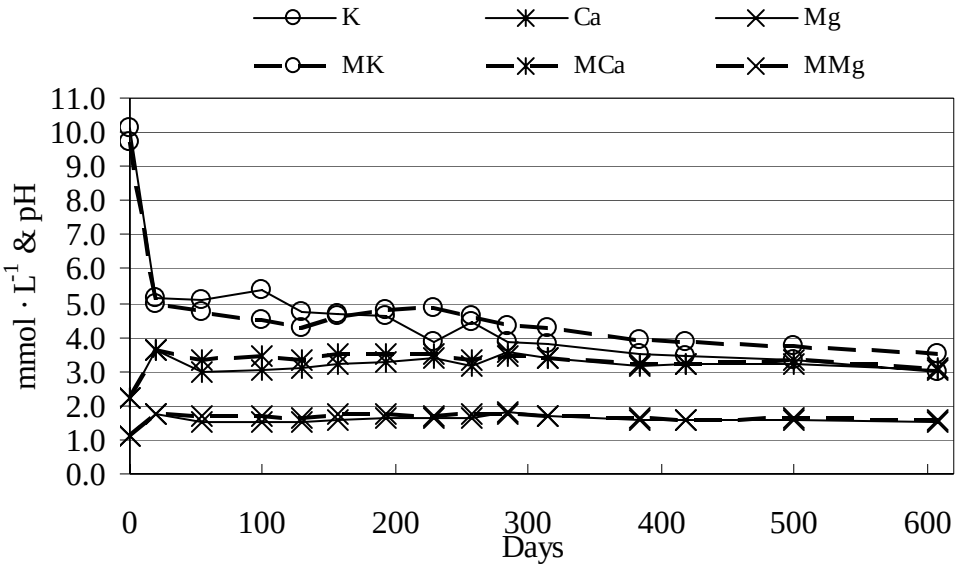

Figure 10. Modeled vs. measured concentrations of important cations within the C-ISM.

Figure 11 presents modeled vs. measured concentrations for important anions and pH of the C-ISM. Br^- concentration output by the model is based on the mixing fraction input, as discussed earlier. The concentration for DIC, SO_4^{2-} [S(6) in PHREEQC-2] and pH are calculated by the model based on the boundary conditions described previously.

Again close agreement between the analytical data and the data output by the model is observed for the minor ions of the C-ISM.

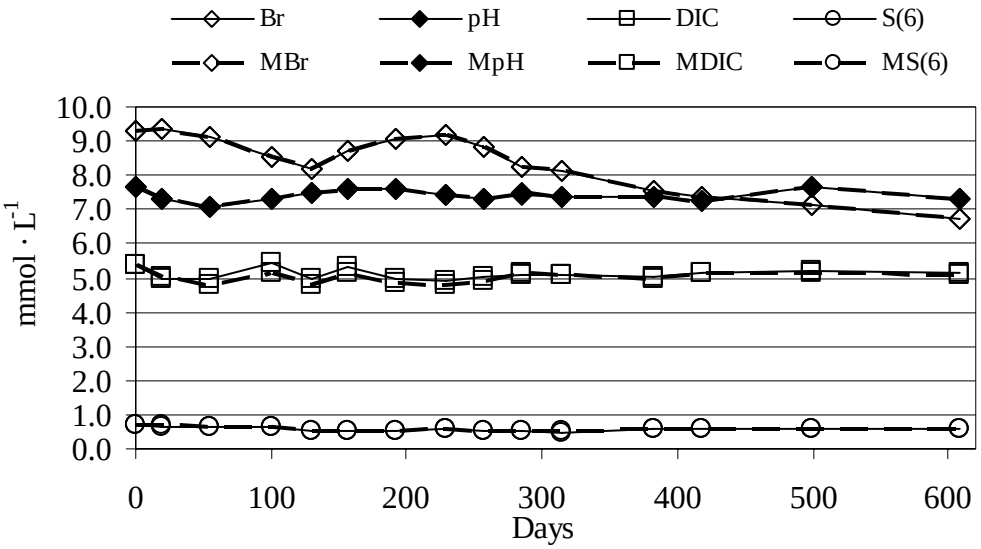

Figure 11. Modeled output vs. analytical data for important anions and pH of the C-ISM.

Overall, close agreement of modeled vs. measured concentrations are observed in Figures 10 and 11. This signifies accomplishment of the first modeling objective to simulate the state of thermodynamic disequilibrium within the C-ISM. The close agreement of measured vs. modeled values validates the model, to some extent, as a plausible description of the in-situ geochemical environment representing the major reactions controlling the water quality within the C-ISM.

Model output concentrations vs. analytical results for the R-ISM are presented as Figures 12 and 13. Again, the dashed lines represent model output values and analytical results are the solid lines with the same symbol. Model concentration output data for the R-SM are presented in Table 13 (Appendix G).

Figure 12 indicates modeled vs. measured concentrations for pH and important anions. Anions include Br^- and the redox sensitive parameters according to Reactions (1-

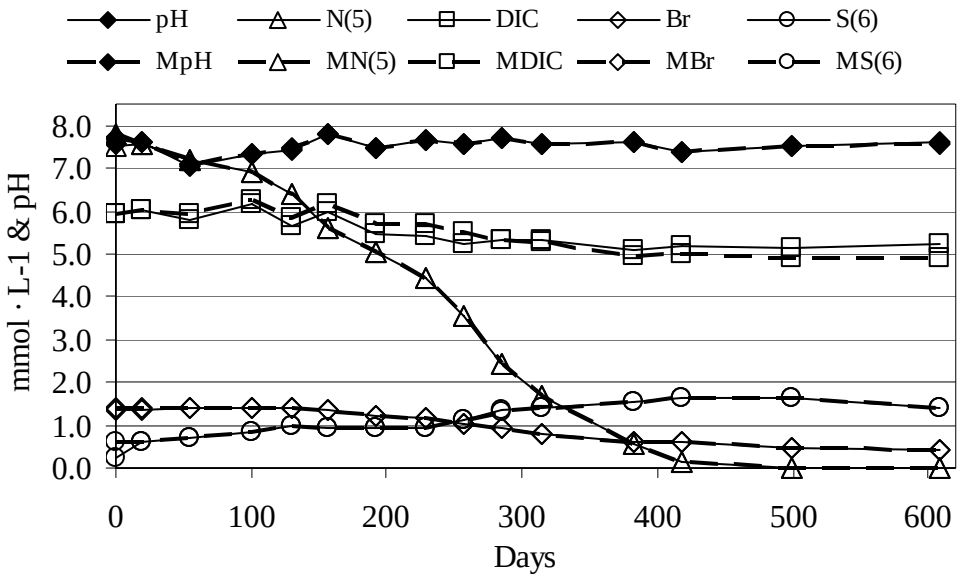

Figure 12. Research ISM model output vs. measured values for pH, Br^- and redox sensititve analytes presented in Reactions (1-4).

4). N(5) and S(6) represents moles of NO_3^--N and sulfur in the form of SO_4^{2-}, respectively. It is expected that N(5), S(6) and Br^- match closely, because these concentrations are directly controlled by the modeler during simulation input via the mixing fraction and addition of electron donating phases. The model calculates pH and concentration of DIC, according to the boundary conditions of the model. For these two parameters a close match between the modeled output values and analytical results is also observed.

Figure 13 indicates modeled output vs. measured values for important cations of the R-ISM. The model output concentrations for Ca^{2+}, Mg^{2+} and K^+ represented by dashed lines, are calculated by the model according to the boundary conditions of the input file and are not explicitly controlled by the modeler. For these analytes, there are

some discrepancies for some data points; however, considering the ion balances and model convergence limits, the modeled vs. measured data correspond well.

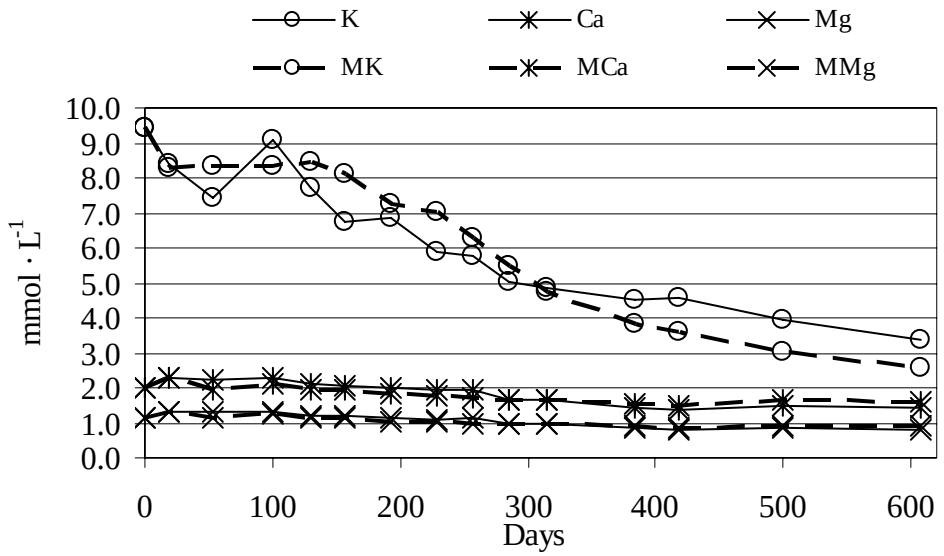

Figure 13. Model output concentrations vs. measured for important cations of the R-ISM.

Figures 20 and 21 (Appendix H) summarize modeled vs. measured concentration for other ions less important to the redox processes observed, based on Reactions (1-4). These figures indicate some discrepancies in Na, Cl and Si concentrations in the modeled vs. measured data; however, a satisfactory match is observed for Mn concentrations. Except for Mn, the other analytes have not been documented to be significantly involved in denitrification processes. The variations in the modeled vs. measured data fo Cl are likely due to natural variability in the R-ISM (Korom et. al., in print) Variability in the Na and Si concentrations may be better modeled by incorporating silicate phases in the model, but doing so is beyond the scope of this research.

Throughout all of the modeling efforts, the concentrations of redox-sensitive parameters and other ions are computed by the model according to the boundary conditions affecting those parameters. A model may produce concentrations that match analytical results very closely; however, the reactions occurring within the model may not make geochemical sense. Accordingly, the final validation of the model and accomplishment of the second and third modeling objectives were achieved by inspecting the phase transfers that occurred. This is done so that the relevance of the reactions presented by the model can be compared to generally accepted geologic and geochemical concepts for the type of physical environment being studied.

Model Phase Mole Transfers

The phase mole transfers that occurred within the model during simulation executions are listed in Tables 14 and 15 of Appendix I. Phase transfers having positive numbers indicate precipitation from solution or formation of that phase via conversion from a different phase. Phase mole transfers having a negative sign indicate dissolution of that phase or loss of that phase from the aquifer solid matrix. All phase transfers listed in Tables 14 and 15 (Appendix I) are totals representing batch reactions starting at time = 0 (10-08-98) and ending at the time of the date in question.

Figures 14 serves as a summary of the phase mole transfers from C-10-08-98 to C-11-30-99 and are indicative of the redox and redox induced phase interactions as presented by the model.

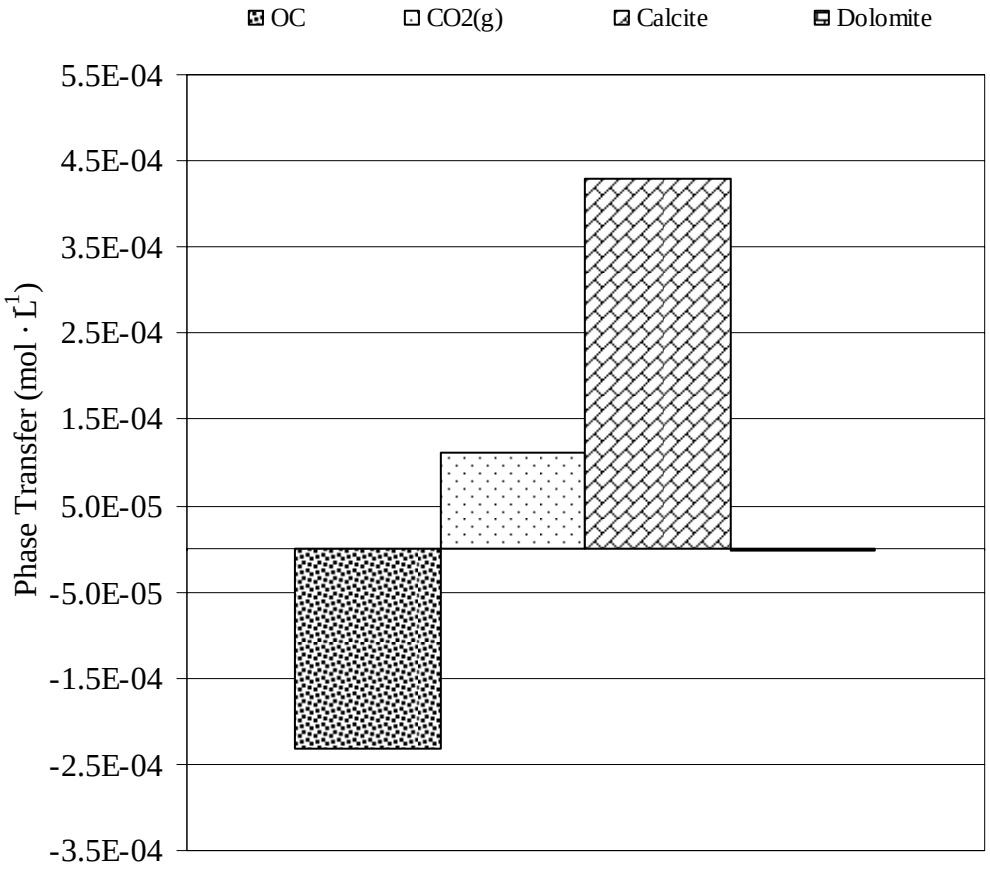

Figure 14. Phase mole transfers in C-ISM for batch reaction from 10-8-98 to 11-30-99.

As discussed earlier and presented by Figure 14, small amounts of OC are allowed to react in the C-ISM. The amount of OC allowed to react in the C-ISM modeled water is determined by the S(6) concentration in the analytical results. As a small amount of OC is allowed to react in the model simulation a small amount of SO_4^{2-} reduction occurs. Hence, the observed fluctuation and overall downward trend in SO_4^{2-} concentrations within the C-ISM is simulated effectively. The lack of appreciable dissolved NO_3^- or the less soluble forms of Mn^{4+} or Fe^{3+} (as indicated by the speciated concentrations for these ions in PHREEQC output from SI query simulation for the C-

ISM) reinforces the probability that reduction of aqueous SO_4^{2-} is occurring. It is the next major available electron acceptor to oxidize the OC in solution.

As OC is used during SO_4^{2-} reduction HCO_3^- is produced within the simulated water. The production of CO_3^{2-} species facilitates precipitation of calcite as represented by the positive phase mole transfers for this phase throughout TT2. This process appears to be driving dolomite dissolution, denoted by the negative phase transfers, via common ion effects. Perhaps the most accurate interpretation of these carbonate phase interactions is a conversion of dolomite to calcite bolstered by additional calcite precipitation. These reactions make geochemical sense because calcite is supersaturated throughout TT2 and expected to be precipitating. Excess CO_3^{2-} produced exits solution as $CO_{2(g)}$ according to the partial pressure of $CO_{2(g)}$ observed in the analytical data. Furthermore, precipitation of carbonate phases and degassing of $CO_{2(g)}$ buffers the pH such that values computed by the model match those measured in the field. The consumption of a small amount of DIC by formation of carbonate phases results in the observed decrease of DIC such that the modeled concentrations closely match those observed in the analytical data.

However, when OC is not added to the C-ISM simulation, the model output concentrations produce a satisfactory match of the analytical data, except for the slight decreasing trend in SO_4^{2-} concentration. This trend is not captured by the model as indicated by Figure 15. This discrepancy could also be explained by natural variability in SO_4^{2-} in C-ISM as for Cl^- in the R-ISM; thus it does not appear that OC oxidation in the C-ISM is essential

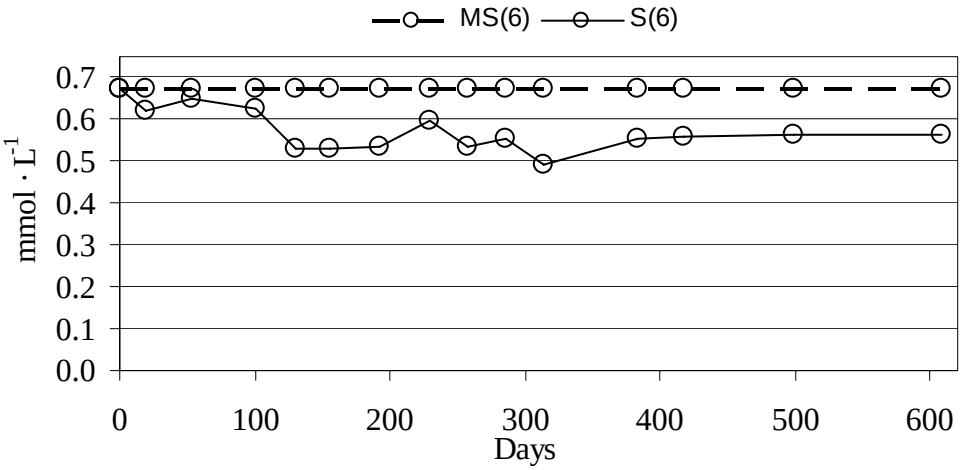

Figure 15. Modeled vs. measured SO_4^{2-} without OC interaction in the C-ISM.

Phase mole transfers for the R-ISM forward simulation are presented in Table 15 (Appendix I). Figure 16 serves as a summary of the phase mole transfers from R-10-08-98 to R-11-30-99 and are indicative of the phase interactions caused by the redox reactions in the model. Table 15 and Figure 16 should be examined frequently in conjunction with Figures 12 and 13, Table 10 (Appendix F) and Table 13 (Appendix G) during the following discussion.

The water quality of the R-ISM is very different than that of the C-ISM; however, the same methodology and assumptions used for simulation of the C-ISM were used for simulation of the R-ISM. The one difference is the activation of two additional phases: pyrite and goethite. Pyrite serves as a major electron donor to NO_3^- as presented in Reaction (4) and is added to the simulation in the manner discussed above. Goethite is allowed to react freely with the R-ISM simulation water, governed only by the state of saturation observed in the SI data for that phase. It acts as a ferric iron sink as described by Reaction (4).

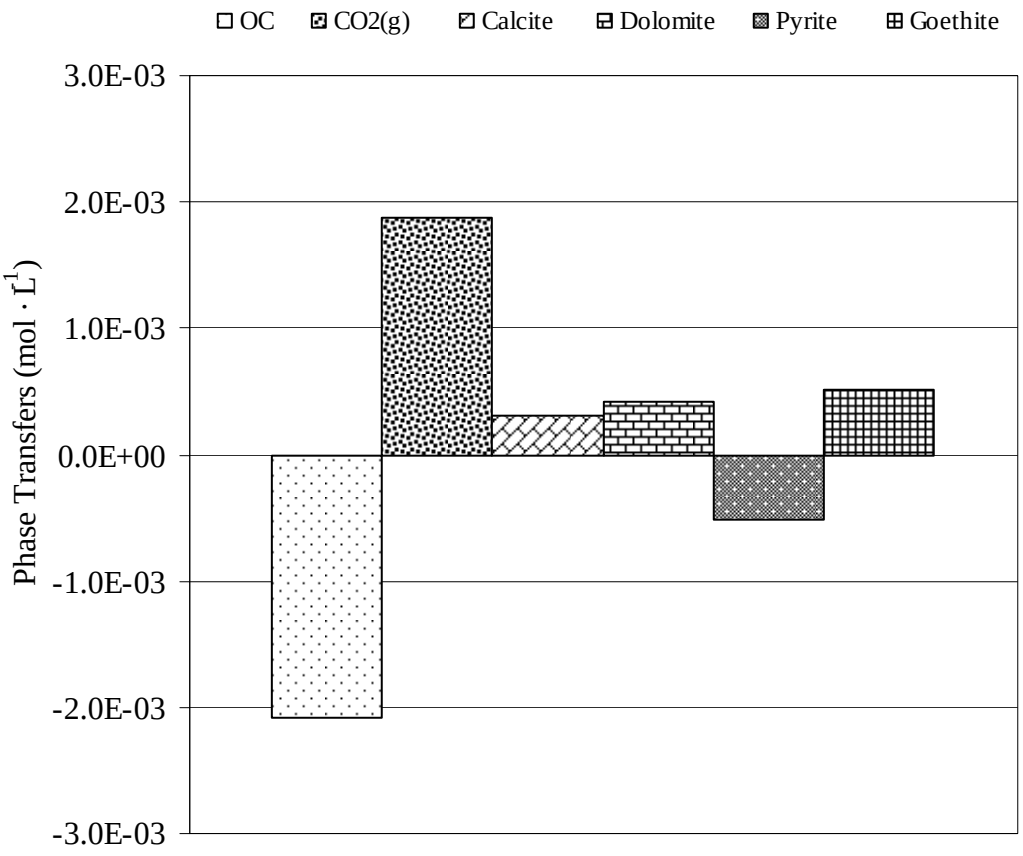

Figure 16. Phase mole transfers within R-ISM from 10-8-98 to 11-30-99.

Within the R-ISM simulation, pyrite is allowed to react according to SO_4^{2-} concentrations observed in the analytical data. This resulted in the reduction of NO_3^--N to $N_{2(g)}$; this reaction also produces dissolved iron. Production of iron caused precipitation of goethite from solution throughout TT2 in the R-ISM simulation results.

After denitrification via pyrite was simulated according to the observed SO_4^{2-} evolution, NO_3^--N concentrations above observed concentrations in the analytical data remained in the simulated R-ISM solution. Therefore, OC was considered as a potential primary electron donor to denitrify the remaining NO_3^- lost from the R-ISM.

OC , in the same form as that used in simulation of the C-ISM, was allowed to react with the R-ISM simulated water according to Reaction (1). OC was allowed to react until all excess NO_3^--N concentrations in the simulation solution were reduced to $N_{2(g)}$. Concentrations of HCO_3^- are observed increasing as would be expected from heterotrophic denitrification described by Reaction (1). The observed DIC increase in the simulation solution was well in excess of values observed in the analytical data, where a slight decrease was observed in DIC. At first inspection this seems to rule out OC as the second electron donor; however, following the insights gathered from the simulation of the C-ISM, and the discussion presented by Schlag (1999) regarding this matter, carbonate phase precipitation was considered as a potential DIC sink.

Calcite and dolomite phases were invoked within the simulation and allowed to react to the observed state of saturation. The model suggests that the production of DIC from the simulation of heterotrophic denitrification facilitates, and perhaps drives, precipitation of both of these phases throughout TT2. This phenomenon results in formation of a Mg-rich Ca carbonate perhaps similar to the sample bottle precipitate observed by Schlag (1999). The model also suggests that the amount of carbonate phase precipitated (calcite + dolomite) is larger in the R-ISM than the C-ISM due to the greater DIC produced in the R-ISM from redox processes. The interaction of these carbonate phases resulted in model-output pH values that were lower than those observed in the field measurements, as well as, a continued excess of DIC. $CO_{2(g)}$ interaction was considered next.

$CO_{2(g)}$ is invoked in the model as a phase and allowed to degas according to the observed partial pressure of this gas as determined by PHREEQC-2 from the analytical

data. The model suggests that $CO_{2(g)}$ is off-gassing. When this occurs DIC concentrations in the simulated water match the analytical results closely. The off-gassing of $CO_{2(g)}$ also buffers the pH to values matching those observed in the field. This does not suggest that $CO_{2(g)}$ is leaving the R-ISM but is merely leaving solution as tiny bubbles.

As observed in the simulation of the C-ISM, cation concentrations in the simulation solution and equilibrium distribution on the exchanger are effected by the carbonate-precipitation cation-sink.

To test whether the interaction of OC is essential in the R-ISM the model was executed again and this phase was turned off. Inherent to the modeling methods dealing with redox parameters NO_3^- concentration output by the model do not agree with those observed in the analytical results, as expected. In addition to this data discrepancy the concentration of Ca^{2+} and DIC output by the model match the analytical data less effectively as shown by Figure 17. As indicated by Figure 17, the model including OC as a primary electron donor (series with short dashes) resulted in a discrepancy of 0.0939 mmol $\cdot$ L^{-1} Ca^{2+} at 418 days vs. 0.379 mmol $\cdot$ L^{-1} Ca^{2+} in the model without OC (series with long dashes). Similarly, DIC concentrations differences output by the model including OC were 0.1646 mmol $\cdot$ L^{-1} vs. 0.5791mmol $\cdot$ L^{-1} output by the model without OC at 418 days.

Overall, the model simulation of the R-ISM suggests that geochemical conditions are appropriate for OC to be a primary electron donor to the observed denitrification. Furthermore, the modeling simulations of the R-ISM suggest that the interaction of OC as a primary electron donor results in a model that more accurately captures the water

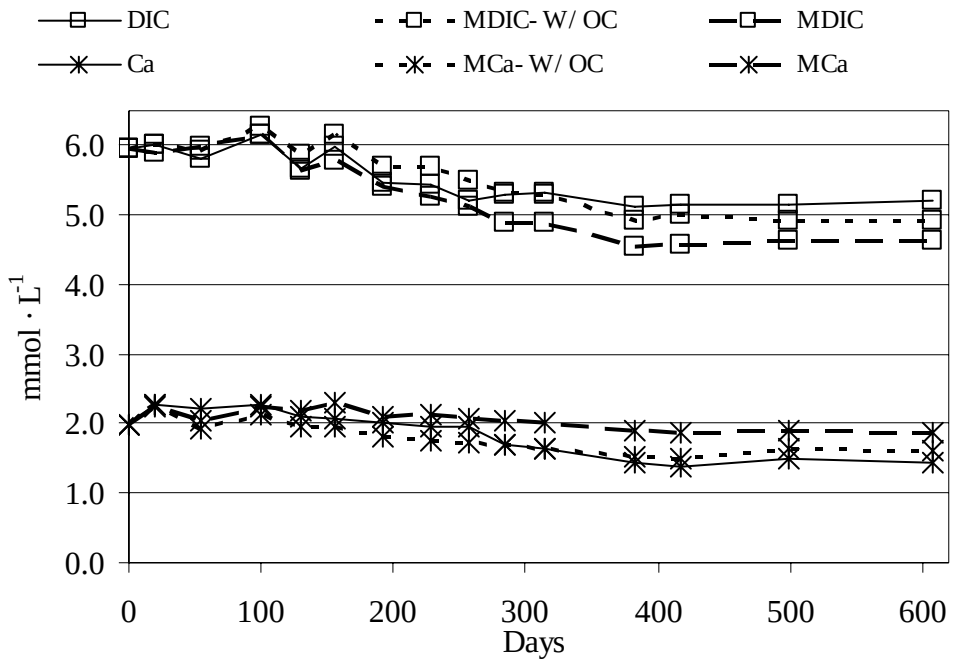

Figure 17. Comparison of Ca^{2+} and DIC concentrations in the R-ISM model output for model including and not including OC as primary electron donor.

quality data observed in the R-ISM. Along with the observed and simulated redox reactions the model also suggests that the amendment methodology with a solution with a relatively strong K^+ concentration to both ISMs causes significant cation exchange, which significantly effects cation concentrations, whereby compounding carbonate precipitation resulting in a slight decreasing trend in DIC concentrations.

Ultimately, the model simulations of the C and R-ISM should be considered as simple conceptual models of the actual geochemical environment and the processes occurring in-situ. None-the-less the model simulations closely capture the major changes and the trends observed in the analytical data, as well as, describe a likely geochemical environment controlling the water quality in the ISMs. Finally, electron donor participation can be quantitatively estimated according to the model phase mole transfers.

Quantification of electron donors in the R-ISM simlutation is shown on Figure 18. These values are given as a total percent of electrons donated to denitrification for OC

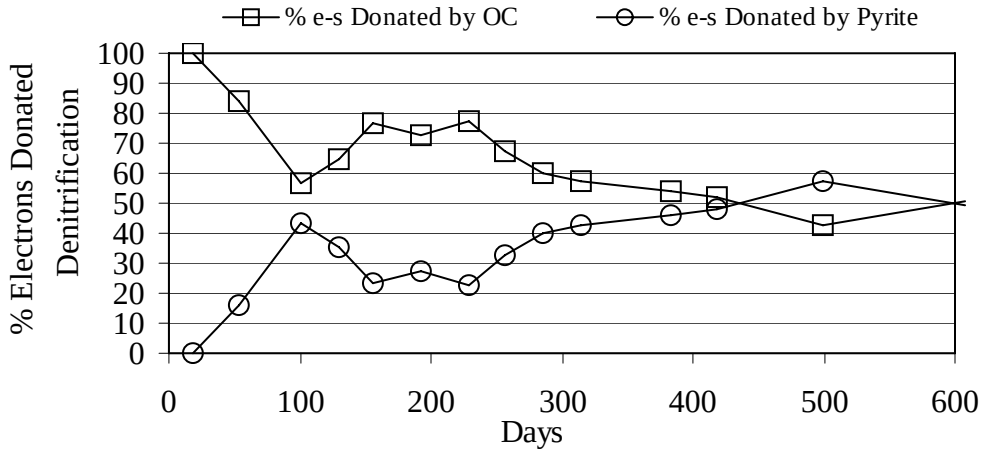

Figure 18. R-ISM PHREEQC-2 simulation output of percent total electrons donated to denitrification by pyrite and OC for each sampling event.

and pyrite from the R-ISM simulation. Figure 18 suggests that 48% of the observed denitrification at 418 days (when the NO_3^- concentration was effectively zeroed) can be attributed to denitrification by pyrite in accord with Reaction (4). The remaining 52% can be attributed to denitrification by OC in accordance with Reaction (1), based on the geochemical conditions observed in the aquifer. Furthermore, the modeling efforts suggest that OC participation as a primary electron donor is a more accurate interpretation of the observed denitrification based on the overall geochemical environment and the observed water quality data.

CHAPTER VII

CONCLUSIONS

The hypotheses of this research were: (1) autotrophic denitrification by sulfides occurs in the EVA, and (2) geochemical conditions are consistent with the occurrence of denitrification by OC in the EVA. The methods used to test these hypotheses included duplicating the tracer test (TT1) done by Schlag (1999) using the in-situ mesocosms, comparing the results of the two tracer tests and modeling the geochemistry of the second tracer test (TT2). The results presented in this thesis provide compelling evidence that supports the hypothesis of denitrification by sulfide phases. It also provides additional evidence substantiating the hypothesis that geochemical conditions are consistent with the occurrence of heterotrophic denitrification by organic carbon (OC).

Three lines of evidence support the conclusion of denitrification during TT2: (1) 3.19 mmol $\cdot L^{-1}$ NO_3^--N were lost in the R-ISM that were not accounted for by dilution of conservative Br^- tracer; (2) $\delta^{15}N$ in the remaining nitrate increased from 4.5 ‰ to 26.95 ‰ over a 418 day period: and (3) 2.05 mmol $\cdot L^{-1}$ SO_4^{2-}-S were generated during the test.

The observed denitrification during TT2 had an average rate of 7.6 μmol $\cdot L^{-1} \cdot day^{-1}$ (0.11 mg $\cdot L^{-1} \cdot day^{-1}$), which was approximately half the 15.0 μmol NO_3^--N $\cdot L^{-1} \cdot day^{-1}$ (0.22mg $\cdot L^{-1} \cdot day^{-1}$) rate observed during TT1 (Schlag, 1999). The observed isotopic enrichment during TT2 resulted in calculation of a Rayleigh enrichment factor (ε) of -27.64 ‰. This indicates a more electron donor-limiting environment during

TT2, compared to the ε of -20.43 ‰ calculated for TT1 (Schlag, 1999). Evolution of SO_4^{2-} in the R-ISM indicates autotrophic denitrification according to Reaction (4) accounts for at least 48 % of observed denitrification during TT2, based on Figure 18. Denitrification by pyrite accounted for at least 61 % of the total observed denitrification during TT1.

Geochemical modeling of the TT2 data was performed using PHREEQC-2. Several assumptions were made to complete the simulation of the ISM waters; however, a calibrated and validated model was achieved. The modeling efforts offer insights with regard to OC role as a primary electron donor in the R-ISM. The model was used to perform a simulation of ISM water quality evolution by invoking dilution, cation exchange, and phase interaction. The results are a calibrated and validated model of the geochemistry resulting in model outputs closely matching observed analytical data associated with denitrification reactions. The reactions and interaction that were allowed to occur in the model simulations are likely, from a geochemical perspective, to be occurring in-situ. Ultimately, it is concluded that geochemical conditions of the aquifer are proper for OC to be a primary electron donor of the observed denitrification. Furthermore, the results of the modeling indicate that the occurrence of denitrification by OC is a more accurate interpretation of the geochemical processes that produced the water quality observed during TT2 and that it likely accounted for a maximum of 52 % of the observed denitrification, based on Figure 18.

Finally, the results of the modeling offer insights regarding redox and amendment-induced reactions. The model suggests that precipitation of goethite and carbonate phases from solution are induced by the observed redox reactions resulting in

the non-detectable iron concentrations and the slight decrease of DIC observed in both ISMs. The model also suggests that a significant amount of K^+ exchange for Ca^{2+} and Mg^{2+} took place as a result of the amendment methodology. This affected the state of saturation with respect to the carbonate system by increasing the concentrations of these ions.

Recommendations for Future Work

The research presented in this thesis has likely raised more questions than it has answered. The following recommendations for future work may provide additional insights into the in-situ workings of denitrification in the Elk Valley Aquifer and other geochemical environments.

(1) Biologic characterization of denitrifying bacteria, including formulation of a stoichiometric equation(s) that incorporates and accounts for biota and inorganic process interactions such as bio-assimilation and bio-accumulation of nutrients.

(2) Investigate and characterize the conditions governing the kinetics of denitrification and mineral phase interaction, with potential for future applications to PHREEQC modeling.

(3) Execute a third tracer test at the LFS using an amendment cation other than K^+. This type of study may facilitate testing of some of the hypothesis made in this research regarding the geochemical environment and reactions occurring in-situ, while allowing for continued characterization of the observed denitrification and the long-term effects of NO_3^- loading on the EVA.

(4) Install a network of ISMs in multiple aquifers, with different physical and chemical characteristics than those found in the EVA. Studying denitrification in

multiple shallow aquifer environments may facilitate a general formulation, or a method for assessing denitrification capacities and maximum allowable nitrate loading, based on the chemical and physical characteristics of the aquifer sediments.

REFERENCES

Appelo, C. A. J., D. Postma, Geochemistry, Groundwater and Pollution, 536pp., A. A. Balkema, Rotterdam, Netherlands, 1996.

Appelo, C. A. J., and A. Willemsen, Geochemical calculations and observations on salt water intrusions, I, A combined geochemical/mixing cell model, Journal of Hydrology, 94, 313-330, 1987.

Appelo, C. A. J., A. Willemsen, H. E. Beekman, and J. Grifioen, Geochemical calculations and observations on salt water intrusions, II, Valication of a geochemical model with laboratory experiments, Journal of Hydrology, 120, 225-250, 1990.

Aravena, R. and W. D. Robertson, Use of multiple isotope tracers to evaluate denitrification in groundwater: study of nitrate from a large-flux septic system plume, Ground Water, 36(6), 975-982, 1998.

Bates, H. K. and R. F. Spalding, Aquifer denitrification as interpreted from in-situ microcosm experiments, Journal of Environmental Quality, 27, 174-182, 1998.

Boggs, S. Jr., Principles of Sedimentology and Stratigraphy, Second Edition, 774pp., Prentice Hall, New Jersey, 1995.

Böttcher, J., O. Strebel, S. Voerkelius and H.-L. Schmidt, Using isotope fractionation of nitrate-nitrogen and nitrate-oxygen for evaluation of microbial denitrification in a sandy aquifer, Journal of Hydrology, 114, 413-424, 1990.

Buresh, R. J. and J. T. Moraghan, Chemical reduction of nitrate by ferrous iron, Journal of Environmental Quality, 5, 320-325, 1976.

Canter, L. W., Nitrates in Groundwater, 263pp., Lewis Publishers, New York, 1997.

Das, B. M., Principles of Geotechnical Engineering, 672pp., PWS Publishing Company, Boston, MA, 1994.

Faure, G. F., Principles and Applications of Geochemistry, 600 pp., Prentice Hall, Upper Saddle River, NJ, 1998.

Firestone, M. K., Biological denitrification, in Nitrogen in Agricultural Soils, edited by F. J. Stevenson, American Society of Agronomy, Madison, Wisconsin, 289-326, 1982.

Gerla, P. J., Pathline and geochemical evolution of ground water in a regional discharge area, Red River Valley, North Dakota, Ground Water, 30(5), 1992.

Gillham, R. W., M. J. L. Robin and C. J. Ptacek, A device fr in-situ determination of geochemical transport parameters 2. Biochemical reactions, Ground Water, 28(6), 1990.

Harris, K. L., Geology of the souther part of the Lake Agassiz Basin, in Prodeedings of the North Dakota Academy of Science 51, Supplement 1: 6-11, 1997.

Howard, K. W. F., Denitrification in a major limestone aquifer, Journal of Hydrology, 76, 265-280, 1985.

Kelly, T. E., and Q. F. Paulson, Geology and ground water resources of Grand Forks County, North Dakota: Ground water resources, North Dakota Geological Survey Bulletin 53, Part III, 58 pp. Bismarck, ND. 1970.

Kammer, A., Laboratory denitrification using sediments from the Elk Valley aquifer, M.S. thesis, 76pp., University of North Dakota, Grand Forks, ND, 2001.

Kinzelbach, W., W. Schäfer and J. Herzer, Modeling of natural and enhanced denitrification processes in aquifers, Water Resources Research, 27(6), 1123-1135, 1991.

Kölle, W., O. Strebel, and J. Bottcher, Formation of sulfate by microbial denitrification in a reducing aquifer, Water Supply, 3(1), 35-40, 1985.

Kölle, W., O. Strebel, and J. Bottcher, 1987, Reduced sulfur compounds in sandy aquifers and their interactions with groundwater, in Proceedings of the Dresden Symposium, Groundwater Monitoring and Management, edited by G. P. Jones, IAHS Publication No. 173, 23-30, 1990.

Korom, S. F., Denitrification in the unconsolidated deposits of the Heber Valley aquifer, Ph.D. thesis, 176 pp., Utah State University, Logan, Utah, 1991.

Korom, S. F., Natural denitrification in the saturated zone: a review, Water Resources Research, 28(6), 1657-1667, 1992.

Korom, S. F., A. J. Schlag, W. M. Schuh and A. K. Schlag, In situ mesocosms: Denitrification in the Elk Valley Aquifer, Ground Water Monitroing and Remediation, in print.

Mariotti, A., J. C. Germon, P. Hubert, P. Kaiser, R. Letolle, A Tardieux and P. Tardieux, Experimental determination of nitrogen kinetic isotope fractionation: Some principles; illustration for the denitrification and nitrification processes, Plant and Soil, 62, 413-430, 1981.

Mariotti, A., J. C. Germon, and A. Leclerc, Nitrogen isotope fractionation associated with the $NO_2 \rightarrow N_2O$ step of denitrification in soils, Canadian Jounal of Soil Science, 62(2), 227-241, 1982.

Mariotti, A., A. Landreau and B. Simon, ^{15}N isotope biogeochemistry and natural denitrification process in groundwater: Application to the chalk aquifer of northern France, Geochimica et Cosmochimica Acta, 52(7), 1869-1878, 1988.

Mayer, G. G., Denitrification in the Elk Valley aquifer, northeastern North Dakota. Ph.D. thesis, 233 pp., University of North Dakota, Frand Forks, ND, 1992.

McMahon, P. B., J. K. Böhlke and B. W. Bruce, Denitrification in marine shales in northeastern Colorado, Water Resources Research, 35(5), 1629-1642, 1999.

Parkhurst, D. L., C. A. J. Appelo, User's guide to PHREEQC (version2)— A computer program for speciation, batch-reaction, on-dimensional transport, and inverse geochemical calculations, U.S. Geological Survey Water Resources Investigations Report 99-4259, 308 pp., 1999.

Patch, J. C., and G. Padmanabhan, Vertical nitrate gradients in a shallow unconfined aquifer in North Dakota, in Proceedings of the North Dakota Water Quality Symposium, 25-34, 1996.

Pauwels, H. O. Legendre, and J.-C. Foucher, High-rate denitrification from several electron donors in a schist aquifer, in Water-Rock Interaction: Proceedings of the 9^{th} International Symposium - WRI - 9, pp. 173-176, Ashgate Publishing Co., Balkema, Rotterdam, Netherlands, 1998.

Pauwels, H., W. Kloppmann, J.-C. Foucher, A. Martelat, and V. Fritsche, Field tracer test in a pyrite-bearing schist aquifer, Applied Geochemistry, 13(6), 767-778, 1998.

Plummer, L. N., B. F. Jones, and A. H. Truesdell, WATEQF: A FORTRAN IV version of WATEQ, a computer program for calculating chemical equilibrium in natural waters, U. S. Geologic Survey Water Resources Investigation, 76-13, 1976.

Plummer, L. N., E. C.Prestemon, and D.L. Parkhurst, An interactive code (NETPATH) for modeling net geochemical reactions along a flow path, U. S. Geologic Survey Water Resources Research, 27, 2027-2045, 1991.

Postma, D., Kinetics of nitrate reduction by detrital Fe(II)-silicates, Geochimica et Cosmochimica Acta, 54, 903-908, 1990.

Postma, D., C. Boesen, H. Kristiansen, and F. Larsen, Nitrate reduction in an unconfined sandy aquifer: water chemistry, reduction processes, and geochemical modeling, Water Resources Research, 27(8), 2027-2045, 1991.

Rush, D., Personal Communication, 2001.

Schlag, A. J., In-situ measurement of denitrification in the Elk Valley aquifer, M.S. thesis, 104 pp., University of North Dakota, Grand Forks, ND, 1999.

Schultz, L. G., H. A. Tourtelot, J. R. Gill and J. G. Boerngen, Composition and properties of the Pierre Shale and equibalent rocks, Northern Great Plains Region, U. S. Geological Survey Professional Paper 1064-B, 114pp., 1980.

Smith, R. L., B. L. Howes and J. K. Duff, Denitrification in nitrate-contaminated groundwater: Occurrence in steep vertical geochemical gradients, Geochimica et Cosmochimica Acta, 55(76), 1815-1825, 1991.

Tesoriero, A. J., H. Liebscher and S. E. Cox, Mechanism and rate of denitrification in an agricultural watershed: Electon and mass balance along hgroundwater flow paths, Water Resources Research, 36(6), 1545-1559, 2000.

Trudell, M. R., R. W. Gillham, and J. A. Cherry, An in-situ study of the occurrence and rate of denitrification in a shallow unconfined sand aquifer, Journal of Hydrology, 83(3/4), 251-268, 1986.

van Beek, C. G. E. M., F. A. M. Hettingas, and R. Straatman, The effects of manure spreading and acid deposition upon groundwater quality in Vierlingsbeek, the Netherlands, in Proceedings of the Symposium held during the Third IAHS Scientific Assembly, Baltimore, Groundwater Contamination, IAHS Publication No. 185, 155-162, 1989.

Vogel, J. C. A., S. Talma and T. H. E. Heaton, Gaseous nitrogen as evidence for denitrification in groudwater, Journal of Hydrology, 50(1/3), 191-200, 1981.

World Wide Web: http://water.usgs.gov/watuse/spread95.html.

World Wide Web: http://www.epa.gov/ow/resources/9698/chap6c.html.

APPENDICES

APPENDIX A

Review of In-Situ Tracer Tests for Denitrification

In-situ Tracer Tests for Denitrification

In-situ studies introduce another layer of complexity to analysis and discussion of data. Uncertainties were introduced by natural heterogeneties that were difficult to evaluate qualitatively or quantitatively without disturbing the in-situ nature of the system (Howard, 1985). Some of the uncertainties introduced involve the variability of parameters associated with solute transport and mixing such as advective and diffusive effects. Isotopic analysis of dissolved N can be used as a tracer to eliminate some of the complexities introduced by in-situ methods. Initial concentrations and isotopic composition of dissolved NO_3^- are generally required for the use of nitrogen isotopes as a tracer or tool for discussion of the denitrification process. In nature these concentrations are often highly variable and difficult to quantify (Howard, 1985).

Aravena and Robertson (1998) used $\delta^{15}N$ and $\delta^{18}O$ analysis in conjunction with $\delta^{34}S$ and $\delta^{13}C$ to trace electron donors to, and the role of denitrification associated with a large flux septic system plume. The septic flux was infiltrated into an unconfined medium sand aquifer primarily composed of carbonate and silica. The aquifer was also noted to contain a substantial organic fraction ranging from 0.15 to 2 % and a sulfur content of 0.02 % by weight.

They report $\delta^{15}N$ having an overall range of +6 to +58.3 ‰ and an ε = -22.9 ‰ for the study area, indicating denitrification. Observed increases in SO_4^{2-} concentration having a depleted $\delta^{34}S$ and ferrous iron behavior in the zone of NO_3^- attenuation indicated iron sulfide as an electron donor. They also report patterns of DIC and ^{13}C to substantiate carbon as a co-electron donor participating in denitrification.

Chemical mass balance calculations were completed with the aide of the stoichiometry presented in Reactions (1 – 4). They conclude that carbon was the major electron donor responsible for an estimated 70 – 75 % of observed denitrification. They observed twice as much HCO_3^- evolving than was to be expected from the stoichiometry. This was explained via calcite dissolution; however, it was substantiated by admittedly incongruent ^{13}C data. Furthermore, they present no direct evidence regarding the state of saturation for calcite or dolomite mineral phases or the effect of advective dilution along the scale of transport considered for discussion. Though the isotope data and evolution of dissolved species was compelling evidence for dentrification, these lines of evidence do not trace the evolution of groundwater quality along a flow path conservatively enough to merit a mass balance analyses.

One methodology for directly monitoring groundwater quality in-situ commonly used to mitigate uncertainties evolving from advective dilution, was the tracer test. This method consists of amending water with a known amount of a non-reactive tracer whose concentration under background conditions was known. The water was then injected into the aquifer. Application of this methodology in many studies has evolved the term “in-situ tracer test”.

Korom (1991) performed an in-situ tracer test for denitrification in a poorly sorted aquifer of Heber Valley, Utah. He used a single well inject and extract methodology where aquifer water was amended with tracer and NO_3^- and injected into the well. The well was then sampled for NO_3^-, the tracer and other redox sensitive analytes and their relative ratios were determined. The tracer allows for direct measurement of dilution and evolution of dissolved species. The test had two-phases using Cl^- then Br^- as

conservative (non-reactive) tracer. He observed production of both HCO_3^- and SO_4^{2-} relative to the tracer used indicating heterotrophic and autotrophic denitrification that reached rates as high as 0.74 mg $N \cdot L^{-1} \cdot day^{-1}$.

It was also determined that the portion of the aquifer undergoing the tracer test had an apparent finite capacity for denitrification; it ceased after 14.9 mg NO_3^--$N \cdot L^{-1}$ were reduced. Coincidentally, Korom (1991) also notes, during an all-aqueous companion lab denitrification experiment on water from the same well, that dissolved phosphorus was a limiting nutrient for denitrification. Therefore, phosphorus deficiency rather than electron donor limitation could be inferred as the cause of the denitrification cessation during the in-situ test; however, probable existence of P sorbed to the aquifer matrix available for microbial use during denitrification seems to indicate this was not the case. Regardless, the role and effects of P availability in the in-situ test was not directly distinguished.

Pauwels et al. (1998) performed an in-situ tracer test in an aquifer of the Coët Dan drainage basin near Rennes in Brittany, France. The aquifer was composed of fractured and fissured Brioverian schist composed mostly of quartz, muscovite, chlorite, and to lessor extent potassium and plagioclase feldspar. The major accessory mineral was pyrite as 0.3 to 5 % of the dry weight. Minor accessory minerals included illite, smectite, ferrous iron hydroxide, jarosite and natroalunite. Organic material was not detected within the schist aquifer solid matrix. Weathered fragments of schist, sand, silt and clay overlay the aquifer.

This tracer test was performed between two wells 15 m apart laterally employing a pitch and catch methodology. Pumping was initiated on the downstream well (DNS1),

which induced a 10 m drawdown of the hydraulic potentiametric surface at that well after two days. Then the first tracer test using Br^- tracer only was initiated with addition of 3 kg of NaBr into the upstream well (F1). After two days pumping was suspended for 10 hours to measure the vertical concentration profile of Br^- in DNS1 indicating successful capture of Br^- concentrations. Eleven days later a denitrification tracer test was initiated by injection of 3 kg of NaBr and 5 kg of $NaNO_3$ mixed in a 50-L container prior to injection.

Conceptually a dual porosity model was developed to represent fracture flow and matrix through-flow transport between the two wells. Evidence of the Br^- and NO_3^- tracer arrived in well DNS1 in a matter of hours with nearly equal to the NO_3^-/Br^- concentration ratio as that injected. This arrival was believed to be representative of rapid flow paths along fractures and fissures. It was estimated that 28 % and 25 % of the total masses of Br^- and NO_3^-, respectively, were recovered from the rapid fracture flow paths. It was also estimated that 45 % and 22 % of total Br^- and NO_3^-, respectively, were recovered from the slow matrix flow portion of the aquifer.

Based on the recovery percentages presented above, after 10 days of pumping, a "global" recovery of 73 % of the total mass of Br^- and a 47 % recovery of the total mass of NO_3^- were reported. The corresponding rate of denitrification was very rapid exhibiting first order kinetics with a nitrogen half-life ranging from 2.1 to 7.9 days. Autotrophic denitrification using pyrite as the electron donor was discussed; however, a significant trend of SO_4^{2-} concentration evolution was not observed in the capture well. No isotope data were reported.

One aspect that was not discussed by Pauwels et al. (1998) was the fate of the Br^- from the first non-nitrate tracer test. Using the dual porosity model, breakthrough of the fracture flow portion of the tracer was quick exhibiting a sharp short-lived peak. It was followed, and in part overlapped, by a second breakthrough peak that was broad and longer-lived that representing the slower matrix flow. Comparing the time dependent concentration profile curve depicting the slower matrix flow breakthrough curve and the time separation of the two tracer tests, it was apparent that a significant portion of the Br^- from the initial tracer could have still been retained within the matrix at the onset of the NO_3^- tracer test. Thus, water from the second tracer containing NO_3^- received by DNS1 could have undergone mixing with the first tracer water still retained in the matrix with simultaneous dilution of background water resulting in an artificially high Br^-/NO_3^- ratio and over estimation of total Br^- recovery. It seems that the reported NO_3^- loss could be, in part, from unconsidered dilution when not supported by isotope data or SO_4^{2-} evolution. An in-depth presentation and discussion of contaminant transport theory was beyond the scope of this review. Regardless, the perspective presented here lends consideration to the complexities and uncertainties introduced with in-situ tracer tests that undergo transport.

Gillham et al. (1990) report the effectiveness of “microcosms” as a means for reducing the complexities introduced by transport processes during in-situ testing. The microcosm was an inert cylindrical chamber open on the bottom that was inserted into the aquifer. The design of the microcosm effectively isolates a volume of the aquifer from lateral transport effects, which are usually the dominant dilution mechanism. The chamber was equipped with the capability to retrieve aquifer water, amend it with

chemicals, injection it back into aquifer and sample it for water quality and evolution analysis. The chamber mitigated losses of injected water to advection.

Bates and Spalding (1998) demonstrate the effectiveness of microcosm application to in-situ work. They performed an in-situ tracer test within microcosms inserted in a sand and gravel aquifer of Pleistocene age near Central City, Nebraska. The microcosm was 61 cm in length and 15 cm in diameter with an interior volume of ~11 L. Br^- was used as the tracer for denitrification in multiple tests that ranged in duration from 50 to 110 hours. They report a peak overall denitrification ($NO_3^- + NO_2^-$) rate of 26 mg $N \cdot L^{-1} \cdot d^{-1}$ when ethanol was simultaneously injected at C/N = 1.25. They computed an ε for overall denitrification ranging from –11 ‰ to –16 ‰, for C/N = 2.5 and = 1.25, respectively. They also observed HCO_3^- evolution within the microcosms correspondent to nitrate attenuation. Sulfate concentrations were not reported.

A “control” tracer test was conducted, being without ethanol. No change was observed in NO_3^-, Br^-, HCO_3^-, or DO concentration after 50 hours. Either the portion of the aquifer isolated by that microcosm was electron donor deficient (Korom, 1991) or the time of observation was insufficient to witness appreciable amounts of denitrification due to metabolic lag or slow kinetics (Pauwels et al. 1998). Regardless of cause, the lack of denitrification during the “control” tracer test limits insights on the overall effects of denitrification on aquifer chemistry. None-the-less the data presented were compelling evidence of denitrification and the stoichiometric consumption of an OC electron donor by biomass, perhaps applicable in remedial design. The relative retention of the tracer observed during the tests indicates the efficacy of the in-situ cosm methodology for mitigating advective effects and defining the boundary conditions of the system. The

latter would allow consideration of the potential for kinetic or mole/mass balance modeling using software capable of giving insights to processes responsible for observed changes in geochemistry.

APPENDIX B

Analytical Methods and Detections Limits

Table 3. Analytical methods.

Parameters*	Lab	Equipment	Method	RDL*****
Na^{+}	NDDH	ICPAES	EPA Method 200.7	0.1mg/L
Mg^{2+}	NDDH	ICPAES	EPA Method 200.7	0.1mg/L
Si^{4+}**	NDDH	ICPAES	EPA Method 200.7	0.02mg/L
K^{+}	NDDH	ICPAES	EPA Method 200.7	1.0mg/L
Ca^{2+}	NDDH	ICPAES	EPA Method 200.7	0.30mg/L
Mn^{2+}*	NDDH	ICPAES	EPA Method 200.7	0.002mg/L
Fe^{2+}*	NDDH	ICPAES	EPA Method 200.7	0.007mg/L
As^{3+}*	NDDH	ICPMS	EPA Method 200.8	0.2mg/L
F^{-}	NDDH	ISE	APHA Method 4500-F-C	0.020mg/L
Cl^{-}	NDDH	CAF AAII	APHA Method 4500-Cl-E	0.30mg/L
NH_4^{+}-N***	NDDH	AFIA	EPA Method 350.1	0.010mg/L
pH	Field	Orion™ Model 250A meter	Orion™ Model 9107 pH Triode	NA
DO	Field	YSI™ Model 57 Dissolved Oxygen Meter	APHA Method 4500-O G	0.1mg/L
CO_3^{2-}	NDDH	Mettler™ DL53 Titrator and DLWIN software	SM Method 2320B	1mg/L
HCO_3^{-}	NDDH	Mettler™ DL53 Titrator and DLWIN software	SM Method 2320B	1mg/L

Table 3. (continued).

Parameters*	Lab	Equipment	Method	RDL*****
TDC	WQL	Shimadzu™ TOC 5050 Analyzer	APHA Method 5310 B	1.0mg/L
DIC	WQL	Shimadzu™ TOC 5050 Analyzer	APHA Method 5310 B	1.0mg/L
DOC	WQL	Shimadzu™ TOC 5050 Analyzer	APHA Method 5310 B	1.0mg/L
Total P	NDDH	AFIA Acid persulfate digestion	EPA Method 365.3 acid persulfate digestion	0.018mg/L
SO_4^{2-}	NDDH	CAMB AAII	APHA Method 4500-SO_4^{2-}F	0.30mg/L
SO_4^{2-}	WQL	Alltech™ IC	Modified APHA Method 4110 B	1.5mg/L
NO_3^- and NO_2^- ****	NDDH	AFIA	CR EPA Method 353.2	0.02mg/L
NO_3^-	WQL	Alltech™ IC	Modified APHA Method 4110 B	1.0mg/L
Br^-	WQL	Alltech™ IC	Modified APHA Method 4110 B	2.0mg/L
S istotope	Geochron Labs	Vg Micromass 903	Mass Spectrometry	NA
N isotope	Environmental Isotope Laboratory, University of Waterloo		Mass Spectrometry	NA
Cation Exchange	NDSU Soil and Water Environmental Laboratory		Modified EPA 9081 Na-OAc/NH_4OAc	NA

* All aqueous parameters are reported as totals, including dissolved complexes. Dissolved Fe, Mn and As are assumed to be in most soluble valence.

** Reported as SiO_2.

*** Reported as Ammonia-N

**** Reported as summation of NO_3^- + NO_2^- as N.

***** RDL = Reported Detection Limit

APPENDIX C

Discussion of Minor Analytes

Ammonium (NH_4^+), iron (Fe), manganese (Mn) and dissolved organic carbon (DOC) were considered as important analytes to monitor. Ammonium (NH_4^+), reported as NH_3 due to conversion during analytical methods, is a product of dissimilatory denitrification which can be a nitrate sink (Korom, 1992). Reduced Fe, Mn and DOC are also important due to their capacity to serve as electron donors for redox reactions. The raw data for NH_4^+, Fe, Mn, DOC and As are reported in Tables 1 and 2 presented earlier.

NH_4^+ concentrations in the C-ISM did not establish a noticeable trend. Concentrations began the tracer test below detection. At 19 days detectable amounts of NH_3 were present in the C-ISM and remained above detectable levels until day 192, ranging in concentration from 2.42e-3 to 4.91e-3 mmol $\cdot L^{-1}$. After 192 days NH_3 concentrations fluctuated between detectable levels to non-detectable levels having a TT2 maximum concentration recorded for the C-06-22-99 of 9.45e-3 mmol $\cdot L^{-1}$.

Within the R-ISM dissolved concentrations of NH_3 behaved similarly. The before amendment sample (BR-10-08-98) concentrations were below detection, a value of 3.70e-3 mmol $\cdot L^{-1}$ was reported for the after amendment sample. After this time concentrations were intermittently above detection ranging in value from 1.49e-3 mmol $\cdot L^{-1}$ to the TT2 maximum of 9.45e-3 mmol $\cdot L^{-1}$ at 257 days. Dissolved NH_3 concentrations within the R-ISM also failed to establish a discernable trend.

Total Fe concentrations within both ISMs were below detection throughout TT2 except two data points recorded from samples C-02-15-99 (130 days) and C-02-19-00 (499 days).

Total Mn in the control ISM began TT2 with a value of 1.15e-2 mmol $\cdot L^{-1}$, jumped to 1.56e-2 mmol $\cdot L^{-1}$ by day 19 and continued on an upward trend until 499 days

(C-02-19-00) when the TT2 maximum was recorded with a concentration of 2.46e-2 mmol $\cdot L^{-1}$. Mn concentrations in the C-ISM finished the tracer test with a concentration of 2.44e-2 mmol $\cdot L^{-1}$ on day 608.

Mn concentrations within the R-ISM behaved similarly to those in C-ISM for the first 19 days, beginning TT2 with a concentration of 1.03e-2 mmol $\cdot L^{-1}$ at day zero and jumping to 1.13 mmol $\cdot L^{-1}$ by day 19. After this time the concentration of Mn within the R-ISM behaved opposite to that in the C-ISM. A steady downward trend was observed reaching the TT2 minimum value of 5.30e-3 mmol $\cdot L^{-1}$ at 383 days. Following the 10-26-99 minimum Mn concentrations rebounded within the R-ISM for the next 225 days, finishing TT2 with a value of 7.32e-3 mmol $\cdot L^{-1}$ at 608 days. The TT2 two minimum Mn concentrations reported at 383 days and 418 days (5.41 mmol/L) principally coincide with the time when NO_3^- concentrations were just being effectively zeroed within the R-ISM.

DOC was also considered to be an important analyte to monitor due to its capacity to contribute as an electron donor. However, the dissolved concentration profiles observed in both ISMs were erratic indicating no discernable trend. Thus, little useful information directly pertinent to the modeling efforts presented in this thesis could be gleaned from this parameter's dissolved concentrations. None-the-less Figure 19 shows DOC data for both ISMs during the tracer test. Concentrations of DOC in the C-ISM (C-DOC) began TT2 at 0.391 mmol $\cdot L^{-1}$ dipped slightly at day 19 to 0.223 mmol $\cdot L^{-1}$ and proceeded to reach its maximum value of 2.038 mmol $\cdot L^{-1}$ at day 54. After 12-01-98 (day 54) C-DOC concentrations varied between 0.815 mmol $\cdot L^{-1}$ to the TT2 minimum of

0.130 mmol · L^{-1}, occurring at both 285 and 314 days. C-DOC continued to vary for the next 294 days finishing TT2 with a concentration of 0.241 mmol · L^{-1} at 608 days.

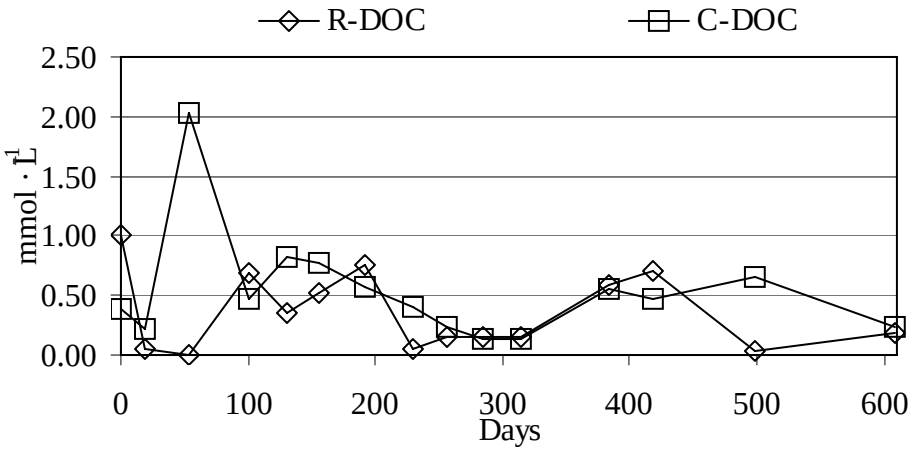

Figure 19. Comparison of R-DOC and C-DOC vs. time. Note: DOC concentrations for both AC and AR-10-08-98 are not reported.

DOC analysis in the R-ISM (R-DOC) ranged from the TT2 high of 1.00 mmol · L^{-1} within the BR-10-08-98 sample to the TT2 minimum of non-detection at 54 days. After 54 days R-DOC continued to vary from 0.761 mmol · L^{-1} on day 192 to 0.042 mmol · L^{-1} at 499 days. R-DOC finished TT2 with a value of 0.182 mmol · L^{-1}. Analyses of C-DOC and R-DOC failed to indicate a steady trend for this analyte in either ISM during TT2; however, the R-DOC maximum value was recorded at the beginning of the tracer test, prior to amendment.

Total arsenic (As) concentrations were also monitored during the tracer test due to its contaminant nature and its potential to be mobilized during redox reactions involving iron-sulfides and organic compounds containing As impurities (van Beek et al., 1989; Kölle et al., 1990). These two source materials for As are known to exist in the Pierre shale, which is believed to have been one of the major rock units supplying sediments for

the proglacial depositional processes that formed the EVA (Schultz et al., 1980 1064-B). As concentration are presented in Tables 1 and 2.

Arsenic concentrations in the C-ISM failed to establish a recognizable trend during the tracer test. As concentrations in the R-ISM, relative to NO_3^- concentrations within the R-ISM and As concentrations in C-ISM, failed to establish a discernable redox-sensitive trend.

APPENDIX D

Denitrification by Pyrite: Quantitative Comparison of TT1 and TT2

Assumptions and Description of Calculations

For discussionary purposes and denitrification evaluation the normalized data for Br^- R-ISM (R-Br^-) has been re-normalized to its maximum value reported for R-02-15-99 (1.41 mmol/L). This Br^- concentration is equal to the expected R-Br^- resulting from the amendment, according to the analytical accuracy of the method and equipment used for analysis. All other data points for the R-ISM with lessor concentration of Br^- are considered to be a dilution of this Br^- concentration. The only data points prior to R-02-15-99 with lessor concentrations of Br^-, with an absolute value of error from the expected amendment concentration greater than the expected error of the analytical method, is AR-10-08-98. This occurrence is attributed to non-thorough mixing of the amendment solution, or the development of slight density stratification within the amendment container. Other data points prior to R-02-15-99 with Br^- concentrations less than those observed in that sample, regardless of the absolute error being within analytical accuracy, are considered to be a dilutive fraction of the original amendment concentration. After R-02-15-99 R-Br^- concentrations less than the expected amendment concentration are considered to be a dilutive fraction of the initial amendment solution.

In this section, for TT1/TT2 comparative purposes the evaluation of the observed denitrification for TT2 is begun with the R-10-27-98 (day 19) as the evaluation of denitrification for TT1 considered day 32 as day 0. Ultimately the TT2 AR-10-27-98 data point does not effect the observation made in a TT1/TT2 comparative discussionary framework.

In lieu of the assumptions made regarding R-Br^-, NO_3^--N concentrations in the R-ISM (R-NO_3^--N) are dealt with in a similar manner. Since, the desired amendment

concentration of $R\text{-}Br^-$ was achieved it is assumed that the desired amendment concentration was also achieved for $R\text{-}NO_3^-\text{-}N$. Therefore, the expected value of $R\text{-}NO_3^-\text{-}N$ concentration for sample R-02-15-99 would be the concentration expected from amendment, 7.82 mmol $\cdot L^{-1}$. This concentration was never achieved within the R-ISM having a maximum $NO_3^-\text{-}N$ concentration reported from the day 19 sample R-10-27-98; however, denitrification is considered to commence within the first 19 days of TT2, resulting in $R\text{-}NO_3^-\text{-}N$ concentrations below those accountable by dilution for this initial stretch of time. Ultimately, based on $R\text{-}Br^-$ concentrations, it is assumed that the $R\text{-}NO_3^-\text{-}N$ concentration expected from the amendment was achieved. However, this expected maximum concentration of 7.82 mmol $\cdot L^{-1}$ is masked in the samples leading up to R-02-15-99 due to analytical uncertainty, non-thorough mixing of the AR-10-08-98 sample, and a small amount of denitrification that occurred within the first days of TT2. Therefore, throughout TT2 any missing $R\text{-}NO_3^-\text{-}N$ not accounted for by dilution, as recorded by Br^- and based on the reasoning and assumptions, is considered to be a result of denitrification. Total $NO_3^-\text{-}N$ attenuated by denitrification and denitrification rates are based on this consideration.

For comparing denitrification rates and the percent of denitrification accounted for by sulfate production during TT1 and TT2 the R-10-27-98 sample for $NO_3^-\text{-}N$ concentration is considered as the starting point and initial $NO_3^-\text{-}N$ concentration. For the total denitrification rate and percent of autotrophic denitrification accounted for by SO_4^{2-} evolution the assumed initial value of 7.82 mmol $\cdot L^{-1}$ $NO_3^-\text{-}N$ is used as the total starting concentration.

Consequent to the assumptions and reasoning used in regard to the R-Br^-, R-NO_3^--N the SO_4^{2-} concentration and evolution in the R-ISM (R-SO_4^{2-}) is based on the value reported for the R-10-27-98 sampling point (0.62 mmol $\cdot L^{-1}$). Therefore the R-SO_4^{2-} concentration of 0.62 reported for day 19 (R-10-27-98) is considered as the starting concentration for evaluation of denitrification accounted for by autotrophic processes resulting in SO_4^{2-} evolution for the purpose of comparing TT1 to TT2. This method results in a conservative estimate of autotrophic denitrification as accounted for by SO_4^{2-} evolution including consideration of dilution, which is inherently accounted for within the calculation method.

The method of accounting used simulates each data point as a unique point in time that is the result of a batch reaction that has occurred from the starting, or reference point, to the time in question instead of a continuous evolution of the amendment water through time. The algorithm for these type of calculations includes multiplying the initial NO_3^-N concentration by the fraction of the amendment remaining according to Br^- concentration, thus inherently accounting for dilution of SO_4^{2-}. However, when considering the likelihood of electron donor geographic heterogeneity, the occurrence and development of preferential flow paths within the ISM and the potential for uneven distribution of amendment water upon injection, it is difficult to defend a continuous geochemical evolution methodology for autotrophic denitrification quantification. 0.62 mmol $\cdot L^{-1}$ is a high value for native SO_4^{2-} as compared to the annual average (0.49 mmol $\cdot L^{-1}$) observed within wells screened at the same depth as the ISMs located approximately 100 meters north of the ISMs (Rush, personal communication). Furthermore, initial concentrations for SO_4^{2-} from R-10-08-98 reported by the WQL were

0.26 and 0.23 mmol · L^{-1}, values that were comparable to NDDH analytical results. However, the method of using 0.62 mmol · L^{-1} as the initial SO_4^{2-} concentration is congruent with that used for TT1 and facilitates direct relative comparison of the two data sets.

Table 4. Data calculations using initial concentration assumption for comparison of TT1 and TT2.

	A	B	C	D	E	F	G	H	I	J	K	L
1			7.82					Total	Expected		Actual	Fraction Missing
2	Sample Number		NO_3^--N**	Br^-	Br^-	N/Br	NO_3^--N	NO_3^--N	SO_4^{2-}	SO_4^{2-}	SO_4^{2-}	N Accounted
3	ISM-mm-dd-yy	Time	mmol · L^{-1}	mmol · L^{-1}	Normal		Expected	Lost to Denit	Production	mmol · L^{-1}	Prod	by SO_4^{2-}
4	BR-10-08-98	0	0.001	nd	NA	NA	NA	NA	NA	0.26	NA	
5	AR-10-08-99	0	7.52	1.33	0.945	5.640	NA	NA	NA	0.23	NA	NA
6	R-10-27-98	19	7.55	1.38	0.974	5.492	NA	NA	NA	0.62	0.00	NA
7	R-12-01-98	54	7.18	1.40	0.993	5.119	7.500	0.3248	0.21654615	0.68	0.06	0.28
8	R-01-16-99	100	6.90	1.39	0.983	4.969	7.426	0.5296	0.35306474	0.85	0.23	0.65
9	R-02-15-99	130	6.38	1.41	1.000	4.518	7.554	1.1753	0.78354026	0.96	0.34	0.44
10	R-03-12-99	156	5.59	1.36	0.965	4.105	7.291	1.6972	1.13146641	0.92	0.30	0.27
11	R-04-17-99	192	5.03	1.22	0.861	4.141	6.503	1.4700	0.98000353	0.93	0.31	0.32
12	R-05-25-99	229	4.45	1.18	0.839	3.755	6.334	1.8892	1.25944011	0.93	0.31	0.25
13	R-06-22-99	257	3.57	1.04	0.740	3.413	5.591	2.0247	1.34977971	1.12	0.50	0.37
14	R-07-20-99	285	2.41	0.92	0.651	2.626	4.917	2.5038	1.66919598	1.33	0.71	0.43
15	R-08-17-99	314	1.66	0.80	0.563	2.085	4.256	2.5974	1.73160437	1.40	0.78	0.45
16	R-10-26-99	383	0.55	0.63	0.446	0.880	3.372	2.8169	1.87796344	1.52	0.90	0.48
17	R-11-30-99	418	0.13	0.60	0.425	0.222	3.208	3.07478	2.04985149	1.63	1.01	0.49
18	R-02-19-00	499	0.001	0.49	0.346	0.002	2.612	2.6106	1.74039474	1.65	1.03	0.59
19	R-06-07-00	608	0.001	0.41	0.294	0.002	2.220	2.2189	1.47923553	1.39	0.76	0.52
20					D7/$D$10		(D7/$D$7)*$C$7		H7*(4/6)		J(n)-J7	K(n)/I(n)
21						C7/D7		G7-C7				

Table 5. Calculations of total denitrification accounted for by SO_4^{2-} evolution during TT2, while excluding initial SO_4^{2-} concentration assumption.

	P	Q	R	S	T	U	V	W	X	Y	Z	AA
1			7.82					Total	Expected		Actual	Fraction Missing
2	Sample Number		NO_3^--N**	Br^-	Br	N/Br	NO_3^--N	NO_3^--N	SO_4^{2-}	SO_4^{2-}	SO_4^{2-}	N Accounted
3	ISM-mm-dd-yy	Time	mmol · L^{-1}	mmol · L^{-1}	Normal		Expected	Lost to Denit	Production	mmol · L^{-1}	prod	by SO_4^{2-}
4	BR-10-08-98	0	0.001	nd	NA	NA	NA	NA	NA	0.26	NA	
5	AR-10-08-99	0	7.52	1.33	0.945	5.640	7.390	-0.1348	-0.0898619	0.23	-0.03	0.36
6	R-10-27-98	19	7.55	1.38	0.974	5.492	7.619	0.0654	0.0436173	0.62	0.36	8.26
7	R-12-01-98	54	7.18	1.40	0.993	5.119	7.765	0.5894	0.39293426	0.68	0.42	1.07
8	R-01-16-99	100	6.90	1.39	0.983	4.969	7.688	0.7916	0.52772047	0.85	0.59	1.12
9	R-02-15-99	130	6.38	1.41	1.000	4.518	7.820	1.4418	0.96118829	0.96	0.70	0.73
10	R-03-12-99	156	5.59	1.36	0.965	4.105	7.548	1.9544	1.30293062	0.92	0.66	0.51
11	R-04-17-99	192	5.03	1.22	0.861	4.141	6.733	1.6994	1.13295197	0.93	0.67	0.59
12	R-05-25-99	229	4.45	1.18	0.839	3.755	6.558	2.1126	1.4084122	0.93	0.67	0.48
13	R-06-22-99	257	3.57	1.04	0.740	3.413	5.788	2.2219	1.4812677	1.12	0.86	0.58
14	R-07-20-99	285	2.41	0.92	0.651	2.626	5.090	2.6773	1.78483492	1.33	1.07	0.60
15	R-08-17-99	314	1.66	0.80	0.563	2.085	4.406	2.7475	1.83168887	1.40	1.14	0.62
16	R-10-26-99	383	0.55	0.63	0.446	0.880	3.491	2.9359	1.95725935	1.52	1.26	0.64
17	R-11-30-99	418	0.13	0.60	0.425	0.222	3.321	3.18793	2.12528891	1.63	1.37	0.64
18	R-02-19-00	499	0.001	0.49	0.346	0.002	2.704	2.7027	1.8018156	1.65	1.39	0.77
19	R-06-07-00	608	0.001	0.41	0.294	0.002	2.298	2.2972	1.53144326	1.39	1.13	0.73
20					S(n)7/$S$10		T(n)*$R$2		H7*(4/6)		J(n)-J7	K(n)/I(n)
21						R(n)/S(n)		V(n)-R(n)				

For comparison of autotrophic denitrification the R-10-27-98 concentration of 0.62 mmol $\cdot L^{-1}$ for SO_4^{2-} is used as the starting point for quantification Table 4. For the total autotrophic denitrification quantification the initial BR-10-08-98 value of 0.26 mmol $\cdot L^{-1}$ is used as the initial SO_4^{2-} concentration in Table 5. Ultimately, this method is expected to result in a slight over-estimation of autotrophic denitrification because of the likelihood that some of the SO_4^{2-} produced in the initial 19 days was a result of reduction of dissolved oxygen that inundated the amendment water during field operations.

APPENDIX E

PHREEQC-2 Input Files

Table 6. PHREEQC-2 Input file for SI query of R-ISM.

```
TITLE Research ISM SI and Ion Balance Test
PHASES
OC
        CH2O + 2H2O = HCO3- + 5H+ + 4e-
        log_k           0.0
TITLE BR-10-08-98
Solution 1
        temp 9.5
        pH      7.58
        units   mmol/kgw

        Na      0.157
        Mg      1.226
        K       0.253
        Ca      2.061
        Br      0.00
        S(6)    0.26
        C       5.947
        Si      0.476
        F       0.026
        Cl      0.149
        Fe      1.25336e-4
        Mn      0.01028
        N(5)    0.001428
        Al      1.89e-7
        P       0.00071
SELECTED_OUTPUT
        -file               R-ISM.prn
        -selected_out       true
        -reset false
        -totals             Na Mg K Ca Br S(6) C F Cl Fe Mn O Si N Al P S
        -pH                 true
        -temp               true
        -percent_error
        -equilibrium_phases     OC CO2(g) Calcite Dolomite
        -saturation_indices     CO2(g) OC Calcite Dolomite Pyrite Goethite
END
```

Table 6. (continued)

```
TITLE AR-10-08-98
SOLUTION 1
        temp    15.9
        pH      7.69
        units   mmol/kgw

        Na      0.191
        Mg      1.168
        K       9.438
        Ca      1.991
        Br      1.334
        S(6)    0.228
        C       5.947
        Si      0.473
        F       0.026
        Cl      0.168
        Fe      1.25336e-4
        Mn      0.01028
        N(5)    7.525
        P       0.00084
        Al      1.89e-7
        Amm     0.00371

END

TITLE R-10-27-98
SOLUTION 1
        temp    15.0
        pH      7.60
        units   mmol/kgw

        Na      0.287
        Mg      1.333
        K       8.389
        Ca      2.278
        Br      1.375
        S(6)    0.620
        C       6.006
        Si      0.429
        F       0.024
        Cl      0.169
        Fe      1.25336e-4
        Mn      0.01132
        N(5)    7.554
        P       0.00142
        Amm     0.0000
        Al      1.89e-7

END
```

Table 6. (continued)

```
TITLE R-12-01-98
SOLUTION 1
        temp    7.9
        pH      7.07
        units   mmol/kgw

        Na      0.391
        Mg      1.292
        K       7.417
        Ca      2.211
        Br      1.402
        S(6)    0.682
        C       5.801
        Si      0.424
        F       0.024
        Cl      0.170
        Fe      1.25336e-4
        Mn      0.010976
        N(5)    7.175
        Amm     0.0000
        P       0.0001
        Al      1.89e-7


END

TITLE R-01-16-99
SOLUTION 1
        temp    6.8
        pH      7.31
        units   mmol/kgw

        Na      0.370
        Mg      1.317
        K       9.105
        Ca      2.261
        Br      1.388
        S(6)    0.849
        C       6.154
        Si      0.438
        F       0.026
        Cl      0.163
        Fe      1.25336e-4
        Mn      0.01074
        N(5)    6.897
        Amm     0.003641
        P       0.0001
        Al      1.89e-7
END
```

Table 6. (continued)

```
TITLE R-02-15-99
SOLUTION 1
        temp    5.4
        pH      7.44
        units   mmol/kgw

        Na      0.391
        Mg      1.214
        K       7.724
        Ca      2.108
        Br      1.412
        S(6)    0.965
        C       5.674798
        Si      0.396
        F       0.028
        Cl      0.168
        Fe      1.25336e-4
        Mn      0.00974
        N(5)    6.378
        Amm     0.00214
        P       0.0001
        Al      1.89e-7
END

TITLE R-03-12-99
SOLUTION 1
        temp    7.0
        pH      7.78
        units   mmol/kgw

        Na      0.331
        Mg      1.193
        K       6.752
        Ca      2.073
        Br      1.363
        S(6)    0.924
        C       5.980
        Si      0.360
        F       0.029
        Cl      0.172
        Fe      1.25336e-4
        Mn      0.00974
        N(5)    5.593
        Amm     0.00001
        P       0.0011
        Al      1.89e-7
END
```

Table 6. (continued)

```
TITLE R-04-17-99
SOLUTION 1
        temp    5.3
        pH      7.47
        units   mmol/kgw

        Na      0.396
        Mg      1.156
        K       6.855
        Ca      2.006
        Br      1.215
        S(6)    0.933
        C       5.4583
        Al      1.89e-7
        Si      0.394
        F       0.031
        Cl      0.183
        Fe      1.25336e-4
        Mn      0.00925
        N(5)    5.033
        P       0.0001
        Amm     0.0461
END

TITLE R-05-25-99
SOLUTION 1
        temp    9.8
        pH      7.66
        units   mmol/kgw

        Na      0.400
        Mg      1.111
        K       5.908
        Ca      1.946
        Br      1.184
        S(6)    0.933
        C       5.4275
        Si      0.361
        F       0.031
        Cl      0.171
        Fe      1.25336e-4
        Mn      0.0088
        N(5)    4.445
        P       0.0112
        Amm     0.0999
        Al      1.89e-7
END
```

Table 6. (continued)

```
TITLE R-06-22-99
SOLUTION 1
        temp    13.3
        pH      7.56
        units   mmol/kgw

        Na      0.413
        Mg      1.115
        K       5.780
        Ca      1.954
        Br      1.045
        S(6)    1.119
        C       5.217
        Si      0.406
        F       0.029
        Cl      0.158
        Fe      1.25336e-4
        Mn      0.00899
        N(5)    3.566
        Amm     0.00864
        P       0.0001
        Al      1.89e-7
END

TITLE R-07-20-99
SOLUTION 1
        temp    13.0
        pH      7.72
        units   mmol/kgw

        Na      0.400
        Mg      0.975
        K       5.013
        Ca      1.684
        Br      0.919
        S(6)    1.331
        C       5.3043
        Si      0.323
        F       0.031
        Cl      0.157
        Fe      1.25336e-4
        Mn      0.0079
        N(5)    2.413
        Amm     0.0001
        P       0.00507
        Al      1.89e-7
END
```

Table 6. (continued)

```
TITLE R-08-17-99
SOLUTION 1
        temp    12.7
        pH      7.56
        units   mmol/kgw

        Na      0.422
        Mg      0.946
        K       4.885
        Ca      1.629
        Br      0.795
        S(6)    1.400
        C       5.321
        Si      0.381
        F       0.034
        Cl      0.167
        Fe      1.25336e-4
        Mn      0.0075
        N(5)    1.658
        Amm     0.00193
        P       0.0005812
        Al      1.89e-7
END

TITLE R-10-26-99
SOLUTION 1
        temp    9.5
        pH      7.62
        units   mmol/kgw

        Na      0.431
        Mg      0.835
        K       4.527
        Ca      1.427
        Br      0.630
        S(6)    1.520
        C       5.113
        Si      0.356
        F       0.042
        Cl      0.166
        Fe      1.25336e-4
        Mn      0.00530
        N(5)    0.555
        Amm     0.0001
        P       0.0001
        Al      1.89e-7
END
```

Table 6. (continued)

```
TITLE R-11-30-99
SOLUTION 1
        temp    7.8
        pH      7.39
        units   mmol/kgw

        Na      0.422
        Mg      0.806
        K       4.553
        Ca      1.392
        Br      0.599
        S(6)    1.628
        C       5.162
        Si      0.341
        F       0.041
        Cl      0.167
        Fe      1.25336e-4
        Mn      0.00541
        N(5)    0.133
        Amm     0.00114
        P       0.0001
        Al      1.89e-7
END

TITLE R-02-19-00
SOLUTION 1
        temp    6.0
        pH      7.53
        units   mmol/kgw

        Na      0.409
        Mg      0.856
        K       3.939
        Ca      1.490
        Br      0.488
        S(6)    1.647
        C       5.147
        Si      0.431
        F       0.037
        Cl      0.169
        Fe      1.25336e-4
        Mn      0.00688
        N(5)    0.0001428
        Amm     0.0001
        P       0.0001
        Al      1.01186e-6
END
```

Table 6. (continued)

```
TITLE R-06-07-00
SOLUTION 1
        temp    11.2
        pH      7.60
        units   mmol/kgw

        Na      0.348
        Mg      0.823
        K       3.351
        Ca      1.432
        Br      0.415
        S(6)    1.385
        C       5.212
        Si      0.394
        F       0.029
        Cl      0.219
        Fe      1.25336e-4
        Mn      0.00732
        N(5)    0.001428
        Amm     0.00164
        P       0.00113
        Al      3.66938e-7
END
```

Table 7. PHREEQC-2 Input file for SI query of C-ISM.

```
TITLE Control ISM SI Test
PHASES
OC
        CH2O + 2H2O = HCO3- + 5H+ + 4e-
        log_k           0.0
TITLE BC-10-08-98
Solution 1
        temp 9.5
        pH      7.55
        units   mmol/kgw

        Na      0.204
        Mg      1.053
        K       0.381
        Ca      2.098
        Br      0.00
        S       0.675
        C       5.404
        Si      0.453
        F       0.033
        Cl      0.144
        Fe      1.25336e-4
        Mn      0.01128
        N(5)    0.001428
        Al      1.89e-7
        P       0.00071
SELECTED_OUTPUT
        -file           C-ISM.prn
        -selected_out   true
        -reset          false
        -totals         Na Mg K Ca Br S(6) C F Cl Fe Mn O Si N Al
        -pH             true
        -temp           true
        -percent_error
-equilibrium_phases     OC CO2(g) Calcite Dolomite
-saturation_indices     CO2(g) OC Calcite Dolomite

END
```

Table 7. (continued)

```
TITLE AC-10-08-98
SOLUTION 1
        temp    15.9
        pH      7.64
        units   mmol/kgw

        Na      0.231
        Mg      1.099
        K       10.128
        Ca      2.198
        Br      9.307
        S       0.673
        C       5.404
        Si      0.471
        F       0.033
        Cl      0.149
        Fe      1.25336e-4
        Mn      0.01182
        N(5)    0.001428
        P       0.0001
        Al      1.89e-7

END

TITLE C-10-27-98
SOLUTION 1
        temp    15.0
        pH      7.32
        units   mmol/kgw

        Na      0.348
        Mg      1.782
        K       5.166
        Ca      3.618
        Br      9.349
        S       0.620
        C       4.997
        Si      0.431
        F       0.031
        Cl      0.153
        Fe      1.25336e-4
        Mn      0.01114
        N(5)    0.002855
        P       0.0001
        Amm     0.0024268
        Al      1.89e-7

END
```

Table 7. (continued)

```
TITLE C-12-01-98
SOLUTION 1
        temp    7.9
        pH      7.10
        units   mmol/kgw

        Na      0.561
        Mg      1.498
        K       5.115
        Ca      2.994
        Br      9.111
        S       0.650
        C       4.9796
        Si      0.414
        F       0.031
        Cl      0.155
        Fe      1.25336e-4
        Mn      0.01515
        N(5)    0.002141
        Amm     0.0034261
        P       0.0001
        Al      1.89e-7


END

TITLE C-01-16-99
SOLUTION 1
        temp    6.8
        pH      7.31
        units   mmol/kgw

        Na      0.483
        Mg      1.506
        K       5.397
        Ca      3.069
        Br      8.560
        S       0.625
        C       5.427524
        Si      0.411
        F       0.030
        Cl      0.147
        Fe      1.25336e-4
        Mn      0.01663
        N(5)    0.0001
        Amm     0.004925
        P       0.0001
        Al      1.89e-7
END
```

Table 7. (continued)

```
TITLE C-02-15-99
SOLUTION 1
        temp    5.4
        pH      7.48
        units   mmol/kgw

        Na      0.474
        Mg      1.522
        K       4.732
        Ca      3.094
        Br      8.160
        S       0.529
        C       4.958787
        Si      0.384
        F       0.031
        Cl      0.153
        Fe      0.000161146
        Mn      0.01721
        N(5)    0.0001
        Amm     0.00271
        P       0.0001
        Al      1.89e-7
END

TITLE C-03-12-99
SOLUTION 1
        temp    7.0
        pH      7.61
        units   mmol/kgw

        Na      0.4675
        Mg      1.5755
        K       4.668
        Ca      3.194
        Br      8.698
        S       0.5315
        C       5.343
        #Alkalinity     5.343 as CO3
        Si      0.339
        F       0.030
        Cl      0.154
        Fe      1.25336e-4
        Mn      0.01692
        N(5)    0.0001
        Amm     0.002783
        P       0.0001
        Al      1.89e-7
END
```

Table 7. (continued)

```
TITLE C-04-17-99
SOLUTION 1
        temp    5.3
        pH      7.62
        units   mmol/kgw

        Na      0.461
        Mg      1.629
        K       4.604
        Ca      3.294
        Br      9.073
        S       0.534
        C       4.992090
        Si      0.389
        F       0.031
        Cl      0.164
        Fe      1.25336e-4
        Mn      0.01934
        N(5)    0.001428
        P       0.0001
        Amm     0.00328
        Al      1.89e-7
END

TITLE C-05-25-99
SOLUTION 1
        temp    9.8
        pH      7.42
        units   mmol/kgw

        Na      0.465
        Mg      1.642
        K       3.888
        Ca      3.368
        Br      9.171
        S       0.596
        C       4.885
        Si      0.358
        F       0.030
        Cl      0.157
        Fe      1.25336e-4
        Mn      0.01970
        N(5)    0.002855
        P       0.00762
        Amm     0.0001
        Al      1.89e-7
END
```

Table 7. (continued)

```
TITLE C-06-22-99
SOLUTION 1
        temp    13.3
        pH      7.33
        units   mmol/kgw

        Na      0.465
        Mg      1.658
        K       4.450
        Ca      3.169
        Br      8.818
        S       0.533
        C       5.008
        Si      0.396
        F       0.025
        Cl      0.146
        Fe      1.25336e-4
        Mn      0.02113
        N(5)    0.001428
        Amm     0.009493
        P       0.0001
        Al      1.89e-7
END

TITLE C-07-20-99
SOLUTION 1
        temp    13.0
        pH      7.48
        units   mmol/kgw

        Na      0.478
        Mg      1.802
        K       3.836
        Ca      3.593
        Br      8.235
        S       0.554
        C       5.08450
        Si      0.325
        F       0.028
        Cl      0.142
        Fe      1.25336e-4
        Mn      0.02095
        N(5)    0.001428
        Amm     0.0001
        P       0.0001
        Al      1.89e-7
END
```

Table 7. (continued)

```
TITLE C-08-17-99
SOLUTION 1
        temp    12.7
        pH      7.39
        units   mmol/kgw

        Na      0.483
        Mg      1.695
        K       3.785
        Ca      3.393
        Br      8.131
        S       0.491
        C       5.09283
        Si      0.393
        F       0.029
        Cl      0.153
        Fe      1.25336e-4
        Mn      0.02167
        N(5)    0.001428
        Amm     0.0014989
        P       0.0005813
        Al      1.89e-7
END

TITLE C-10-26-99
SOLUTION 1
        temp    9.5
        pH      7.36
        units   mmol/kgw

        Na      0.470
        Mg      1.568
        K       3.530
        Ca      3.144
        Br      7.533
        S       0.556
        C       5.040
        Si      0.361
        F       0.032
        Cl      0.159
        Fe      1.25336e-4
        Mn      0.02149
        N(5)    0.0001428
        Amm     0.0001
        P       0.0001
        Al      1.89e-7

END
```

Table 7. (continued)

```
TITLE C-11-30-99
SOLUTION 1
        temp    7.8
        pH      7.27
        units   mmol/kgw

        Na      0.472
        Mg      1.584
        K       3.4275
        Ca      3.194
        Br      7.349
        S       0.558
        C       5.168
        Si      0.346
        F       0.031
        Cl      0.164
        Fe      1.25336e-4
        Mn      0.02185
        N(5)    0.0001428
        Amm     0.00471
        P       0.0005813
        Al      1.89e-7

END

TITLE C-02-19-00
SOLUTION 1
        temp    6.0
        pH      7.66
        units   mmol/kgw

        Na      0.474
        Mg      1.600
        K       3.325
        Ca      3.244
        Br      7.132
        S       0.564
        C       5.205
        Si      0.431
        F       0.031
        Cl      0.179
        Fe      0.0001969
        Mn      0.02417
        N(5)    0.0001428
        Amm     0.0001
        P       0.0001
        Al      1.012e-6
END
```

Table 7. (continued)

```
TITLE C-06-07-00
SOLUTION 1
        temp    11.2
        pH      7.30
        units   mmol/kgw

        Na      0.435
        Mg      1.526
        K       2.967
        Ca      3.044
        Br      6.708
        S       0.566
        C       5.158
        Si      0.396
        F       0.025
        Cl      0.210
        Fe      1.25336e-4
        Mn      0.02399
        N(5)    0.001428
        Amm     0.00164
        P       0.0001
        Al      1.038e-6
END
```

Table 8. Input data block for C-ISM forward model.

```
TITLE Control ISM SI Controlled Forward Model

PHASES
OC
        CH2O + 2H2O = HCO3- + 5H+ + 4e-
        log_k           0.0
TITLE BC-10-08-98
Solution 0
        temp 9.5
        pH      7.55
        units   mmol/kgw

        Na      0.204
        Mg      1.053
        K       0.381
        Ca      2.098
        Br      0.00
        S       0.675
        C       5.404
        Si      0.453
        F       0.033
        Cl      0.144
        Fe      1.25336e-4
        Mn      0.01128
        N(5)    0.001428
        Al      1.89e-7
        P       0.00071
EXCHANGE 1
        -equilibrate 0
        X       0.039509399
SAVE EXCHANGE 1
SELECTED_OUTPUT
        -file           C-ISM.prn
        -selected_out   true
        -reset          false
        -totals         Na Mg K Ca Br S(6) C F Cl Fe Mn O Si N Al
        -pH             true
        -temp           true
        -percent_error
-equilibrium_phases     OC CO2(g) Calcite Dolomite
saturation_indices      CO2(g) OC Calcite Dolomite
END
```

Table 8. (continued)

```
TITLE AC-10-08-98
SOLUTION 1
        temp    15.9
        pH      7.64
        units   mmol/kgw

        Na      0.231
        Mg      1.099
        K       9.73
        Ca      2.198
        Br      9.307
        S       0.673
        C       5.404
        Si      0.471
        F       0.033
        Cl      0.149
        Fe      1.25336e-4
        Mn      0.01182
        N(5)    0.001428
        P       0.0001
        Al      1.89e-7

END


TITLE C-10-27-98

MIX 1
        0       -0.004512732
        1       1.004512732
USE Exchange 1

EQUILIBRIUM_PHASES 1
        #OC                     0.0             2.64e-4
        Dolomite                0.0983          10
        Calcite                 0.206           10.0
        #Pyrite                 0.0             4.5e-5
        CO2(g)                  -1.9786         0.0
REACTION_TEMPERATURE 1
        15
END
```

Table 8. (continued)

```
TITLE C-12-01-98

MIX 1
        1       0.978940582
        0       0.021059418
REACTION_TEMPERATURE 1
        7.9

USE Exchange 1
Equilibrium_Phases 1
        OC                              0.0             3.999e-5
        Dolomite                        -0.8949         10.0
        Calcite                         -0.2302         10.0
        #Pyrite                         0.0             4.5e-5
        CO2(g)                          -1.829          10.0
END


TITLE C-01-16-99

MIX 1
        1       0.919737832
        0       0.080262168
REACTION_TEMPERATURE 1
        6.8
USE exchange 1
Equilibrium_Phases 1
        OC              0.0             .86e-4
        Dolomite        -0.3935         10.0
        Calcite 0.0358          10.0
        #Pyrite 0.0             4.5e-5
        CO2(g)          -1.9793         10
END


TITLE C-02-15-99

MIX 1
        1       0.876759428
        0       0.123240572
REACTION_TEMPERATURE 1
        5.4
USE exchange 1
Equilibrium_Phases 1
        OC                      0.0             2.98e-4
        Dolomite                -0.1562         10.0
        Calcite                 0.1683          10
        #Pyrite                 0.0             4.5e-5
        CO2(g)                  -2.1794         0
END
```

Table 8. (continued)

```
TITLE C-03-12-99

MIX 1
        1       0.934565381
        0       0.065434619
REACTION_TEMPERATURE 1
        7.0
USE exchange 1
Equilibrium_Phases 1
        OC                      0.0             2.75e-4
        Dolomite                0.2898          10.0
        Calcite                 0.3743          10
        #Pyrite                 0.0             4.5e-5
        CO2(g)                  -2.2608         10
END


TITLE C-04-17-99

MIX 1
        1       0.974857634
        0       0.025142366
REACTION_TEMPERATURE 1
        5.3
USE exchange 1
EQUILIBRIUM_PHASES 1
        OC                      0.0             2.78e-4
        Dolomite                0.1867          10.0
        Calcite                 0.3394          10
        #Pyrite                 0.0             4.5e-5
        CO2(g)                  -2.3091         10
END


TITLE C-05-25-99

MIX 7
        1       0.985387343
        0       0.014612657
REACTION_TEMPERATURE 1
        9.8
USE exchange 1
Equilibrium_Phases 1
        OC                      0.0             1.88e-4
        Dolomite                -0.0096         10.0
        Calcite                 0.1999          10
        #Pyrite                 0.0             4.5e-5
        CO2(g)                  -2.1084         10
END
```

Table 8. (continued)

```
TITLE C-06-22-99

MIX 1
        1       0.947458902
        0       0.052541098
REACTION_TEMPERATURE 1
        13.3
USE exchange 1
Equilibrium_Phases 1
        OC                      0.0             2.78e-4
        Dolomite                -0.0257         10.0
        Calcite                 0.1452          10
        #Pyrite                 0.0             4.5e-5
        CO2(g)                  -1.9944         10
END


TITLE C-07-20-99

MIX 1
        1       0.884817879
        0       0.115182121
REACTION_TEMPERATURE 9
        13
USE exchange 1
Equilibrium_Phases 1
        OC                      0.0             2.48e-4
        Dolomite                0.3768          10.0
        Calcite                 0.3582          10
        #Pyrite                 0.0             4.5e-5
        CO2(g)                  -2.1296         10
END


TITLE C-08-17-99

MIX 1
        1       0.873643494
        0       0.126356506
REACTION_TEMPERATURE 1
        12.7
USE exchange 1
Equilibrium_Phases 1
        Equilibrium_Phases 1
        OC                      0.0             3.48e-4
        Dolomite                0.1309          10.0
        Calcite                 0.2388          10
        #Pyrite                 0.0             4.5e-5
        CO2(g)                  -2.0459         10
END
```

Table 8. (continued)

```
TITLE C-10-26-99

MIX 1
        1       0.809390781
        0       0.190609219
REACTION_TEMPERATURE 1
        9.5
USE exchange 1
Equilibrium_Phases 1
        OC                      0.0             2.36e-4
        Dolomite                -0.1593         10.0
        Calcite                 0.1232          10
        #Pyrite                 0.0             4.5e-5
        CO2(g)                  -2.0398         10
END


TITLE C-11-30-99

MIX 1
        1       0.789620716
        0       0.210379284
REACTION_TEMPERATURE 1
        7.8
USE exchange 1
Equilibrium_Phases 1
        OC                      0.0             2.32e-4
        Dolomite                -0.4148         10.0
        Calcite                 0.013           10
        #Pyrite                 0.0             4.5e-5
        CO2(g)                  -1.9587         10
END


TITLE C-02-19-00

MIX 1
        1       0.766304932
        0       0.233695068
REACTION_TEMPERATURE 1
        6.0
USE exchange 1
Equilibrium_Phases 1
        OC                      0.0             2.20e-4
        Dolomite                0.3449          10.0
        Calcite                 0.412           10
        #Pyrite                 0.0             4.5e-5
        CO2(g)                  -2.3237         10
END
```

Table 8. (continued)

```
TITLE C-06-07-00

MIX 1
        1       0.720747824
        0       0.279252176
REACTION_TEMPERATURE 14
        11.2
USE exchange 1
Equilibrium_Phases 1
        OC                              0.0             2.16e-4
        Dolomite                        -0.2004         10.0
        Calcite                         0.0858          10
        #Pyrite                         0.0             4.5e-5
        CO2(g)                          -1.9645         10
END
```

Table 9. Input data block forward model simulation of R-ISM.

```
TITLE Research ISM FORWARD SI GOVERNED
PHASES
OC
        CH2O + 2H2O = HCO3- + 5H+ + 4e-
        log_k           0.0
TITLE BR-10-08-98
Solution 0
        temp 9.5
        pH      7.58
        units   mmol/kgw
        Na      0.157
        Mg      1.226
        K       0.253
        Ca      2.061
        Br      0.00
        S(6)    0.620
        C       5.947
        Si      0.476
        F       0.026
        Cl      0.149
        Fe      1.25336e-4
        Mn      0.01028
        N(5)    0.001428
        Al      1.89e-7
        P       0.00071
        #S(-2)  0.318

EXCHANGE 1
-equilibrate 0
        X       0.0036509399
SAVE Solution 0
SAVE Exchange 1

SELECTED_OUTPUT
        -file               R-ISM.prn
        -selected_out       true
        -reset              false
        -totals              Na Mg K Ca Br S(6) C F Cl Fe Mn O Si N(5) Al P S
        -pH                 true
        -temp               true
        -percent_error
        -equilibrium_phases     CO2(g) OC Calcite Dolomite Goethite Pyrite
        -saturation_indices     CO2(g) OC Calcite Dolomite Goethite Pyrite
END
```

Table 9. (continued)

```
TITLE AR-10-08-98
SOLUTION 1
        temp    15.9
        pH      7.69
        units   mmol/kgw

        Na      0.191
        Mg      1.168
        K       9.438
        Ca      1.991
        Br      1.4120
        S(6)    0.620
        C       5.947
        Si      0.473
        F       0.026
        Cl      0.168
        Fe      1.25336e-4
        Mn      0.01028
        N(5)    7.8199
        P       0.00084
        Al      1.89e-7
        Amm     0.00371
        #S(-2)  0.392

SAVE Solution 1
END

TITLE R-10-27-98

MIX 1
        0       0.02266289
        1       0.97733711
REACTION_TEMPERATURE 1
        15
USE Exchange 1
EQUILIBRIUM_PHASES 1
        OC                      0.0             1.14e-4
        Dolomite                0.5427          10.0
        Calcite                 0.3907          10.0
        #Pyrite                 0.0             4.0e-4
        CO2(g)                  -2.1535         0.0
        Goethite                6.8899          0
END
```

Table 9. (continued)

```
TITLE R-12-01-98

MIX 1
        1       0.991501416
        0       0.008498584
REACTION_TEMPERATURE 1
        7.9
USE Exchange 1
Equilibrium_Phases 1
        OC                      0.0             6.00e-4
        Dolomite                -1.0225         10.0
        Calcite                 -0.3275         10.0
        Pyrite                  0.0             .31e-4
        CO2(g)                  -1.7353         10.0
        Goethite                5.5015          0
END


TITLE R-01-16-99

MIX 1
        1       0.984419263
        0       0.015580737
REACTION_TEMPERATURE 1
        6.8
USE exchange 1
Equilibrium_Phases 1
        OC                      0.0             5.69e-4
        Dolomite                -0.4871         10.0
        Calcite                 -0.0484         10.0
        Pyrite                  0.0             1.145e-4
        CO2(g)                  -1.9228         10.0
        Goethite                6.1542          0
END


TITLE R-02-15-99

MIX 1
        1       1
        0       0
REACTION_TEMPERATURE 1
        5.4
USE exchange 1
Equilibrium_Phases 1
        OC                      0.0             11.550e-4
        Dolomite                -0.4018         10.0
        Calcite                 0.0107          10.0
        Pyrite                  0.0             1.705e-4
        CO2(g)                  -2.0808         10.0
        Goethite                6.501           0
END
```

Table 9. (continued)

```
TITLE R-03-12-99

MIX 1
        1       0.963172805
        0       0.036827195
REACTION_TEMPERATURE 1
        7.0
USE exchange 1
Equilibrium_Phases 1
        OC                      0.0             18.550e-4
        Dolomite                0.4407          10.0
        Calcite                 0.4158          10.0
        Pyrite                  0.0             1.525e-4
        CO2(g)                  -2.368          10.0
        Goethite                7.3218          0
END


TITLE R-04-17-99

MIX 1
        1       0.864022663
        0       0.135977337
REACTION_TEMPERATURE 1
        5.3
USE exchange 1
EQUILIBRIUM_PHASES 1
        OC                      0.0                     15.550e-4
        Dolomite                -0.3994         10.0
        Calcite                 0.013           10.0
        Pyrite                  0.0             1.569e-4
        CO2(g)                  -2.1236         10.0
        Goethite                6.5915          0
END


TITLE R-05-25-99

MIX 1
        1       0.835694051
        0       0.164305949
REACTION_TEMPERATURE 1
        9.8
USE exchange 1
Equilibrium_Phases 1
        OC                      0.0                     20.150e-4
        Dolomite                0.2128          10.0
        Calcite         0.2768          10.0
        Pyrite          0.0             1.569e-4
        CO2(g)          -2.2782         10.0
        Goethite        7.0821          0
END
```

Table 9. (continued)

```
TITLE R-06-22-99

MIX
        1       0.743626062
        0       0.256373938
REACTION_TEMPERATURE 1
        13.3
USE exchange 1
Equilibrium_Phases 1
        OC                      0.0             19.150e-4
        Dolomite                0.1425          10.0
        Calcite                 0.2106          10.0
        Pyrite                  0.0             2.480e-4
        CO2(g)                  -2.1805         10.0
        Goethite                6.8662          0
END


TITLE R-07-20-99

MIX 1
        1       0.650849858
        0       0.349150142
REACTION_TEMPERATURE 1
        13.
USE exchange 1
Equilibrium_Phases 1
        OC                      0.0             20.150e-4
        Dolomite                0.3598          10.0
        Calcite                 0.3185          10.0
        Pyrite                  0.0             3.550e-4
        CO2(g)                  -2.3245         10.0
        Goethite                7.1101          0
END


TITLE R-08-17-99

MIX 1
        1       0.563031161
        0       0.436968839
REACTION_TEMPERATURE 1
        12.7
USE exchange 1
Equilibrium_Phases 1
        OC                      0.0             19.650e-4
        Dolomite                -0.0083         10.0
        Calcite                 0.1365          10.0
        Pyrite                  0.0             3.900e-4
        CO2(g)                  -2.1714         10.0
        Goethite                6.8728          0
END
```

Table 9. (continued)

```
TITLE R-10-26-99

MIX 1
        1       0.446175637
        0       0.553824363
REACTION_TEMPERATURE 1
        9.5
USE exchange 1
Equilibrium_Phases 1
        OC                      0.0             19.80e-4
        Dolomite                -0.1731         10.0
        Calcite                 0.0809          10.0
        Pyrite                  0.0             4.500e-4
        CO2(g)                  -2.2607         10.0
        Goethite                7.016           0
END


TITLE R-11-30-99

MIX 1
        1       0.424220963
        0       0.575779037
REACTION_TEMPERATURE 1
        7.8
USE exchange 1
Equilibrium_Phases 1
        OC                      0.0             20.750e-4
        Dolomite                -0.7721         10.0
        Calcite                 -0.2003         10.0
        Pyrite                  0.0             5.090e-4
        CO2(g)                  -2.0528         10.0
        Goethite                6.434           0
END


TITLE R-02-19-00

MIX 1
        1       0.345609065
        0       0.654390935
REACTION_TEMPERATURE 1
        6.0
USE exchange 1
Equilibrium_Phases 1
        OC                      0.0             14.5175e-4
        Dolomite                -0.5111         10.0
        Calcite                 -0.0505         10.0
        Pyrite                  0.0             5.140e-4
        CO2(g)                  -2.1924         10.0
        Goethite                6.7795          0
END
```

Table 9. (continued)

```
TITLE R-06-07-00

MIX 1
        1       0.293909348
        0       0.706090652
REACTION_TEMPERATURE 1
        11.2
USE exchange 1
Equilibrium_Phases 1
        OC                      0.0             14.477e-4
        Dolomite                -0.0977         10.0
        Calcite                 0.1073          10.0
        Pyrite                  0.0             3.80e-4
        CO2(g)                  -2.2224         10.0
        Goethite                6.9694          0
END
```

APPENDIX F

Important Saturation Indices

Table 10. R-ISM important SIs.

ISM-mm-dd-yy	Time	$CO_2(g)$	OC	Calcite	Dolomite	Goethite	Pyrite
BR-10-08-98	0	-2.157	-56.207	0.309	0.286	6.940	-101.166
AR-10-08-99	0	-2.237	-56.761	0.449	0.675	6.973	-105.991
R-10-27-98	19	-2.154	-56.313	0.391	0.543	6.890	-103.179
R-12-01-98	54	-1.735	-53.737	-0.328	-1.023	5.502	-91.675
R-01-16-99	100	-1.923	-54.879	-0.048	-0.487	6.154	-94.971
R-02-15-99	130	-2.081	-55.551	0.011	-0.402	6.501	-96.403
R-03-12-99	156	-2.368	-57.206	0.416	0.441	7.322	-102.706
R-04-17-99	192	-2.124	-55.713	0.013	-0.399	6.592	-96.853
R-05-25-99	229	-2.278	-56.650	0.277	0.213	7.082	-101.733
R-06-22-99	257	-2.181	-56.171	0.211	0.143	6.866	-101.229
R-07-20-99	285	-2.325	-56.953	0.319	0.360	7.110	-103.726
R-08-17-99	314	-2.171	-56.158	0.137	-0.008	6.873	-100.756
R-10-26-99	383	-2.261	-56.471	0.081	-0.173	7.016	-100.424
R-11-30-99	418	-2.053	-55.334	-0.200	-0.772	6.434	-95.907
R-02-19-00	499	-2.192	-56.025	-0.051	-0.511	6.780	-97.503
R-06-07-00	608	-2.222	-56.361	0.107	-0.098	6.969	-100.813

Table 11. C-ISM important SIs.

Sample #		SI = log [IAP/K]			
ISM-mm-dd-yy	Time	$CO_{2(g)}$	OC	Calcite	Dolomite
BC-10-08-98	0	-2.170	-56.100	0.235	0.065
AC-10-08-98	0	-2.241	-56.606	0.395	0.497
C-10-27-98	19	-1.979	-55.018	0.206	0.098
C-12-01-98	54	-1.829	-53.951	-0.230	-0.895
C-01-16-99	100	-1.979	-54.936	0.036	-0.394
C-02-15-99	130	-2.179	-55.809	0.168	-0.156
C-03-12-99	156	-2.261	-56.418	0.374	0.290
C-04-17-99	192	-2.309	-56.499	0.339	0.187
C-05-25-99	229	-2.108	-55.520	0.200	-0.010
C-06-22-99	257	-1.994	-55.064	0.145	-0.026
C-07-20-99	285	-2.130	-55.798	0.358	0.377
C-08-17-99	314	-2.046	-55.353	0.239	0.131
C-10-26-99	383	-2.040	-55.210	0.123	-0.159
C-11-30-99	418	-1.959	-54.760	0.013	-0.415
C-02-19-00	499	-2.324	-56.677	0.412	0.345
C-06-07-00	608	-1.965	-54.903	0.086	-0.201

APPENDIX G

Forward Model Concentration Output

Table 12. C-ISM model output concentrations.

Sample #					mole · L^{-1}					
ISM-mm-dd-yy	Time	pH	temp	pct_err	Na	Mg	K	Ca	Br	S(6)
BC-10-08-98	0	7.55	9.5	2.53	2.0E-04	1.1E-03	3.8E-04	2.1E-03	0.0E+00	6.8E-04
AC-10-08-98	0	7.64	15.9	1.75	2.3E-04	1.1E-03	9.7E-03	2.2E-03	9.3E-03	6.7E-04
C-10-27-98	19	7.33	15	1.84	3.4E-04	1.7E-03	5.0E-03	3.5E-03	9.3E-03	6.7E-04
C-12-01-98	54	7.09	7.9	1.90	5.7E-04	1.6E-03	5.2E-03	3.1E-03	9.1E-03	6.5E-04
C-01-16-99	100	7.31	6.8	1.83	4.9E-04	1.5E-03	5.5E-03	3.1E-03	8.6E-03	6.3E-04
C-02-15-99	130	7.47	5.4	1.91	4.9E-04	1.6E-03	4.3E-03	3.3E-03	8.2E-03	5.3E-04
C-03-12-99	156	7.60	7	1.82	4.8E-04	1.7E-03	4.8E-03	3.4E-03	8.7E-03	5.4E-04
C-04-17-99	192	7.61	5.3	1.85	4.7E-04	1.7E-03	4.7E-03	3.5E-03	9.1E-03	5.3E-04
C-05-25-99	229	7.40	9.8	1.87	4.8E-04	1.8E-03	4.1E-03	3.7E-03	9.2E-03	5.8E-04
C-06-22-99	257	7.32	13.3	1.88	4.8E-04	1.7E-03	4.6E-03	3.3E-03	8.8E-03	5.4E-04
C-07-20-99	285	7.48	13	1.86	4.7E-04	1.8E-03	3.8E-03	3.5E-03	8.2E-03	5.5E-04
C-08-17-99	314	7.39	12.7	1.89	4.9E-04	1.7E-03	3.8E-03	3.4E-03	8.1E-03	5.0E-04
C-10-26-99	383	7.35	9.5	1.93	4.8E-04	1.6E-03	3.6E-03	3.3E-03	7.5E-03	5.6E-04
C-11-30-99	418	7.27	7.8	1.93	4.8E-04	1.6E-03	3.8E-03	3.2E-03	7.3E-03	5.6E-04
C-02-19-00	499	7.65	6	1.90	4.8E-04	1.7E-03	3.4E-03	3.4E-03	7.1E-03	5.6E-04
C-06-07-00	608	7.30	11.2	1.96	4.5E-04	1.5E-03	3.5E-03	3.1E-03	6.7E-03	5.7E-04

		mole · L^{-1}							
ISM-mm-dd-yy	Time	Mn	Si	N	Al	F	Cl	Fe	DIC
BC-10-08-98	0	1.1E-05	4.5E-04	1.4E-06	1.9E-10	3.3E-05	1.4E-04	1.3E-07	5.4E-03
AC-10-08-98	0	1.2E-05	4.7E-04	1.4E-06	1.9E-10	3.3E-05	1.5E-04	1.3E-07	5.4E-03
C-10-27-98	19	1.6E-05	4.3E-04	1.4E-06	1.9E-10	3.3E-05	1.5E-04	1.3E-07	4.9E-03
C-12-01-98	54	1.5E-05	4.1E-04	1.4E-06	2.0E-10	3.3E-05	1.5E-04	5.3E-08	4.9E-03
C-01-16-99	100	1.5E-05	4.1E-04	1.4E-06	1.9E-10	3.3E-05	1.5E-04	5.8E-08	5.4E-03
C-02-15-99	130	1.5E-05	3.8E-04	1.4E-06	1.9E-10	3.3E-05	1.5E-04	9.1E-08	4.9E-03
C-03-12-99	156	1.7E-05	3.4E-04	1.4E-06	1.8E-10	3.3E-05	1.5E-04	9.3E-08	5.2E-03
C-04-17-99	192	1.7E-05	3.9E-04	1.4E-06	1.9E-10	3.3E-05	1.5E-04	9.3E-08	4.9E-03
C-05-25-99	229	1.6E-05	3.6E-04	1.4E-06	1.8E-10	3.3E-05	1.5E-04	7.8E-08	4.7E-03
C-06-22-99	257	1.6E-05	4.0E-04	1.4E-06	1.9E-10	3.3E-05	1.5E-04	8.8E-08	4.9E-03
C-07-20-99	285	1.6E-05	3.3E-04	1.4E-06	1.9E-10	3.3E-05	1.5E-04	8.9E-08	5.1E-03
C-08-17-99	314	1.6E-05	3.9E-04	1.4E-06	1.9E-10	3.3E-05	1.5E-04	9.8E-08	5.1E-03
C-10-26-99	383	1.5E-05	3.6E-04	1.4E-06	1.9E-10	3.3E-05	1.5E-04	8.1E-08	5.0E-03
C-11-30-99	418	1.5E-05	3.5E-04	1.4E-06	1.9E-10	3.3E-05	1.5E-04	7.6E-08	5.2E-03
C-02-19-00	499	1.6E-05	4.3E-04	1.4E-06	1.0E-09	3.3E-05	1.5E-04	8.5E-08	5.1E-03
C-06-07-00	608	1.5E-05	4.0E-04	1.4E-06	1.0E-09	3.3E-05	1.5E-04	7.5E-08	5.1E-03

Table 13. R-ISM model output concentrations.

Sample #					mol · L^{-1}					
ISM-mm-dd-yy	Time	pH	temp	pct_err	Na	Mg	K	Ca	Br	S(6)
BR-10-08-98	0	7.58	9.5	-0.05	0.0002	0.0012	0.0003	0.0021	0.0000	0.0006
AR-10-08-99	0	7.69	15.9	-1.35	0.0002	0.0012	0.0094	0.0020	0.0014	0.0006
R-10-27-98	19	7.59	15	-1.36	0.0003	0.0014	0.0077	0.0024	0.0014	0.0006
R-12-01-98	54	7.08	7.9	-1.47	0.0004	0.0013	0.0073	0.0021	0.0014	0.0007
R-01-16-99	100	7.33	6.8	-1.38	0.0004	0.0012	0.0086	0.0020	0.0014	0.0008
R-02-15-99	130	7.44	5.4	-1.48	0.0004	0.0012	0.0077	0.0021	0.0014	0.0010
R-03-12-99	156	7.77	7	-1.48	0.0003	0.0013	0.0069	0.0022	0.0014	0.0009
R-04-17-99	192	7.48	5.3	-1.44	0.0004	0.0011	0.0067	0.0019	0.0012	0.0009
R-05-25-99	229	7.66	9.8	-1.46	0.0004	0.0011	0.0059	0.0020	0.0012	0.0009
R-06-22-99	257	7.57	13.3	-1.40	0.0004	0.0010	0.0056	0.0018	0.0010	0.0011
R-07-20-99	285	7.71	13	-1.33	0.0004	0.0010	0.0051	0.0017	0.0009	0.0013
R-08-17-99	314	7.57	12.7	-1.23	0.0004	0.0009	0.0048	0.0016	0.0008	0.0014
R-10-26-99	383	7.63	9.5	-1.11	0.0004	0.0008	0.0044	0.0014	0.0006	0.0015
R-11-30-99	418	7.41	7.8	-1.09	0.0004	0.0007	0.0044	0.0013	0.0006	0.0016
R-02-19-00	499	7.54	6	-0.92	0.0004	0.0008	0.0038	0.0014	0.0005	0.0016
R-06-07-00	608	7.60	11.2	-0.84	0.0003	0.0008	0.0033	0.0014	0.0004	0.0014

Sample #		mol · L^{-1}								
ISM-mm-dd-yy	Time	Si	N(5)	Al	P	Cl	Fe	Mn	DIC	F
BR-10-08-98	0	4.8E-04	1.4E-06	1.9E-10	7.1E-07	1.5E-04	1.3E-07	1.0E-05	5.9E-03	2.6E-05
AR-10-08-99	0	4.7E-04	7.8E-03	1.9E-10	8.4E-07	1.7E-04	1.3E-07	1.0E-05	5.9E-03	2.6E-05
R-10-27-98	19	4.3E-04	7.6E-03	1.9E-10	8.4E-07	1.7E-04	6.9E-08	1.1E-05	5.9E-03	2.6E-05
R-12-01-98	54	4.2E-04	7.2E-03	2.0E-10	8.4E-07	1.7E-04	1.8E-09	1.1E-05	5.9E-03	2.6E-05
R-01-16-99	100	4.4E-04	6.9E-03	1.9E-10	8.4E-07	1.7E-04	5.1E-09	1.1E-05	6.4E-03	2.6E-05
R-02-15-99	130	4.0E-04	6.4E-03	1.9E-10	8.4E-07	1.7E-04	8.3E-09	1.1E-05	5.7E-03	2.6E-05
R-03-12-99	156	3.6E-04	5.6E-03	1.8E-10	8.4E-07	1.7E-04	5.4E-08	1.1E-05	5.8E-03	2.6E-05
R-04-17-99	192	3.9E-04	5.0E-03	1.9E-10	8.2E-07	1.7E-04	9.7E-09	1.0E-05	5.6E-03	2.6E-05
R-05-25-99	229	3.6E-04	4.5E-03	1.9E-10	8.2E-07	1.6E-04	4.9E-08	1.1E-05	5.4E-03	2.6E-05
R-06-22-99	257	4.1E-04	3.5E-03	1.9E-10	8.1E-07	1.6E-04	5.2E-08	1.0E-05	5.4E-03	2.6E-05
R-07-20-99	285	3.2E-04	2.4E-03	1.9E-10	7.9E-07	1.6E-04	8.1E-08	1.0E-05	5.2E-03	2.6E-05
R-08-17-99	314	3.8E-04	1.7E-03	1.9E-10	7.8E-07	1.6E-04	4.9E-08	9.9E-06	5.4E-03	2.6E-05
R-10-26-99	383	3.6E-04	5.6E-04	1.9E-10	7.7E-07	1.6E-04	4.1E-08	9.5E-06	5.2E-03	2.6E-05
R-11-30-99	418	3.4E-04	1.3E-04	1.9E-10	7.7E-07	1.6E-04	1.0E-08	9.0E-06	5.3E-03	2.6E-05
R-02-19-00	499	4.3E-04	1.4E-07	1.0E-09	7.5E-07	1.6E-04	1.5E-08	9.3E-06	5.3E-03	2.6E-05
R-06-07-00	608	3.9E-04	1.2E-06	3.7E-10	7.5E-07	1.5E-04	4.8E-08	9.4E-06	5.2E-03	2.6E-05

APPENDIX H

Modeled vs. Measured Concentrations for Less Important Ions

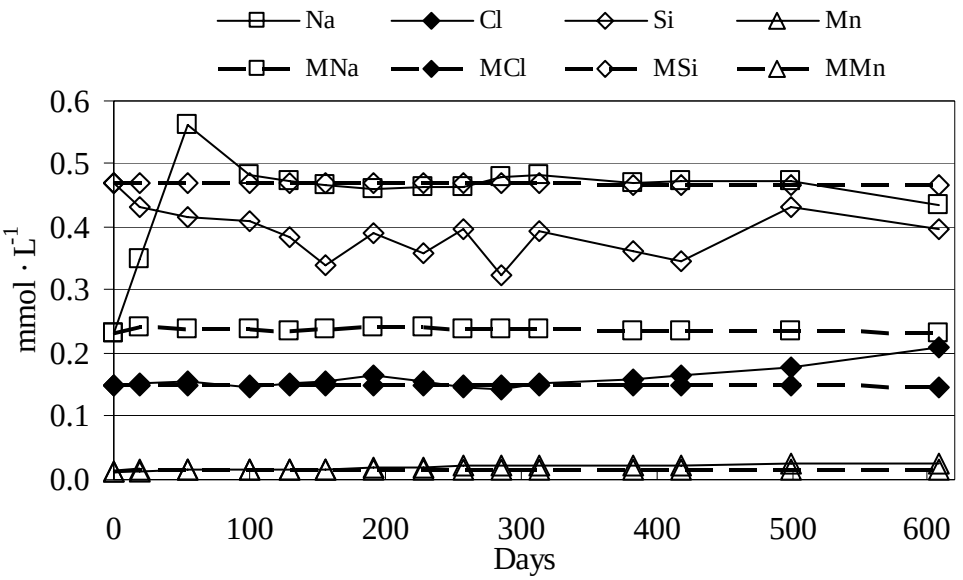

Figure 20. Modeled vs. measured concentrations for less important ions in the C-ISM.

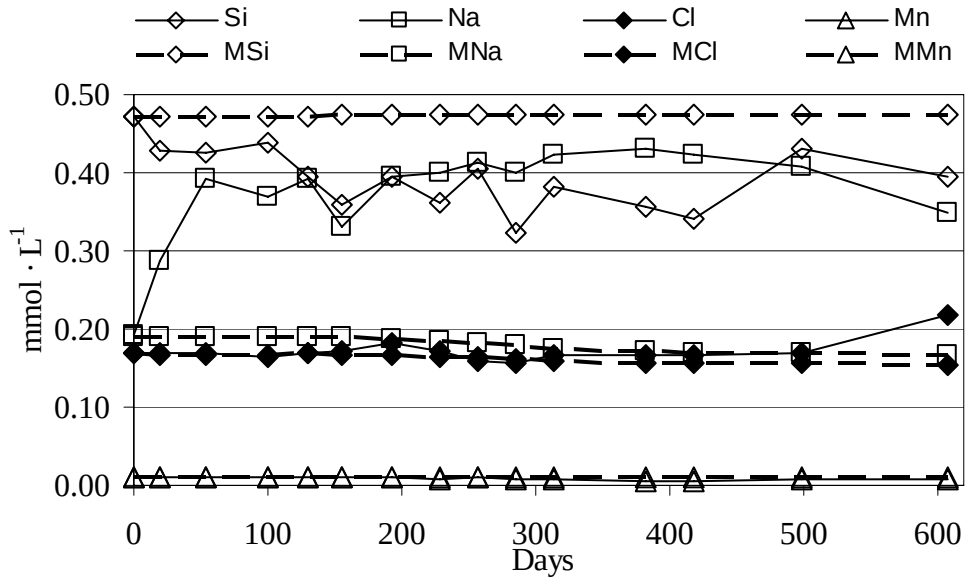

Figure 21. Modeled vs. measured concentrations for less important ions in the R-ISM.

APPENDIX I

Forward Model Phase Mole Transfers

Table 14. Phase mole transfers in the C-ISM forward model.

Sample #		Total phase transfer (mole · L^{-1})			
ISM-mm-dd-yy	Days	OC	CO2(g)	Calcite	Dolomite
BC-10-08-98	0	0.00E+00	0.00E+00	0.00E+00	0.00E+00
AC-10-08-98	0	0.00E+00	0.00E+00	0.00E+00	0.00E+00
C-10-27-98	19	0.00E+00	9.45E-05	4.39E-04	-5.24E-05
C-12-01-98	54	-4.00E-05	5.36E-05	6.77E-04	-3.29E-06
C-01-16-99	100	-8.60E-05	1.14E-05	3.76E-04	-6.17E-07
C-02-15-99	130	-2.98E-04	4.41E-04	4.25E-04	4.27E-05
C-03-12-99	156	-2.75E-04	3.19E-04	3.96E-04	-5.18E-05
C-04-17-99	192	-2.78E-04	4.61E-04	4.86E-04	-3.05E-05
C-05-25-99	229	-1.88E-04	3.54E-04	3.91E-04	4.14E-05
C-06-22-99	257	-2.78E-04	3.32E-04	9.86E-04	-2.49E-04
C-07-20-99	285	-2.48E-04	2.54E-04	5.18E-04	-1.26E-04
C-08-17-99	314	-3.48E-04	3.04E-04	5.16E-04	-7.10E-05
C-10-26-99	383	-2.36E-04	2.68E-04	4.89E-04	-2.75E-05
C-11-30-99	418	-2.32E-04	1.11E-04	4.30E-04	-2.38E-06
C-02-19-00	499	-2.20E-04	2.95E-04	3.02E-04	-3.72E-05
C-06-07-00	608	-2.16E-04	1.60E-04	4.83E-04	-4.89E-05

Table 15. Phase mole transfers in the R-ISM forward model.

Sample #		Total Phase Transfers (mol · L^{-1})					
ISM-mm-dd-yy	Days	CO2(g)	OC	Calcite	Dolomite	Goethite	Pyrite
BR-10-08-98	0	0.00E+00	0.00E+00	0.00E+00	0.00E+00	0.00E+00	0.00E+00
AR-10-08-99	0	0.00E+00	0.00E+00	0.00E+00	0.00E+00	0.00E+00	0.00E+00
R-10-27-98	19	0.00E+00	-1.14E-04	8.90E-05	-2.30E-05	5.72E-08	0.00E+00
R-12-01-98	54	0.00E+00	-6.00E-04	2.30E-04	1.70E-04	3.11E-05	-3.10E-05
R-01-16-99	100	0.00E+00	-5.69E-04	1.35E-04	5.76E-05	1.15E-04	-1.15E-04
R-02-15-99	130	6.77E-04	-1.16E-03	2.03E-04	1.82E-04	1.71E-04	-1.71E-04
R-03-12-99	156	1.09E-03	-1.86E-03	1.95E-04	1.82E-04	1.53E-04	-1.53E-04
R-04-17-99	192	1.02E-03	-1.56E-03	2.49E-04	2.65E-04	1.57E-04	-1.57E-04
R-05-25-99	229	1.41E-03	-2.02E-03	2.53E-04	3.06E-04	1.57E-04	-1.57E-04
R-06-22-99	257	1.47E-03	-1.92E-03	2.48E-04	3.18E-04	2.48E-04	-2.48E-04
R-07-20-99	285	1.74E-03	-2.02E-03	2.73E-04	3.21E-04	3.55E-04	-3.55E-04
R-08-17-99	314	1.69E-03	-1.97E-03	2.75E-04	3.32E-04	3.90E-04	-3.90E-04
R-10-26-99	383	1.93E-03	-1.98E-03	3.11E-04	3.80E-04	4.50E-04	-4.50E-04
R-11-30-99	418	1.87E-03	-2.08E-03	3.13E-04	4.20E-04	5.09E-04	-5.09E-04
R-02-19-00	499	1.61E-03	-1.45E-03	2.14E-04	3.32E-04	5.14E-04	-5.14E-04
R-06-07-00	608	1.58E-03	-1.45E-03	2.09E-04	3.41E-04	3.80E-04	-3.80E-04

REFERENCES

Appelo, C. A. J., D. Postma, Geochemistry, Groundwater and Pollution, 536pp., A. A. Balkema, Rotterdam, Netherlands, 1996.

Appelo, C. A. J., and A. Willemsen, Geochemical calculations and observations on salt water intrusions, I, A combined geochemical/mixing cell model, Journal of Hydrology, 94, 313-330, 1987.

Appelo, C. A. J., A. Willemsen, H. E. Beekman, and J. Grifioen, Geochemical calculations and observations on salt water intrusions, II, Valication of a geochemical model with laboratory experiments, Journal of Hydrology, 120, 225-250, 1990.

Aravena, R. and W. D. Robertson, Use of multiple isotope tracers to evaluate denitrification in groundwater: study of nitrate from a large-flux septic system plume, Ground Water, 36(6), 975-982, 1998.

Bates, H. K. and R. F. Spalding, Aquifer denitrification as interpreted from in-situ microcosm experiments, Journal of Environmental Quality, 27, 174-182, 1998.

Boggs, S. Jr., Principles of Sedimentology and Stratigraphy, Second Edition, 774pp., Prentice Hall, New Jersey, 1995.

Böttcher, J., O. Strebel, S. Voerkelius and H.-L. Schmidt, Using isotope fractionation of nitrate-nitrogen and nitrate-oxygen for evaluation of microbial denitrification in a sandy aquifer, Journal of Hydrology, 114, 413-424, 1990.

Buresh, R. J. and J. T. Moraghan, Chemical reduction of nitrate by ferrous iron, Journal of Environmental Quality, 5, 320-325, 1976.

Canter, L. W., Nitrates in Groundwater, 263pp., Lewis Publishers, New York, 1997.

Das, B. M., Principles of Geotechnical Engineering, 672pp., PWS Publishing Company, Boston, MA, 1994.

Faure, G. F., Principles and Applications of Geochemistry, 600 pp., Prentice Hall, Upper Saddle River, NJ, 1998.

Firestone, M. K., Biological denitrification, in Nitrogen in Agricultural Soils, edited by F. J. Stevenson, American Society of Agronomy, Madison, Wisconsin, 289-326, 1982.

Gerla, P. J., Pathline and geochemical evolution of ground water in a regional discharge area, Red River Valley, North Dakota, Ground Water, 30(5), 1992.

Gillham, R. W., M. J. L. Robin and C. J. Ptacek, A device fr in-situ determination of geochemical transport parameters 2. Biochemical reactions, Ground Water, 28(6), 1990.

Harris, K. L., Geology of the souther part of the Lake Agassiz Basin, in Prodeedings of the North Dakota Academy of Science 51, Supplement 1: 6-11, 1997.

Howard, K. W. F., Denitrification in a major limestone aquifer, Journal of Hydrology, 76, 265-280, 1985.

Kelly, T. E., and Q. F. Paulson, Geology and ground water resources of Grand Forks County, North Dakota: Ground water resources, North Dakota Geological Survey Bulletin 53, Part III, 58 pp. Bismarck, ND. 1970.

Kammer, A., Laboratory denitrification using sediments from the Elk Valley aquifer, M.S. thesis, 76pp., University of North Dakota, Grand Forks, ND, 2001.

Kinzelbach, W., W. Schäfer and J. Herzer, Modeling of natural and enhanced denitrification processes in aquifers, Water Resources Research, 27(6), 1123-1135, 1991.

Kölle, W., O. Strebel, and J. Bottcher, Formation of sulfate by microbial denitrification in a reducing aquifer, Water Supply, 3(1), 35-40, 1985.

Kölle, W., O. Strebel, and J. Bottcher, 1987, Reduced sulfur compounds in sandy aquifers and their interactions with groundwater, in Proceedings of the Dresden Symposium, Groundwater Monitoring and Management, edited by G. P. Jones, IAHS Publication No. 173, 23-30, 1990.

Korom, S. F., Denitrification in the unconsolidated deposits of the Heber Valley aquifer, Ph.D. thesis, 176 pp., Utah State University, Logan, Utah, 1991.

Korom, S. F., Natural denitrification in the saturated zone: a review, Water Resources Research, 28(6), 1657-1667, 1992.

Korom, S. F., A. J. Schlag, W. M. Schuh and A. K. Schlag, In situ mesocosms: Denitrification in the Elk Valley Aquifer, Ground Water Monitroing and Remediation, in print.

Mariotti, A., J. C. Germon, P. Hubert, P. Kaiser, R. Letolle, A Tardieux and P. Tardieux, Experimental determination of nitrogen kinetic isotope fractionation: Some principles; illustration for the denitrification and nitrification processes, Plant and Soil, 62, 413-430, 1981.

Mariotti, A., J. C. Germon, and A. Leclerc, Nitrogen isotope fractionation associated with the $NO_2 \rightarrow N_2O$ step of denitrification in soils, Canadian Jounal of Soil Science, 62(2), 227-241, 1982.

Mariotti, A., A. Landreau and B. Simon, ^{15}N isotope biogeochemistry and natural denitrification process in groundwater: Application to the chalk aquifer of northern France, Geochimica et Cosmochimica Acta, 52(7), 1869-1878, 1988.

Mayer, G. G., Denitrification in the Elk Valley aquifer, northeastern North Dakota. Ph.D. thesis, 233 pp., University of North Dakota, Frand Forks, ND, 1992.

McMahon, P. B., J. K. Böhlke and B. W. Bruce, Denitrification in marine shales in northeastern Colorado, Water Resources Research, 35(5), 1629-1642, 1999.

Parkhurst, D. L., C. A. J. Appelo, User's guide to PHREEQC (version2)— A computer program for speciation, batch-reaction, on-dimensional transport, and inverse geochemical calculations, U.S. Geological Survey Water Resources Investigations Report 99-4259, 308 pp., 1999.

Patch, J. C., and G. Padmanabhan, Vertical nitrate gradients in a shallow unconfined aquifer in North Dakota, in Proceedings of the North Dakota Water Quality Symposium, 25-34, 1996.

Pauwels, H. O. Legendre, and J.-C. Foucher, High-rate denitrification from several electron donors in a schist aquifer, in Water-Rock Interaction: Proceedings of the 9th International Symposium - WRI - 9, pp. 173-176, Ashgate Publishing Co., Balkema, Rotterdam, Netherlands, 1998.

Pauwels, H., W. Kloppmann, J.-C. Foucher, A. Martelat, and V. Fritsche, Field tracer test in a pyrite-bearing schist aquifer, Applied Geochemistry, 13(6), 767-778, 1998.

Plummer, L. N., B. F. Jones, and A. H. Truesdell, WATEQF: A FORTRAN IV version of WATEQ, a computer program for calculating chemical equilibrium in natural waters, U. S. Geologic Survey Water Resources Investigation, 76-13, 1976.

Plummer, L. N., E. C.Prestemon, and D.L. Parkhurst, An interactive code (NETPATH) for modeling net geochemical reactions along a flow path, U. S. Geologic Survey Water Resources Research, 27, 2027-2045, 1991.

Postma, D., Kinetics of nitrate reduction by detrital Fe(II)-silicates, Geochimica et Cosmochimica Acta, 54, 903-908, 1990.

Postma, D., C. Boesen, H. Kristiansen, and F. Larsen, Nitrate reduction in an unconfined sandy aquifer: water chemistry, reduction processes, and geochemical modeling, Water Resources Research, 27(8), 2027-2045, 1991.

Rush, D., Personal Communication, 2001.

Schlag, A. J., In-situ measurement of denitrification in the Elk Valley aquifer, M.S. thesis, 104 pp., University of North Dakota, Grand Forks, ND, 1999.

Schultz, L. G., H. A. Tourtelot, J. R. Gill and J. G. Boerngen, Composition and properties of the Pierre Shale and equibalent rocks, Northern Great Plains Region, U. S. Geological Survey Professional Paper 1064-B, 114pp., 1980.

Smith, R. L., B. L. Howes and J. K. Duff, Denitrification in nitrate-contaminated groundwater: Occurrence in steep vertical geochemical gradients, Geochimica et Cosmochimica Acta, 55(76), 1815-1825, 1991.

Tesoriero, A. J., H. Liebscher and S. E. Cox, Mechanism and rate of denitrification in an agricultural watershed: Electon and mass balance along hgroundwater flow paths, Water Resources Research, 36(6), 1545-1559, 2000.

Trudell, M. R., R. W. Gillham, and J. A. Cherry, An in-situ study of the occurrence and rate of denitrification in a shallow unconfined sand aquifer, Journal of Hydrology, 83(3/4), 251-268, 1986.

van Beek, C. G. E. M., F. A. M. Hettingas, and R. Straatman, The effects of manure spreading and acid deposition upon groundwater quality in Vierlingsbeek, the Netherlands, in Proceedings of the Symposium held during the Third IAHS Scientific Assembly, Baltimore, Groundwater Contamination, IAHS Publication No. 185, 155-162, 1989.

Vogel, J. C. A., S. Talma and T. H. E. Heaton, Gaseous nitrogen as evidence for denitrification in groudwater, Journal of Hydrology, 50(1/3), 191-200, 1981.

World Wide Web: http://water.usgs.gov/watuse/spread95.html.

World Wide Web: http://www.epa.gov/ow/resources/9698/chap6c.html.